UNIVERSITY COLLEGE LONDON

Department of Electronic and Electrical Engineering

Wideband Modulation and Tuning of Semiconductor Lasers using Novel Quantum well Structures

Contract F6170896C0008

Final Report

prepared by

Xuan Huang and Alwyn Seeds

December, 1997

TORRINGTON PLACE LONDON WC1E 7JE UK
Telephone: +44 171-380 7928
Facsimile: +44 171-387 4350
e-mail: a.seeds @ eleceng.ucl.ac.uk

REPORT DOCUMENTATION PAGE

Form Approved OMB No. 0704-0188

1. AGENCY USE ONLY (Leave blank)	2. REPORT DATE	3. REPORT TYPE AND DATES COVERED
	December 1997	Final Report

4. TITLE AND SUBTITLE

Wideband Modulation and Tuning Of Semiconductor Lasers Using Novel Quantum Well Structures

5. FUNDING NUMBERS

F6170896C0008

6. AUTHOR(S)

Dr. Alwyn Seeds

7. PERFORMING ORGANIZATION NAME(S) AND ADDRESS(ES)

University College London
Gower Street
London WC1E 6BT
United Kingdom

8. PERFORMING ORGANIZATION REPORT NUMBER

N/A

9. SPONSORING/MONITORING AGENCY NAME(S) AND ADDRESS(ES)

EOARD
PSC 802 BOX 14
FPO 09499-0200

10. SPONSORING/MONITORING AGENCY REPORT NUMBER

SPC 96-4065

11. SUPPLEMENTARY NOTES

12a. DISTRIBUTION/AVAILABILITY STATEMENT

Approved for public release; distribution is unlimited.

12b. DISTRIBUTION CODE

A

13. ABSTRACT (Maximum 200 words)

This report results from a contract tasking University College London as follows: The objective of the tasking was to realize GaAs/AlGaAs tunable lasers which use the quantum-confined Stark effect (QCSE) as a tuning mechanism to produce a uniform frequency modulation (FM) response. A detailed analysis of optical frequency modulation analogue link is presented. It is shown that these enable non-linear limits on the dynamic range of long (>100km) links to be overcome. Using realistic system parameters signal to noise ratios exceeding 156 dB. Hz are predicted for 1000km links.

14. SUBJECT TERMS

Computers, Lasers

15. NUMBER OF PAGES

104

16. PRICE CODE

N/A

17. SECURITY CLASSIFICATION OF REPORT	18. SECURITY CLASSIFICATION OF THIS PAGE	19. SECURITY CLASSIFICATION OF ABSTRACT	20. LIMITATION OF ABSTRACT
UNCLASSIFIED	UNCLASSIFIED	UNCLASSIFIED	UL

Abstract

This is the final report for a three year programme to realise GaAs/AlGaAs tunable lasers which use the quantum-confined Stark effect (QCSE) to as a tuning mechanism to produce an uniform frequency modulation (FM) response. It focuses on work carried out under the present contract over the last year. However, for completeness reference is made to pertinent work carried out under the previous two contracts SPC-93-4072 and F61708-94-C0009.

A detailed analysis of optical frequency modulation analogue links is presented. It is shown that these enable non-linear limits on the dynamic range of long (> 100 km) links to be overcome. Using realistic system parameters signal to noise ratios exceeding 156 dB.Hz are predicted for 1,000 km links.

Detailed modelling of QCSE tuning performance has been carried out. The results for wavelength de-tuning, insertion loss, tuning section length and static FM response are presented. In device fabrication development, a successful O+ implantation isolated two section laser with very high isolation resistance and very low leakage current has been obtained, its performance evaluated and techniques for further improvements proposed. Results on an air-bridged room temperature CW operating laser with an order of magnitude lower parasitic capacitance are presented. Extensive further studies of quantum well disordering by cap annealing have been carried out, leading to successful fabrication of a two-section tunable laser having a disordered tuning section.

Using the above techniques in combination, monolithically integrated QCSE tuned lasers having peak deviation > 10 GHz, an FM response uniform within ± 2 dB from 10 kHz to 6 GHz, residual intensity modulation less than 5%, linewidth less than 10 MHz and room temperature CW output power greater than 10 mW/facet have been successfully fabricated. The upper frequency limit could be further extended with more complex fabrication techniques.

Preliminary work on InP based tunable lasers has also started, covering both device design/modelling and laser fabrication.

Chapter 1 Introduction

This is the final report for a three year programme to realise GaAs/AlGaAs tunable lasers which use the quantum-confined Stark effect (QCSE) to as a tuning mechanism to produce an uniform frequency modulation (FM) response. It focuses on work carried out under the present contract over the last year. However, for completeness reference is made to pertinent work carried out under the previous two contracts SPC-93-4072 and F61708-94-C0009. This earlier work is summarised below.

In the first year of the programme, funded under contract SPC-93-4072, we reviewed existing approaches to tunable lasers, presented different tuning configurations from external cavity tuning to integrated monolithic tuning, and discussed different tuning mechanisms including the electro-optic effect, the acoust-optic effect, the carrier injection effect (CIE) and the quantum confined Stark effect (QCSE) in a multiple quantum well (MQW) structure. We decided to use QCSE as the tuning mechanism and described the design of a 2-section integrated Fabry-Perot cavity ridge waveguide tunable laser, to demonstrate fast tuning and uniform modulation response. A room temperature CW operating two section laser, with threshold current 25 mA, was fabricated successfully and preliminary experimental results were presented.

In the second year, funded under contract F61708-94-C0009, modelling and calculation was performed on the optical field profile in the waveguide, optical confinement factor, tuning performance and absorption - refractive index conversion. Fabrication techniques were developed to reduce the contact resistance, improve the die soldering technique using eutectic alloy instead of indium, and improve the trench etching technique to give uniform ridge dimensions. These developments gave improved power output and single mode operation. Ion implantation by H^+ and O^+ was carried out over a range of different doses and energies. H^+ implantation gave well isolated two section lasers. Experiments on impurity free vacancy diffusion (IFVD) by SiO_2 and SrF_2 cap annealing were performed, leading to a photoluminescence wavelength shift of up to 17nm. A new IFVD technique for better device performance was suggested. Due to the improvements in device fabrication, static and dynamic tuning performance could be evaluated, giving tuning exceeding the Fabry-Perot mode spacing of 60GHz and highly uniform FM response with a cut-off frequency of 500MHz, which was parasitic capacitance limited. The experimental results were analysed in great detail to reveal the mechanisms involved and the route to further performance enhancement.

Work under the current contract has built on these foundations. More detailed modelling of the tuning performance has been carried out. The results for wavelength de-tuning, insertion loss, tuning section length and static FM response are presented. In device fabrication development, a successful O+ implantation isolated two section laser with very high isolation resistance and very low leakage current has been obtained, its performance evaluated and techniques for further improvements proposed. First results on an air-bridged room temperature CW operating laser with an order of magnitude lower parasitic capacitance are presented. Extensive further studies of quantum well disordering by cap annealing have been carried out, leading to successful fabrication of a two-section tunable laser having a disordered tuning section.

The work described above was brought together to produce reverse bias tuned quantum well lasers offering room temperature CW output power well in excess of 10mW/facet, sidemode suppression exceeding 10 dB over 2:1 bias current ranges with best values exceeding 20 dB, linewidths of < 10 MHz FWHM, FM tuning slopes of 12 GHz/V, residual intensity modulation below 5% for 5 GHz peak deviation and FM frequency response uniform within ± 2.5 dB from 10 kHz to over 2 GHz. The upper cut-off frequency for these devices would be expected to be raised to between 3 GHz and 5 GHz, by the use of low parasitic microwave mounts. Further increases would be posssible by using more complex fabrication procedures, with an estimated upper - 3 dB limit of about 40 GHz A specially attractive feature of these lasers is the independence of the tuning response from changes in gain section bias current, in complete contrast to current tuned lasers. The successful realisation of these lasers enabled us to complete the realisation of the major objectives of this programme.

Preliminary work on InP based tunable lasers has also started, covering both device design/modelling and laser fabrication. Initial successful CW laser operation of an oxide isolated stripe laser has been obtained, using epitaxial material grown at the Laboratory for Physical Sciences, albeit at very low output powers. Important processing techniques toward the realisation of ridge guide and other advanced structures have also been developed. Finally, we have placed our work in a systems context with a study of optical FM transmission systems for wide dynamic range analogue signals. This indicates that it should be possible to achieve signal to noise ratios exceeding 150 dB.Hz for transmission distances in excess of 1,000 km.

The report is organised as follows. Chapter 2 describes optical FM transmission systems leading to the identification of key parameters for the optical source laser.

Chapter 3 describes device tuning performance analyses; Chapter 4, device fabrication progress in ion implantation isolation; Chapter 5, device fabrication progress on a low parasitic capacitance laser; Chapter 6, studies of quantum well disordering for tunable lasers using cap annealing techniques. Chapter 7 reports fabrication procedures and the measured performance of our complete QCSE tuned laser and Chapter 8, some initial tunable laser work on the InP based semiconductor material system. Finally, Chapter 9 contains the conclusions from our work on GaAs/AlGaAs tunable lasers and directions for our future work on tunable lasers in the InP based material system.

Chapter 2. Optical FM Transmission Systems

2.1 Introduction

Most optical fibre analogue transmission systems use intensity modulation of the optical source with direct detection of the modulated optical signal in a depletion photo-detector. In this chapter coherent techniques are introduced and their advantages and disadvantages relative to intensity modulation/direct detection (IMDD) systems considered. Coherent techniques will be defined broadly to include all transmission systems where the precise frequency of the optical signal is important.

Section 2.2 will introduce analogue coherent transmission systems and contrast their performance with that of IMDD systems. In Section 2.3 optical source requirements for coherent analogue transmission will be discussed. Section 2.4 will review coherent analogue transmission techniques and show why optical frequency modulation (OFM) is an attractive option. Section 2.5 will present results for an experimental coherent analogue transmission system using OFM. Finally, Section 2.6 will discuss future prospects for coherent analogue transmission systems, including requirements for an optimised laser source for OFM systems.

2.2 Coherent analogue transmission systems

Figure 2.1 contrasts IMDD and coherent optical transmission systems. In the IMDD system, Figure 2.1(a), the optical source intensity is either directly modulated by the input analogue signal or passes through an external intensity modulator. The resulting intensity modulated signal passes through the optical fibre to the photodiode where the modulation is returned to the electrical domain.

In the coherent system, Figure 2.1(b), the optical source is modulated in intensity, frequency or phase by the input analogue signal, either directly or by passage through an external modulator. The modulated signal passes through the optical fibre to the receiver, where it is combined with the output from a local oscillator (LO) laser. The combined signal illuminates the photodiode to produce an electrical signal centered on the difference frequency between the unmodulated optical source and the LO laser. This signal is further processed to recover the analogue output signal.

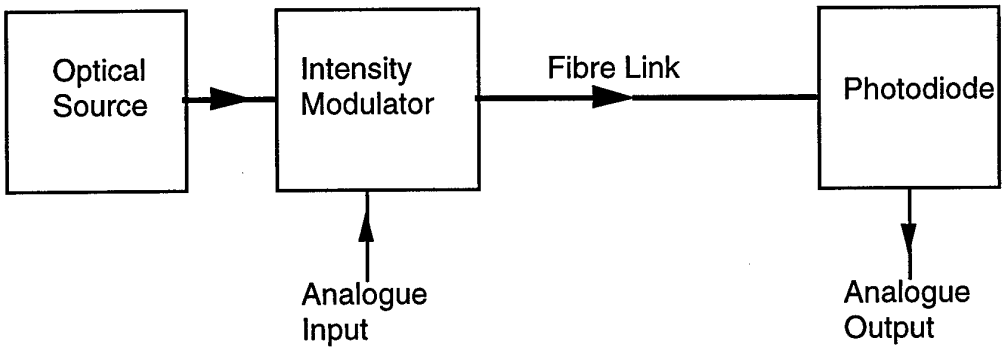

(a) IMDD transmission system

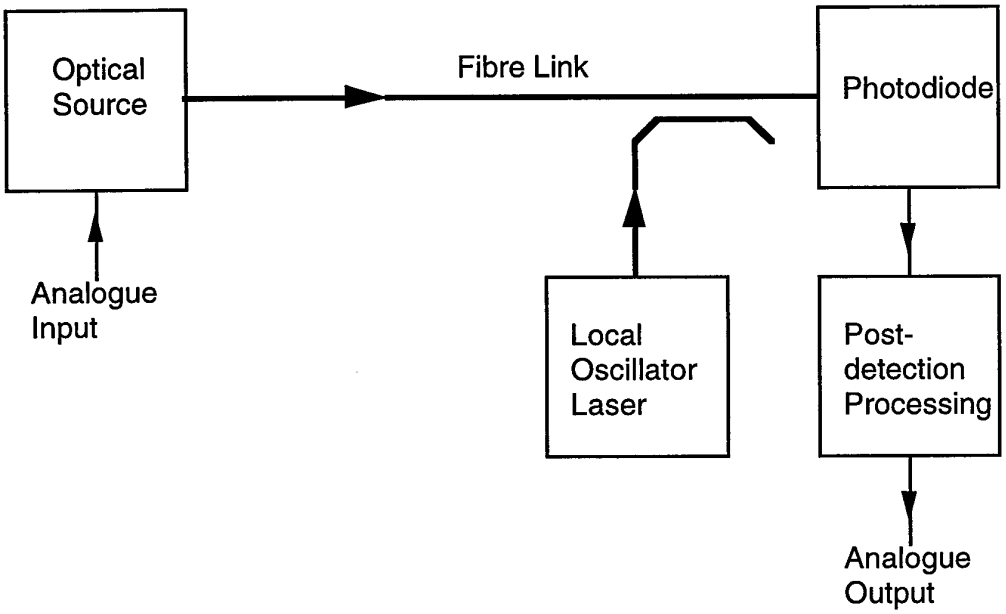

(b) Coherent transmission system

Figure 2.1 *IMDD and coherent analogue transmission systems*

2.2.1 Transmission system model- direct detection

Consider first the IMDD system, Figure 2.1(a). Let the analogue signal to be transmitted be represented by m{t}. The optical power at the output of the intensity modulator is

$$P_o = P_u (1 + k\, m\{t\}) \qquad (2.1)$$

where P_u is the mean optical power and k is the modulation sensitivity (k m{t} > -1). The mean squared signal current at the detector output is

$$I_s^2 = (R G_l P_u k)^2 \overline{m^2\{t\}} \qquad (2.2)$$

where R is the photodiode responsivity and G_l the fibre path gain ($G_l < 1$ unless optical amplifiers are used). Noise at the detector output arises from several sources. These include

(i) Thermal noise current generated in the photodiode load, with mean square value

$$I_{nt}^2 = \frac{4kTB}{R_L} \qquad (2.3)$$

where k is Boltzmann's constant, T the absolute temperature, B the bandwidth and R_L the load resistance value.

(ii) Shot noise generated in the photodiode

$$I_{ns}^2 = 2e(\overline{i_d} + i_{dk})B \qquad (2.4)$$

where e is the electronic charge, $\overline{i_d}$ is the mean optically generated current in the photodiode and i_{dk} is the photodiode dark current.

(iii) Optical source relative intensity noise

$$I_{nRIN}^2 = \overline{i_d}^2 RIN B \qquad (2.5)$$

where RIN is the source relative intensity noise value.

(iv) Noise generated by any optical amplifiers used, I_{na}^2.

Assuming these noise sources to be uncorrelated the signal to noise ratio at the detector output can be written

$$SNR=\frac{(RG_1P_u k)^2\overline{m^2\{t\}}}{\left(\frac{4kT}{R_L}+2e\left(RG_1P_u+i_{dk}\right)+\left(RG_1P_u\right)^2 RIN\right)B+I_{na}^2}. \qquad (2.6)$$

It can be seen that the thermal noise contribution is independent of unmodulated optical power, P_u, as is the optical amplifier noise contribution if non-linear effects can be neglected. Thus the signal to noise ratio can be improved by increasing the unmodulated optical power until the source relative intensity noise limit is reached, giving

$$SNR=\frac{k^2\overline{m^2\{t\}}}{RINB} \qquad (2.7a)$$

For optical powers below the RIN limit shot noise limited reception can be achieved if the thermal and optical amplifier contributions are sufficiently small, giving

$$SNR=\frac{RG_1P_u k^2\overline{m^2\{t\}}}{2eB} \qquad (2.7b)$$

where the photodiode dark current has been assumed negligible relative to the photocurrent. For low received optical powers thermal and optical amplifier contributions are dominant, with signal-spontaneous beat noise being dominant in optically filtered and pre-amplified systems, giving

$$SNR=\frac{P_u k^2\overline{m^2\{t\}}}{2P_nB} \qquad (2.8)$$

where P_n is the optical amplifier amplified spontaneous emission (ASE) power spectral density.

The strategy of increasing the source power, P_u, in order to reach the shot moise limit is limited by the onset of stimulated Brillouin scattering (SBS) and other non-linear effects in optical fibre [2.1]. The SBS threshold for 1 dB forward transmission loss is given by

$$P_c=\frac{42A_e}{g_BL_e}, \qquad L_e=\frac{1-e^{-\alpha L}}{\alpha} \qquad (2.9)$$

where A_e is the core area of the fibre, g_B is the Brillouin gain coefficient, L_e is the effective interaction length, L is the fibre length and α the fibre loss. For a 30 km long 1,550 nm wavelength system using silica fibre of 9 μm core diameter and 0.2 dB/km loss, with $g_B = 4 \times 10^{-9}$ cm/W and continuous wave (CW) excitation, $P_c = 4.1$ mW. Thus, from equation (2.8), the shot noise limited SNR, for a narrow bandwidth link with photodiode responsivity 0.9 A/W and $k^2\overline{m^2\{t\}} = 1$, would be limited by SBS to 155 dB.Hz. Longer links would be limited by the increased importance of receiver noise or by optical amplifier noise, leading to SNR values worse than the shot noise limit. Strategies to reduce the effect of SBS by deliberately broadening the optical spectrum, such as are used in cable television links, have the disadvantage of incurring dispersion penalties. Thus coherent transmission remains of interest, for other than short distance systems, when high SNR is required.

2.2.2 Transmission system model- coherent detection

Consider now the coherent system, Figure 2.1(b), and assume that polarisation control techniques are used so that the signal and local oscillator electric fields incident on the photodiode have the same polarisation. The signal electric field is defined by

$$E_S = \hat{E}_S \cos(\omega_S t + \phi_S), \tag{2.10}$$

where ω_S is the signal frequency and ϕ_S the signal phase, and the local oscillator field by

$$E_{LO} = \hat{E}_{LO} \cos(\omega_{LO} t + \phi_{LO}) \tag{2.11}$$

with ω_{LO} the local oscillator frequency and ϕ_{LO} the local oscillator phase. Defining the intermediate frequency (IF), ω_I, by $\omega_I = \omega_{LO} - \omega_S$ the analytic signal incident on the photodiode is

$$V_{in} = \left(\hat{E}_S \exp j\phi_S + \hat{E}_{LO} \exp j(\omega_I + \phi_{LO})\right) \exp j\omega_S t \tag{2.12}$$

For $\omega_I << \omega_S$ the output current from the photodiode is proportional to $V_{in}V_{in}^*$ so that

$$i \propto \hat{E}_S^2 + \hat{E}_{LO}^2 + 2\hat{E}_S \hat{E}_{LO} \cos(\omega_I t + \phi_{LO} - \phi_S) \tag{2.13}$$

It is convenient to re-write equation 2.12 in terms of optical power since that is a directly measurable quantity. Using

$$\hat{E}_s^2 = \frac{2 Z_o P_o G_l}{A} \tag{2.14a}$$

and

$$\hat{E}_{LO}^2 = \frac{2 Z_o P_{LO}}{A} \tag{2.14b}$$

where Z_o is the impedance of the medium where the power is measured, P_o is the source output power and A is the photodiode area,

$$i = R\left(P_o G_l + P_{LO} + 2\sqrt{P_o G_l P_{LO}} \cos\left(\omega_I t + \phi_{LO} - \phi_s\right)\right) \tag{2.15}$$

The first two terms represent direct detection of the signal and local oscillator respectively. The third term is of more interest. First, its magnitude is proportional to the square root of the local oscillator power. Thus the detected signal can be made larger simply by increasing the local oscillator power. Second, the detected signal is proportional to the square root of the source output power. Thus linear modulation of the source electric field will yield linear modulation of the detected photo-current at the intermediate frequency. Alternatively linear modulation of the source intensity will yield linear modulation of the output of a square law detector fed with the photo-detected IF signal. Third, the term is at the IF, ω_I, so that modulation of the source frequency, ω_s, leads directly to modulation of the IF, which can be recovered using a suitable discriminator. Fourth, the term contains the signal phase, ϕ_s, and the local oscillator phase, ϕ_{LO}, so that phase modulation of the source leads directly to phase modulation of the IF output. Thus coherent systems can use amplitude, intensity, frequency or phase modulation while direct detection systems are limited to either amplitude or intensity modulation. When $\omega_I = 0$ the coherent system is said to be homodyne but when $\omega_I \neq 0$ the coherent system is said to be heterodyne.

The sources of noise in a coherent system are similar to those in a direct detection system, Section 2.2.1, giving an IF carrier to noise ratio after photo-detection of

$$CNR = \frac{2 P_o G_1 P_{LO} R^2}{\left(\frac{4kT}{R_L} + 2e(R P_{LO} + i_{dk}) + (R P_{LO})^2 RIN \right) B + I_{na}^2} \qquad (2.16)$$

where it is assumed that $P_{LO} >> P_o G_1$ and RIN is the relative intensity noise of the local oscillator laser. It is normal practice in coherent receivers to use a balanced detection scheme to cancel local oscillator laser RIN [2.2] so that by increasing the local oscillator power shot noise limited reception is obtained, giving

$$CNR = \frac{P_o G_1 R}{e B} \qquad (2.17)$$

if the contribution from optical amplifier noise is small or

$$CNR = \frac{P_o G_1}{P_n B} \qquad (2.17a)$$

if the local oscillator-ASE beat noise term predominates.

2.2.3 Comparison between coherent and direct detection systems

Coherent transmission systems offer three main advantages over systems using direct detection:

(i) Shot noise limited reception can be achieved even at low received signal powers, simply by increasing the local oscillator power.

(ii) Intensity, frequency or phase modulation modes can be used whereas direct detection systems are limited to intensity modulation.

(iii) The excellent frequency selectivity that can be achieved using electrical post-photo-detector filters is translated into the optical domain by the coherent detection technique enabling the realisation of dense wavelength division multiplex schemes for multi-channel transmission or channel selection schemes.

Reviewing these advantages in turn, the first is of reduced importance for systems operating at a wavelength of 1550 nm now that effective optical amplifiers are available. However, there is interest in systems operating at 1300 nm wavelength in order to take advantage of the silica fibre dispersion minimum and the low noise and high output power of semiconductor laser pumped Nd-YAG lasers. There is also interest in systems operating at 850 nm wavelength for compatibility with GaAs microwave monolithic integrated circuit (MMIC) technology. Effective optical fibre amplifiers are not available for either of these wavelengths. The alternative strategy for shot noise limited IMDD systems of increasing the source power P_u is limited by the onset of stimulated Brillouin scattering (SBS) as discussed in Section 2.2.1, so that the high source power strategy is limited to system lengths of a few km or less. Thus coherent transmission remains of interest for other than short distance systems operating at wavelengths other than 1550 nm.

The second advantage enables SBS to be reduced by broadening the optical signal bandwidth beyond the SBS linewidth (~28 MHz at 1300 nm wavelength) using frequency or phase modulation. Use of frequency or phase modulation also enables a trade-off to be made between optical signal bandwidth and received signal to noise ratio.

The importance of the third advantage depends upon whether the ability to switch between many sources carried on the same fibre is required. An example of such a requirement would be a distributed receive antenna remoting application.

There are three main disadvantages of coherent transmission systems relative to those using direct detection:

(i) The frequencies of the local oscillator laser and signal must be controlled to differ by the required IF, whereas in the direct detection system it is only necessary that the source laser frequency be suitable for the photodiode used.

(ii) The linewidths of source and local oscillator lasers must be suitable for the modulation mode used, whereas in direct detection systems the required source linewidth is mainly determined by the optical fibre dispersion penalty.

(iii) The polarisation state of the local oscillator and signal must be matched at the photodiode.

The requirement for source frequency control is an exacting one. An operating wavelength of 1550 nm corresponds to a frequency of 194 THz, so that to maintain an heterodyne signal within 10% of band centre in an IF bandwidth of 2 GHz, control to within 1 part in 10^6 is required. For semiconductor lasers with typical temperature tuning sensitivities of 30 GHz K^{-1} and current tuning sensitivities of 3 GHz mA^{-1} this requires temperature control to within 7 mK and current control to within 7 μA.

The source linewidth requirement will be considered in more detail in Section 2.4. Advanced semiconductor lasers can offer linewidths in the kHz region coupled with wavelength tuning ranges in excess of 10 nm [2.3] although the commercial availability of such lasers is currently limited. Homodyne systems require the local oscillator frequency to be phase-locked to that of the received signal in an optical phase-lock loop (OPLL). Realising such loops with other than narrow linewidth lasers presents formidable challenges [2.4].

Polarisation matching can be achieved by active polarisation control of the local oscillator signal for maximum detected signal output [2.5] or using polarisation diversity reception [2.6].

Whilst the disadvantages of coherent transmission systems can all be overcome, the penalty is a significant increase in system complexity relative to direct detection systems. Whether the coherent system approach is used in a particular application therefore depends upon whether the performance advantages are sufficient to justify the increase in complexity.

2.3 Optical sources for coherent analogue transmission

The key performance parameters for sources used in coherent analogue transmission systems are

(i) Output wavelength
(ii) Output power
(iii) Linewidth and intensity noise
(iv) Tunability
(v) Frequency modulation response

The main optical sources are fibre lasers, crystal and waveguide lasers and semiconductor lasers. Only semiconductor lasers offer direct modulation capability.

The capabilities and limitations of the various source technologies are discussed below.

2.3.1 Fibre lasers

The use of optically pumped fibre doped with an appropriate lasing ion has made a key contribution to optical communication through the optical fibre amplifier. With appropriate feedback fibre optical sources can also be realised.

The required doped fibre length depends on cavity losses, pump power and lasing ion doping concentration. The latter is limited by clustering, so that practical erbium doped fibre lasers for operation at 1,530 nm wavelength typically require doped fibre lengths of 1 to 5 m, giving laser mode separations of 100 MHz to 20 MHz. Obtaining stable single mode operation is therefore difficult. Unidirectional ring configurations, which eliminate spatial hole burning, can offer narrow (kHz) linewidths [2.7] but active stabilisation of the fibre length and polarisation state is required to eliminate mode hopping.

2.3.2 Crystal and waveguide lasers

Diode-pumped crystal lasers are attractive sources of high power (> 100 mW), narrow linewidth (< 1 kHz), low RIN (< - 170 dBc Hz-1) optical signals [2.8]. They are finding application as sources in wide dynamic range direct detection analogue optical transmission systems for cable TV and related applications. For general application, they suffer from limited tunability (< 60 GHz) and high optical complexity. However, the relatively narrow linewidth and good frequency stability have made them the main vehicle for early work on optical phase lock loops [2.9].

Improved optical confinement and potential for integration with other optical and electro-optic components make rare earth doped waveguide lasers of interest. The two main fabrication technologies are silica on silicon and titanium in-diffused lithium niobate. To realise lasers with reasonably small chip area it is necessary to achieve doping densities much higher than for fibre lasers. This is especially challenging for erbium doped guides. Kitagawa et al have achieved an output power of 1-2 mW from a 45 mm long erbium doped silica on silicon laser pumped at 980 nm wavelength [2.10]. In-diffusion has been used to realise an erbium doped laser in lithium niobate.

A waveguide of length 10.5 mm gave a threshold of 8 mW for pumping at 1477 nm wavelength [2.11]. Non-semiconductor waveguide lasers require an optical pump source, which is generally desired to be a diode laser. Thus a fully integrated source technology is not possible.

2.3.3 Semiconductor lasers

Semiconductor lasers are used as sources in most current optical communication systems. They offer the advantages of electrical pumping and direct modulation capability. Key performance aspects requiring improvement for coherent analogue optical transmission systems are:

(i) Narrow linewidth operation

(ii) Tunability for wavelength matching

(iii) Uniform FM frequency response for OFM and phase-locked applications.

Careful design of the laser structure to minimise spatial hole burning effects has led to the realisation of multiple quantum well (MQW) distributed feedback (DFB) lasers having linewidths below 100 kHz [2.3].

Renewed interest in wavelength division multiplexed (WDM) systems, both for increased channel capacity and for their use in all-optical routeing, has placed emphasis on the need for widely tuneable laser sources. A number of approaches are possible. Multi-section DFB lasers have been realised with tuning ranges of 10 nm, while maintaining linewidths less than 20 MHz [2.12]. Wider tuning ranges have been achieved in vertically coupled structures [2.13], culminating in the 55 nm tuning range reported by Kim et al [2.14], although the linewidth obtained was not reported.

A novel approach, yielding discontinuous tuning over a wide range with simple control, is the Y junction laser [2.15] where vernier effects have been used to increase the tuning range to 38 nm.

For use as an OFM source and current controlled oscillator (CCO) operation in phase-locked applications a major difficulty has been the interaction between thermal and

carrier density effects, leading to an highly non-uniform FM response. The most common approach to achieving uniform FM response has been to use a multi-section DFB laser with the section currents adjusted for best uniformity of response. Using this approach Ogita et al [2.16] have achieved a -3 dB bandwidth of 15 GHz, although neither the peak frequency deviation nor the residual intensity modulation is stated. An alternative approach, capable of an intrinsically flat FM response, is to use the refractive index change resulting from the quantum confined Stark effect (QCSE) in a reverse biased multiple quantum well (MQW) section. This was first demonstrated in external cavity laser systems [2.17] and has been the approach investigated in the current programme.

Reviewing the state of semiconductor laser research it is clear that widely tunable sources with linewidths small enough for use in coherent analogue systems are realisable although not widely commercially available.

2.4 Coherent analogue transmission systems

As discussed in Section 2.2 coherent analogue transmission systems offer the choice of intensity, amplitude, frequency or phase modulation. To date demonstrator systems have been reported for intensity, frequency and phase modulation. In this section the relative merits of the various modulation formats are discussed.

2.4.1. Intensity modulation

Reference to equation (2.15) shows that if the source is intensity modulated and heterodyne detection followed by envelope detection is used the output is proportional to $\sqrt{P_0}$ so that a square law detector must be used to provide overall system linearity. Fong et al have demonstrated this approach using semiconductor laser sources [2.18]. The system has the attraction that the main linewidth penalty arises from heterodyned source power falling outside the IF bandwidth. Thus by using a wide IF filter bandwidth and a post-detection filter the system can be made relatively insensitive to source linewidth and drift in source and local oscillator laser frequencies allowing commercially available semiconductor lasers with linewidths of > 10 MHz to be used.

The system offers the advantage of improved receiver sensitivity through coherent detection and thus is useful at wavelengths where good optical pre-amplifiers are not available. System linearity is limited by the linearity of the source intensity modulation characteristic and by the accuracy of the square law detector characteristic. It therefore can be no better than for an IMDD system. Processing gain from the

modulation system is also not available. Thus the overall dynamic range is comparable with an optically pre-amplified IMDD system.

2.4.2. Amplitude modulation

In an amplitude modulation system the peak electric field produced by the source is linearly proportional to the modulating signal. Thus the source power is proportional to the square of the modulating signal. From equation (2.15) it can be seen that heterodyne detection followed by envelope detection would give an output linearly proportional to the modulating signal. Thus a square law detector is not required. Unfortunately, directly modulated semiconductor lasers have a near linear intensity modulation characteristic, whilst interferometric external modulators have a raised sine intensity modulation characteristic. A convenient linear amplitude modulator is therefore not available.

An amplitude modulated heterodyne coherent detection transmission system would be expected to have similar advantages of linewidth insensitivity and improved receiver sensitivity to an intensity modulated coherent detection system, with the linearity advantage of not requiring a square law post detection element in the receiver. Performance would again be expected to be comparable with an optically pre-amplified IMDD system.

2.4.3. Frequency modulation

Frequency modulation is extensively used in radio communication systems because it enables modulated signal bandwidth to be traded for improved receive signal to noise ratio. Similar advantages are available in the optical domain and are attractive since the available transmission bandwidth is large. The main practical difficulty has been to obtain an optical source capable of uniform FM response up to microwave frequencies, as discussed in Section 2.3. However, this problem has now largely been overcome by the development of the reverse bias quantum well laser tuning technique [2.17] which is the subject of the present programme.

The fundamental limitation to signal to noise ratio in an optical FM (OFM) system arises from the finite laser linewidth

$$SNR = \frac{\pi \Delta f^2}{2 f_m \delta f_l} \qquad (2.18)$$

where Δf is the peak frequency deviation, f_m is the modulating frequency and δf_l is the source laser FWHM linewidth. For the reverse biased quantum well tuned laser of [2.17] Δf was 2 GHz and δf_l 50 kHz, giving a signal to noise ratio of 61 dB (141 dB Hz) for a modulating frequency of 100 MHz. Commercially available semiconductor lasers would give considerably inferior performance.

Recovery of the modulating signal requires heterodyne detection followed by a suitable FM discriminator. An elegant approach to this problem is to use an heterodyne OPLL with output taken from the voltage controlled oscillator (VCO) laser control terminal. Figure 2.2 shows the arrangement.

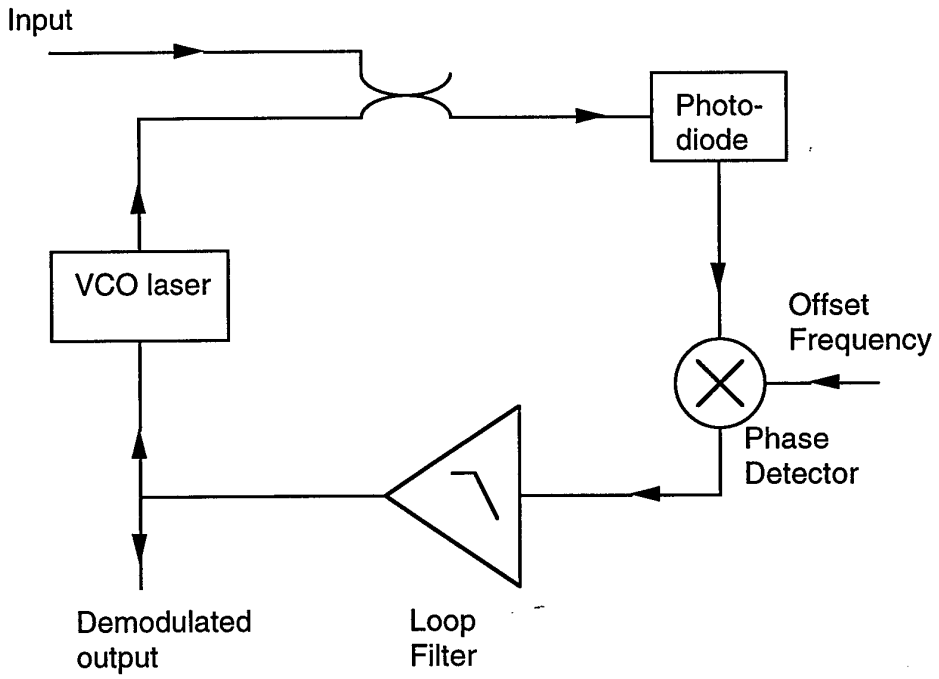

Figure 2.2 *OFM demodulator using optical phase lock loop.*

Whilst the OPLL is conceptually straight-forward, realisation presents formidable technical challenges. First, the difference frequency between master and slave lasers must be set to obtain a difference frequency within the bandwidth of the photodetector. This is not difficult with diode pumped crystal lasers, however the temperature and current dependence of frequency for semiconductor lasers requires active temperature

and current control techniques to obtain a medium term (hour) stability of the difference frequency of about 250 MHz [2.20].

The second challenge arises from the linewidth of the laser sources used. The OPLL must correlate the phase noise components contributing to the linewidths of the two sources in order to generate a high spectral purity difference signal, matching the supplied offset frequency. Large laser linewidths require wide loop bandwidths to achieve this. The loop bandwidth is limited by three main factors

(i) Signal propagation delay around the loop.

(ii) The FM frequency response of the slave laser.

(iii) The bandwidth of the loop filter and transformed bandwidth of other loop components.

For the OFM demodulation application the loop bandwidth must be greater than the base bandwidth of the signal to be demodulated. Design rules for OPLLs have been formulated [2.4] and in practice signal propagation delay limits base bandwidth to a few hundred mega-Hertz for loops constructed with discrete components [2.20, 2.21].

An alternative approach, capable of wide base bandwidth operation, is to use an heterodyne receiver followed by a limiting amplifier and microwave delay line frequency discriminator.

For the OFM receiver the carrier to noise ratio is given by equation (2.16) reducing to equation (2.17) for shot noise limited reception. The improvement in signal to noise ratio above threshold resulting from the use of FM is

$$SNR = 3\left(\frac{\Delta f}{f_m}\right)^3 CNR \qquad (2.19)$$

where $\Delta f >> f_m$. For $\Delta f = 2$ GHz and $f_m = 100$ MHz the improvement would be about 44 dB. This is a powerful argument for the use of OFM in long distance, wide dynamic range systems, since a trade off becomes possible between peak deviation and received optical power for a given signal to noise ratio.

Cai and Seeds [2.22 and Appendix 2.1] have carried out a detailed study of the relative

advantages of IMDD and OFM systems, treating both systems without optical amplifiers and transparent systems where low gain optical amplifiers are distributed within the system to compensate the transmission loss exactly. The recent development of high performance Fibre Grating Lasers (FGL) [2.23], which could use the QCSE tuning technique developed in this programme to produce a robust source laser for OFM systems having a linewidth of order 1 kHz, with peak frequency deviation 10 GHz and uniform FM response (+ 3 dB) to 9 GHz, has potential to permit the realisation of practical, long distance wide dynamic range analogue optical transmission systems. As an example of the performance that might be possible consider short haul, 1,000 km and 5,000 km transparent systems with base-bandwidth 1 GHz based on either IMDD or OFM using FGLs of the parameters above as both source and local oscillator lasers. Unlimited source laser power and RIN of - 170 dBc/Hz is assumed in each case, with full modulation, $k^2\overline{m^2\{t\}} = 1$. For transparent systems with fully inverted amplifiers the ASE power spectral density at the receiver is $P_n = 2hc\alpha L/\lambda$, with h Planck's constant, c the velocity of light in vacuo and λ the operating wavelength. The SNR is calculated from equations 2. 8, 2.9, 2.17a, 2.18 and 2.19 and is shown in Table 2.1.

Link Length (km)	IMDD SNR (dB.Hz)	OFM SNR (dB.Hz)
0	170	169
1,000	125	156
5,000	111	142

Table 2.1 *Signal to noise ratios for transparent IMDD and OFM links.*

The SNR for the short IMDD link is limited by RIN, whilst that for the short OFM link is limited by laser linewidth. The SNR for the longer IMDD links is limited by SBS and signal-spontaneous beat noise. For the longer OFM links the post-detection carrier to noise ratio is limited by SBS and local oscillator-spontaneous beat noise, but the SNR is enhanced by FM processing gain. Higher SNR than in this example would be possible by increasing the modulation index.

2.4.4. Phase modulation

Phase modulation places stringent requirements on optical source linewidth. The signal to noise ratio limit due to source linewidth, assuming white Gaussian frequency noise broadening, is given by

$$SNR = \frac{\pi \Delta\phi_m^2}{\delta f_l \int_{B_{min}}^{B_{max}} f^{-2}\, df} \qquad (2.20)$$

where $\Delta\phi_m$ is the RMS phase deviation and the signal bandwidth limits are given by B_{max} and B_{min}. For an RMS phase deviation of 45 degrees and bandwidth from 100 kHz to 100 MHz a laser of 50 kHz linewidth would give a signal to noise ratio of only 12 dB. For this reason phase modulation analogue transmision systems have received relatively little attention. A method of overcoming the phase noise sensitivity by using a common laser in an heterodyne arrangement has been studied by Kalman and Kazovsky [2.24]. However, since this requires the local oscillator signal to be transmitted with the signal it would be difficult to apply to long links.

2.5 Experimental optical frequency modulation system

As an example of a coherent analogue transmission system a brief description of an OFM link with base bandwidth 1 GHz will be given [2.22, 2.25]. The source laser was a reverse biased quantum well tuned GaAs/AlGaAs laser, having an external cavity length of 15 mm [2.17]. The local oscillator laser was a grating tuned external cavity laser of similar cavity length, which could be tuned over a wavelength range of 5nm for channel selection in a multi-channel system. Linewidths of less than 100 kHz were achieved for both lasers.

A peak deviation of 2 GHz was chosen to give good signal to noise ratio, while avoiding the danger of mode hopping in the source laser. An IF of 10 GHz was used to allow adequate demodulation linearity. The receiver used a 20 GHz bandwidth Schottky barrier photodiode, followed by a delay line discriminator for baseband signal recovery.

The link transmission response which was uniform, with a -3 dB cut-off frequency of 1.3 GHz due to the source laser tuning element capacitance. A mid-band signal to noise ratio of 120 dB.Hz was achieved for a received optical power of -27 dBm, limited by low local oscillator laser launch power (-18 dBm). Calculations indicate that increasing the local oscillator laser launch power to -3 dBm would improve the signal to noise ratio to 140 dB.Hz. Nevertheless, the result achieved was some 20 dB better than an IMDD link operating at the same received power [2.26].

2.6 Conclusion

In this chapter coherent analogue transmission systems have been analysed and their performance compared with direct detection systems. The availability of high quality optical amplifiers for the 1,550nm optical fibre transmission window makes it possible to realise high quality IMDD transmission systems at that wavelength. However, the capability of the coherent systems to select between many channels present on the same optical fibre makes them attractive in applications such as multiple antenna remoting. They also enable wide dynamic range transmission systems to be realised at wavelengths where high quality optical amplifiers are not available.

Of the modulation techniques available for coherent systems, intensity modulation enables simple, linewidth insensitive links to be constructed. Frequency modulation offers the potential for modulated bandwidth signal to noise ratio trade-off at the expense of somewhat more exacting linewidth requirements and makes possible long distance wide dynamic range links. A key requirement in such systems is a source laser having narrow linewidth and uniform FM frequency response. This requirement can be met using the reverse biased quantum well laser tuning technique which has been studied in this programme, particularly if coupled with recently developed high performance fibre grating laser techniques.

For the future there is considerable scope for component development, leading to improved transmission system performance. Particular priorities for research include source modulator linearisation, narrow linewidth monolithic and fibre grating tunable laser development, the monolithic integration of OPLLs in opto-electronic integrated circuit (OEIC) format to achieve wide demodulation bandwidth and improvements to receiver electronics to give enhanced demodulator linearity.

It is anticipated that whilst many single channel point to point transmission system requirements will be met by pre-amplified receiver IMDD systems, multi-channel networks will increasingly apply the coherent techniques discussed here.

2.7 References

2.1 CHRAPLAVY, A. R.:'Nonlinear effects in optical fibers', in *Topics in Lightwave Transmission Systems*, ed. Li, T., (Academic Press, San Diego, 1991), pp. 267-295.

2.2 ABBAS, G. L., CHAN, V. W. S., and LEE, T. K.:'Local-oscillator excess noise suppression for heterodyne and homodyne detection', *Opt. Lett.*, 1983, 8, pp. 419-421.

2.3. OKAI, M. and TSUCHIYA, T.:'Tunable DFB lasers with ultra-narrow spectral linewidth', *Electron Lett.*, 1993, 29, pp. 349-351.

2.4. RAMOS, R. T. and SEEDS, A. J.:'Delay, linewidth and bandwidth limitations in optical phase-locked loop design', *Electron. Lett.*, 1990, 26, pp. 389- 391.

2.5 WALKER, N. G. and WALKER, G. R.:'Polarisation control for coherent communications', *J. Lightwave Tech.*, 1990, LT-8, pp. 438-458.

2.6. GLANCE, B.:'Polarisation independent optical receiver', *J. Lightwave Tech.*, 1987, LT-5, pp. 274-276.

2.7. MORKEL, P. R., COWLE, G. J., and PAYNE, D. N.:'Travelling-wave erbium fibre ring laser with 60 kHz linewidth', *Electron.Lett.*, 1990, 26, pp. 632-634.

2.8. WILLIAMS, K. J., DANDRIDGE, A., KERSEY, A. D., WELLER, J. F., YUREK, A. M., and TVETEN, A. B.:'Interferometric measurement of low-frequency phase noise characteristics of diode laser-pumped Nd:YAG ring laser', *Electron. Lett.*, 1989, 25, pp. 774-776.

2.9. WILLIAMS, K. J., GOLDBERG, L., ESMAN, R. D., DAGENAIS, M. and WELLER, J. F.:'6-34 GHz offset locking of Nd:YAG 1319nm nonplanar ring laser', *Electron. Lett.*, 1989, 25, pp. 1242-1243.

2.10. KITAGAWA, T., HATTORI, K., SHIMIZU, M., OHMORI, Y. and KOBAYASHI, M.:'Guided-wave laser based on erbium-doped silica planar lightwave circuit', *Electron. Lett.*, 1991, 27, pp. 334-335.

2.11. BRINKMANN, R., SOHLER, W. and SUCHE, M:'Continuous-wave erbium-diffused $LiNb0_3$ waveguide laser', *Electron. Lett.*, 1991, 27, pp. 415-416.

2.12. KOCH, T. L. and KOREN, U.:'Semiconductor lasers for coherent optical fibre communications', *J. Lightwave Tech.*, 1990, LT-8, pp. 274-293.

2.13. ILLEK, S., THULKE, W. and AMANN, M.-C.: 'Codirectionally coupled twin-guided laser diode for broadband electronic wavelength tuning', *Electron. Lett.*, 1991, 27, pp. 2207-2209.

2.14. KIM, I., ALFERNESS, R. C., BUHL, L. L., KOREN, U., MILLER, B. I., NEWKIRK, M. A., YOUNG, M. G. and KOCH, T. L:'Broadly tunable InGaAsP/InP vertical coupler filtered laser with low tuning current', *Electron. Lett.*, 1993, 29, pp. 664-666.

2.15. IDLER, W., SCHILLING, M., BAUMS, D., LAUBE, G., WUNSTEL, K. and HILDEBRAND, O.:'Y Laser with 38 nm tuning range', *Electron. Lett.*, 1991, 27, pp. 2268-2270.

2.16. OGITA, S., KOTAKI, Y., MATSUDA, M., KUWAHARA, Y., ONAKA, H., MIYATA, H. and OSHIKAWA, H.:'FM response of narrow linewidth, multielectrode, λ/4 shift DFB laser", *IEEE Photonics Tech. Lett.*, 1990, 2, pp. 165-166.

2.17. CAI, B., SEEDS, A. J. and ROBERTS, J. S.:'MQW tuned semiconductor lasers with uniform frequency response', *IEEE Photonics Tech. Lett.*, 1994, 6, pp. 496-498.

2.18. FONG, T., SABIDO IX, D. J. M. and KAZOVSKY, L. G.:'Linewidth insensitive coherent AM analog optical links using semiconductor lasers', *IEEE Photonics Tech. Lett.*, 1993, 4, pp. 469-471.

2.19. SEEDS, A. J. and CAI, B.:'Optical FM for wide dynamic range links', *Workshop on Microwave Opto-electronics, European Microwave Conf.*, 1991, Stuttgart, pp. 64-70.

2.20. RAMOS, R. T. and SEEDS, A. J.:'Fast heterodyne optical phase-lock loop using double quantum well laser diodes', *Electron. Lett.*, 1992, 28, pp. 82-83.

2.21. GLIESE, U., NIELSEN, T. N., LINTZ CHRISTENSEN, E., STUBKJAER, K. E., LINDGREN, S. and BROBERG, B.:'A wideband heterodyne optical phase-locked loop for generation of 3-18 GHz microwave carriers', *IEEE Photonics. Tech. Lett.*, 1992, 4, pp. 936-938.

2.22. CAI, B. and SEEDS, A. J..:'Optical frequency modulation links: theory and experiments', *IEEE Trans.*, 1997, MTT 45, pp. 505-511.

2.23. TIMOFEEV, F. N., BENNETT, S., GRIFFIN, R., BAYVEL, P., SEEDS, A.J., WYATT, R., KASHYAP, R. and ROBERTSON, M.:'High spectral purity millimetre-wave modulated optical signal generation using fibre grating lasers', submitted to *Electron. Lett.*, 1997.

2.24. KALMAN, R. F. and KAZOVSKY, L. G.:'Demonstration of an analog heterodyne interferometric phase-modulated link', *IEEE Photonics. Tech. Lett.*, 1994, 6, pp. 1271-1273.

2.25. CAI, B. and SEEDS, A. J.:'Optical frequency modulation link for microwave signal transmission', *IEEE MTT-S Digest*,1994, San Diego, pp. 163-166.

2.26. SEEDS, A. J.:'Microwave opto-electronics', *Optical and Quantum Electronics*, 1993, 25, pp. 219-229.

Chapter 3 Tuning Performance Analyses

For the two section laser investigated in this programme, gain and tuning sections interact with each other to produce quite complicated performance for the complete device. This is because tuning is achieved by refractive index variation with bias, which is associated, through the Kramers-Kronig relations, with the variation of absorption coefficient. The absorption change in the cavity will require gain change to compensate for it. Two effects are associated with the gain change: gain peak shift which can affect the tuning behaviour, and output power variation. It is therefore desirable to have a detailed analysis of the device performance when tuning is applied.

3.1 Insertion Loss in the Tuning Section

For a Fabry-Perot two section tunable laser, normally the maximum continuous tuning range is a Fabry-Perot mode spacing. That is

$$\Delta\lambda_{max} = \frac{\lambda_0^2}{2nL} \tag{3.1}$$

where λ_0 is the oscillation wavelength, n the mode index and L the physical length of the whole cavity as shown in Figure 3.1.

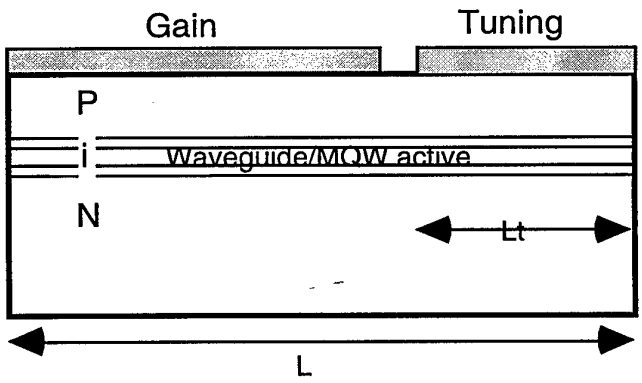

Figure 3.1 *Schematic diagram of two section Fabry-Perot tunable laser.*

For a typical GaAs/AlGaAs laser, if L=800 μm, n=4.5 and the lasing wavelength is 850nm, we have $\Delta\lambda_{max} = 0.1$nm, or 41.5 GHz.

If the refractive index change of Δn is produced in a tuning section of length L_t, within the same mode, the wavelength shift $\Delta\lambda$ will be

$$\frac{\Delta\lambda}{\lambda_0} = \Gamma \frac{\Delta n}{n} \bullet \frac{L_t}{L} \tag{3.2}$$

where Γ is the confinement factor. Let $\Delta\lambda = \Delta\lambda_{max}$ giving

$$\Gamma \Delta n L_t = \frac{nL}{\lambda_0} \frac{\lambda_0^2}{2nL} = \frac{\lambda_0}{2} \tag{3.3}$$

which means a half wavelength change of optical path, or a π phase shift in a single pass is needed for maximum continuous tuning. The tuning section length required for π shift is then

$$L_t = \frac{\lambda_0}{2\Gamma\Delta n} \tag{3.4}$$

For such a length, the insertion loss, for an absorption coefficient of α is

$$\text{Loss} = 10\Gamma\alpha L_t \log_{10} e \quad \text{(dB)} \tag{3.5}$$

Figures.3.2-3.4 show the absorption coefficient for sample QT703R which has an exciton peak at a wavelength of ~838nm at zero field. It is obvious, that in order to have low insertion loss and small absorption variation, the working wavelength in the tuning section should be de-tuned to beyond ~850nm.

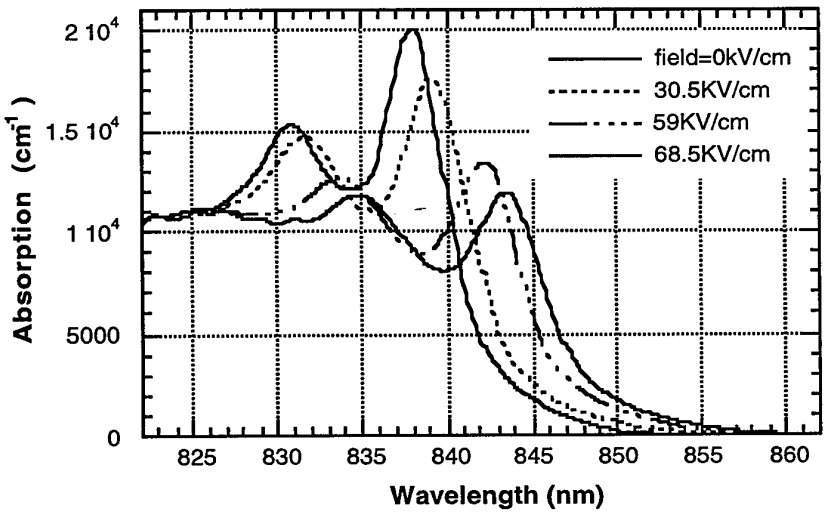

Figure 3.2. *Absorption spectra for sample QT703R. Different field strengths were applied to the sample. Zero field corresponds to 1.42 V forward bias. 30.5kV/cm is a 0.58V forward bias, 59kV/cm 0.22V reverse bias and 68.5kV/cm 0.49V reverse bias.*

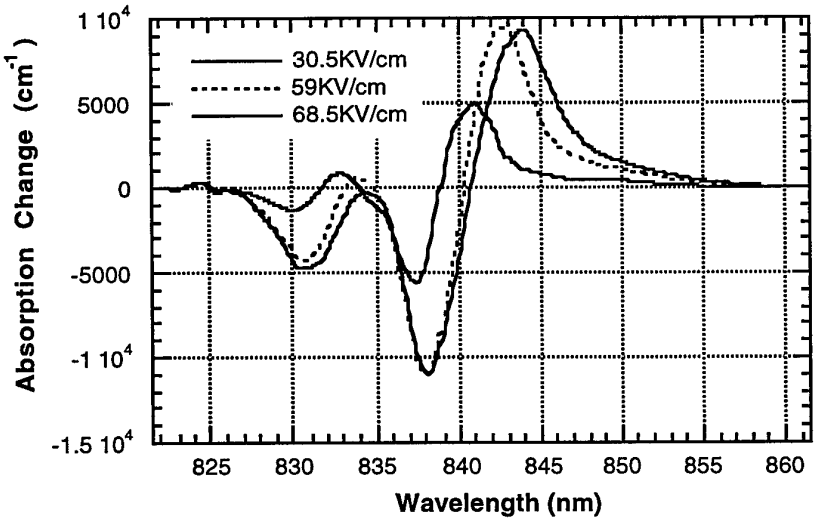

Figure 3.3. *Absorption change spectra for sample QT703R as a function of applied electric field.*

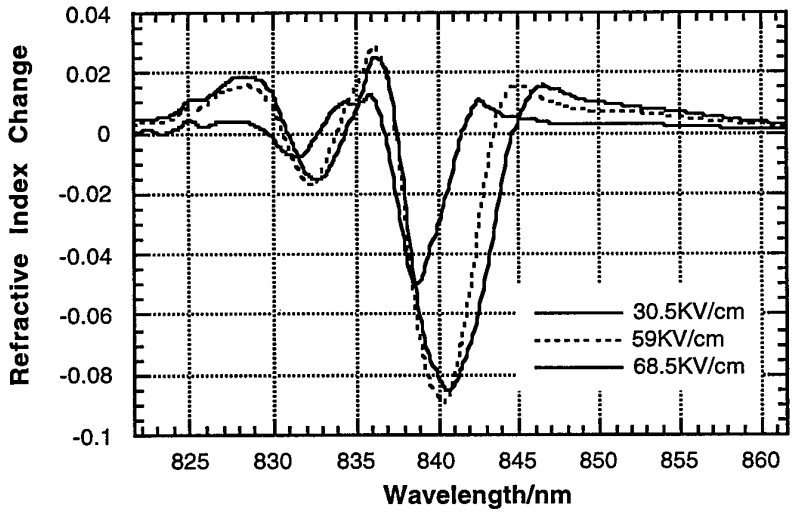

Figure 3.4. *Refractive index change spectra for sample QT703R as a function of applied electric field.*

From equations 3.4 and 3.5, π phase shift tuning section lengths and corresponding insertion losses for field strengths 30.5, 59 and 68.5kV/cm are plotted in Figure 3.5. It is clearly seen that in order to keep insertion loss lower than 3dB, low applied fields require long tuning sections (> 1mm). Considering other internal loss mechanisms within the cavity, such a long tuning section is not acceptable, therefore, medium fields (> 60kV/cm) with a tuning section length 300~400μm are a more suitable choice.

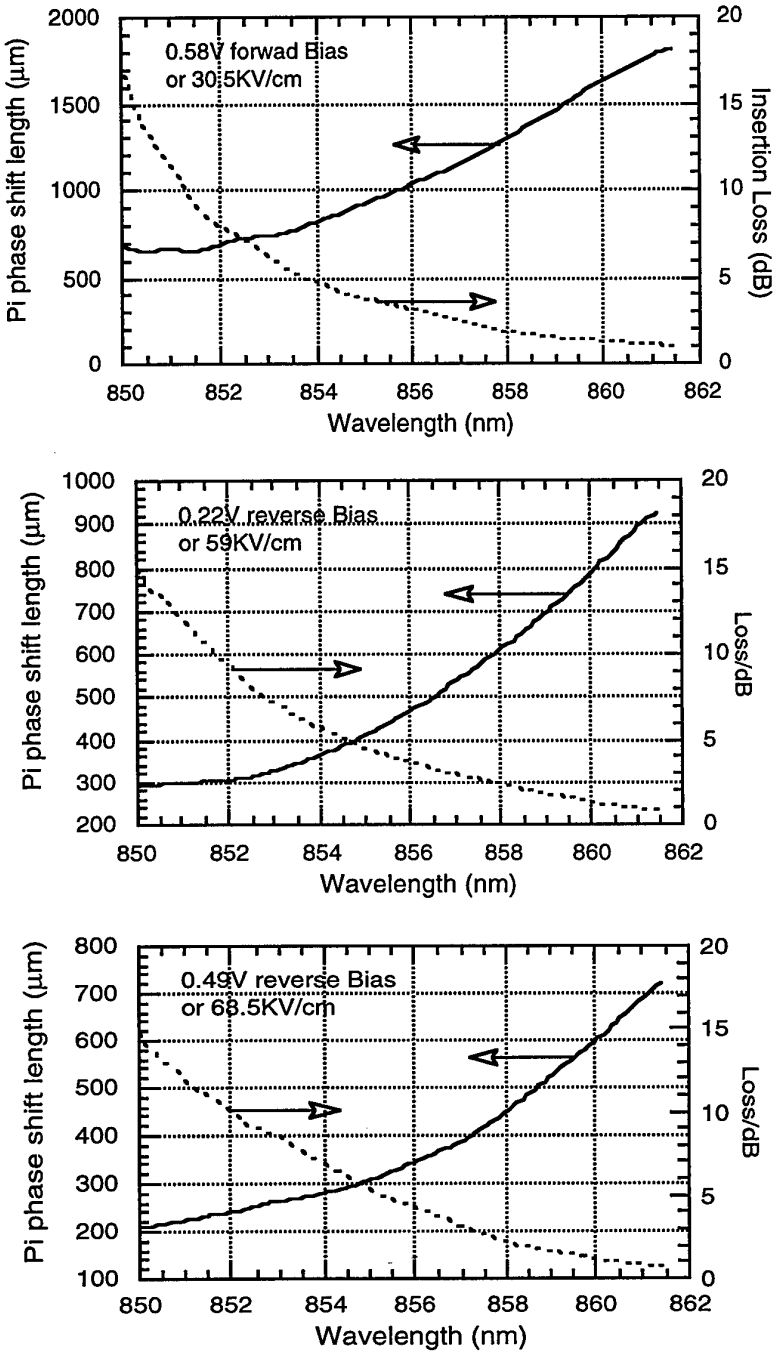

Figure 3.5. *Tuning section length required for π phase shift and corresponding insertion loss at different electric fields.*

3.2 Static tuning performance

For a certain tuning section length, from equation 3.2, it is easy to obtain the maximum frequency deviation

$$\Delta\nu = \frac{c}{\lambda_0^2}\Delta\lambda = \Gamma\frac{c}{\lambda_0}\frac{\Delta n}{n}\bullet\frac{L_t}{L} \qquad (3.6)$$

which is both wavelength and electric field dependent. We check first the wavelength dependence. If we choose L=800 μm and tuning section length of 300 and 400 μm respectively, the maximum frequency deviation calculated from equation 3.6 is plotted in Figure 3.6 for a fixed field variation of 68.5kV/cm, which corresponds to a bias variation of 1.9V (from 1.42 V forward bias to 0.49V reverse bias). The maximum frequency deviation decreases with wavelength almost linearly with a slope of 4.15GHz/nm for 300 μm tuning section length, or 5.53GHz/nm for 400 μm tuning section length. This is a small variation considering the mode space of ~0.1nm, which in the worst case gives a maximum frequency deviation non-uniformity <2% due to the wavelength shift.

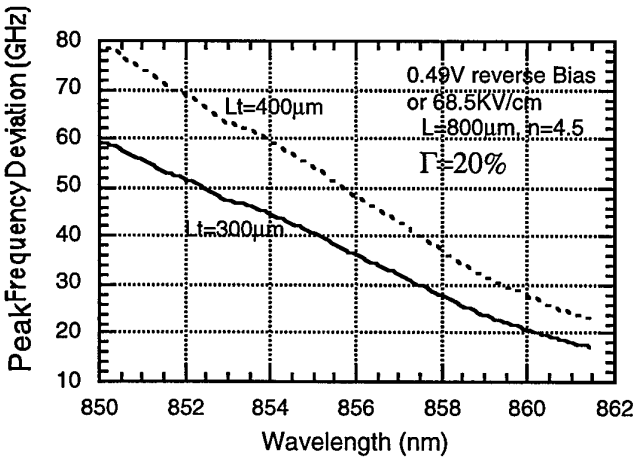

Figure 3.6. *Maximum frequency deviation variation with wavelength for a 800μm long two section laser, with tuning section lengths of 300 and 400 μm, respectively.*

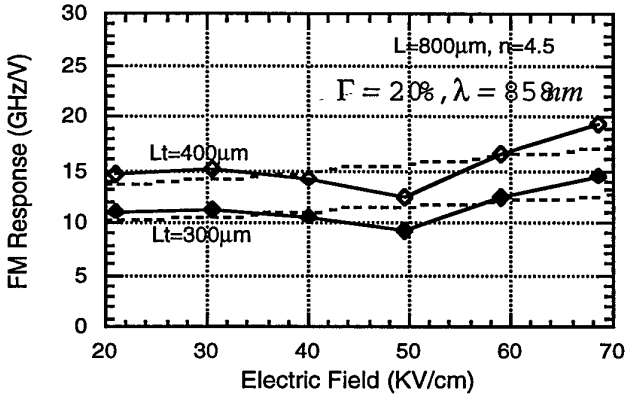

Figure 3.7. *Frequency modulation sensitivity variation with applied field for wavelength 858nm. Dashed lines are theoretical prediction.*

We now examine field strength effects on frequency modulation. As an example, we pick 858nm as the fixed wavelength. Given in Fig.1.7 is the calculated and measured FM sensitivity (the maximum frequency deviation divided by the total voltage applied to the structure) change with field strength. Curves show a linear function of field strength. This is well understood from the electro-optic response, the refractive index change, is best described by both linear and quadratic term of electric field [3.1],

$$\Delta n = -\frac{1}{2} n_o{}^3 \left[rE + sE^2 \right] \tag{3.7}$$

where n_o is zero-field index. The plot in Figure 3.8 shows how the refractive index change varies with field for 858nm (20 nm de-tuning from exciton peak) and its fitting results. The fitting gives a linear coefficient of r= 2.37×10^{-9} cm/V and a quadratic one s= -6×10^{-14} cm^2/V^2. Compared to Zucker's results for a de-tuning of 40nm from the exciton peak [3.1], our results, both 3.2 times hers, is highly credible.

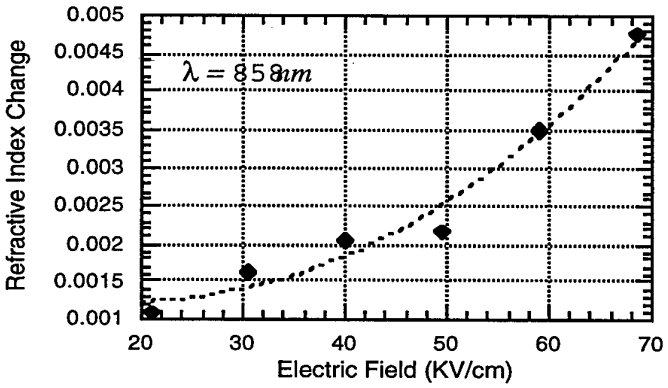

Figure 3.8 *Refractive index change as a function of applied field at wavelength 858nm, which is 20nm de-tuning from exciton peak. Dashed line is fitted curve.*

From equation 3.6, the frequency deviation for small changes in field is a linear function of the field, therefore

$$\text{FM response} = \frac{\Delta v}{V} \propto \frac{\Delta v}{E} \propto \frac{\Delta n}{E} \propto E \tag{3.8}$$

For static tuning at a certain applied bias, E is a constant, giving an uniform FM response. But for dynamic tuning, due to the device impedance dependence on modulating frequency, it is likely the FM response will not be constant above a certain frequency. To reduce device parasitic parameters in order to achieve a wider

modulation frequency bandwidth with constant FM response is therefore important.

3.3. Phase modulation induced intensity modulation

It is desirable to have only frequency shift with no intensity variation in our device. Although it is impossible, from the Kramers-Kronig relations, that pure frequency modulation can exist, it is useful to characterise the relative importance of FM to intensity modulation (IM).

A generalised linewidth parameter

$$a = \Delta n / \Delta k \tag{3.9}$$

is used for this purpose [3.1, 3.2], where Δk is the field induced change of extinction coefficient

$$\Delta k \equiv \frac{\lambda \Delta \alpha}{4\pi} \tag{3.10}$$

The parameter *a* is also field and wavelength dependent. Figure 3.9 shows the $\Delta n/\Delta k$ variation with wavelength for field strength 68.5kV/cm. It is seen, further de-tuning from exciton peak gives not only lower insertion loss, but also purer FM, the trade-off being reduced FM sensitivity.

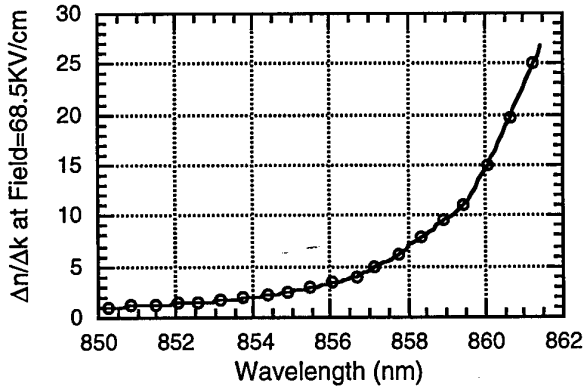

Figure 3.9 *"Chirp" parameter Δn/Δk variation with wavelength for field strength of 68.5kV/cm.*

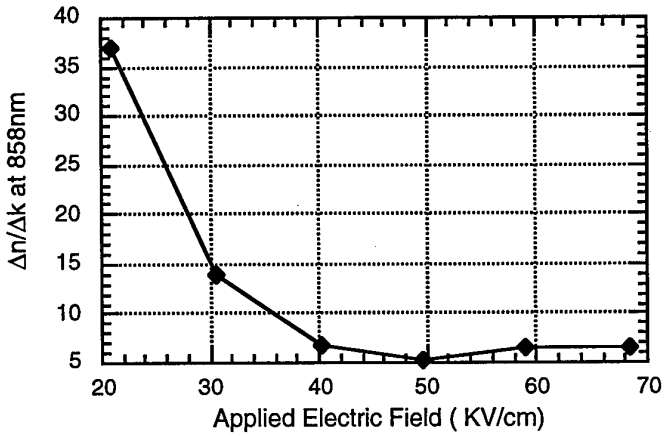

***Figure 3.10** Δn/Δk changes with applied field strength for wavelength 858nm.*

Figure 3.10 shows Δn/Δk as a function of electric field at wavelength 858nm. A general trend is that the residual intensity modulation tends to increase with field strength, confirmed by other researchers. A trade-off has to be made between purer FM and wider maximum frequency deviation.

3.4 Conclusion

In this chapter the trade-offs between tuning section length and loss, FM sensitivity and residual intensity modulation, as a function of applied electric field and detuning between gain and tuning sections, have been presented. The results show that for our device structure detunings of about 20 nm between the zero field e1-hh1 exciton peak wavelength and the emisssion wavelength are optimum. Such shifts are within the range of the quantum well disordering techniques to be described in Chapter 6.

3.5 References

3.1 ZUCKER, J.E., HENDRICKSON, T.L. and BURRUS, C.A.:'Low voltage phase modulation in GaAs/AlGaAs quantum well optical waveguide", *Electron.. Lett.*, 1988, 24 (2), pp. 112-113

3.2. KOREN, U., KOCH, T.L., PRESTING, H. and MILLER, B.I.:'InGaAs/InP MQW waveguide phase modulator', *Appl. Phys. Lett.*, 1987, 50 (7), pp. 368-370.

Chapter 4 Ion Implantation Techniques for Multi-Section Laser Isolation

Since the success in fabricating H+ implantation isolated two-section CW operating lasers [4.1] O+ implantation has been further explored in order to overcome the power degradation problems arising from H+ implantation. We have now successfully fabricated O+ implanted two-section CW laser with stable power output. Detailed results are presented below.

4.1. Isolation results

Since the success of the latest H+ implanted two section laser, in which the implantation depth ended just above the upper core layer of the waveguide, as shown in Figure 4.1 below, new progress has been made on the O+ implanted 2-section laser. In the new isolation scheme, O+ was implanted through the whole active layer, and then annealed at optimised temperature by RTA, as shown in Figure 4.2.

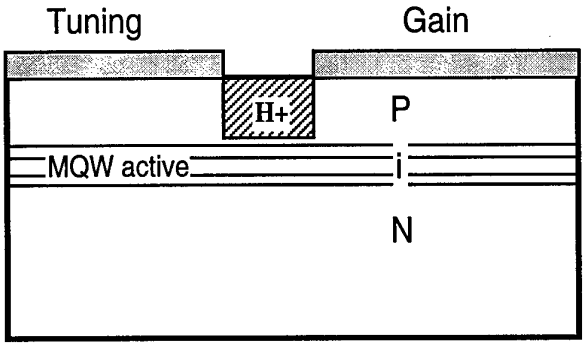

Figure 4.1 *H+ implantation as the isolation scheme: implantation depth must be above the waveguide in order not to stop the device from lasing.*

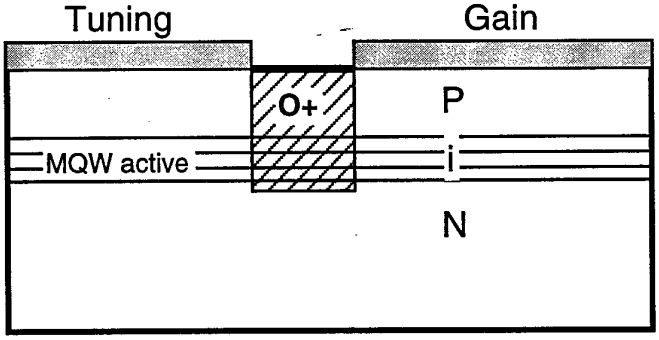

Figure 4.2 *O^+ implantation as the isolation scheme: implantation is through the whole guiding and active layer in order to achieve a fully isolated two-section device.*

In the first scheme, although high isolation resistance was achieved (normally better than 20 kΩ, maximum >100kΩ), there was incomplete isolation between the two sections, since when the gain section was pumped, significant carrier injection through the waveguide to the tuning section resulted. Due to the large potential drop from the gain section to the reverse biased tuning section (2~5 V), and the large carrier density gradient between them, carriers could move from gain to tuning section through the active layer

$$J_{p,n} = \pm qp(\text{or } n)\mu_{p,n}E \mp D_{p,n}\frac{\partial p(\text{or } \partial n)}{\partial x} \qquad (4.1)$$

where q is the elementary charge, p or n is the hole or electron density, E is the electric field, $\mu_{p,n}$ is the hole or electron mobility, and $D_{p,n}$ is the hole or electron diffusion coefficient. Both μ and D vary only slightly with doping levels; therefore, except within the implanted volume where μ and D are changed completely due to the implantation process, μ and D retain high values throughout the active layer. Carriers therefore drift and diffuse through the active layer freely, although larger isolation resistance is presented relative to non-implanted samples (typical resistance 200~600 Ω) due to the lack of leakage through the p^+-doped cap layer. Active layer leakage can be examined using the circuit arrangement of Figure 4.3a, in which the gain section is forward biased and the tuning section reverse biased. Figure 4.3b shows measured results for one of our devices.

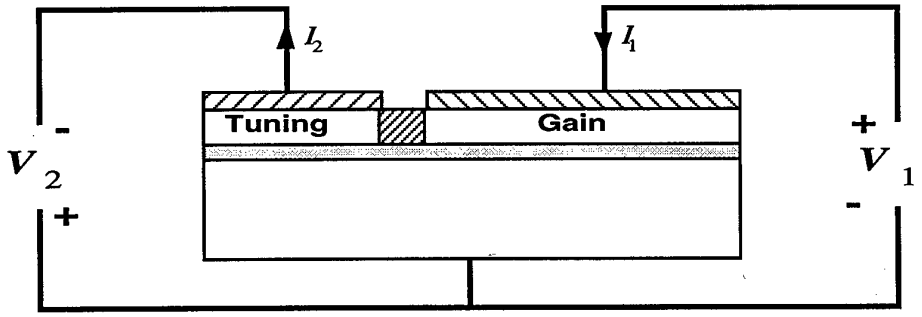

Figure 4.3a. *Device biasing arrangement for detecting lateral carrier leakage.*

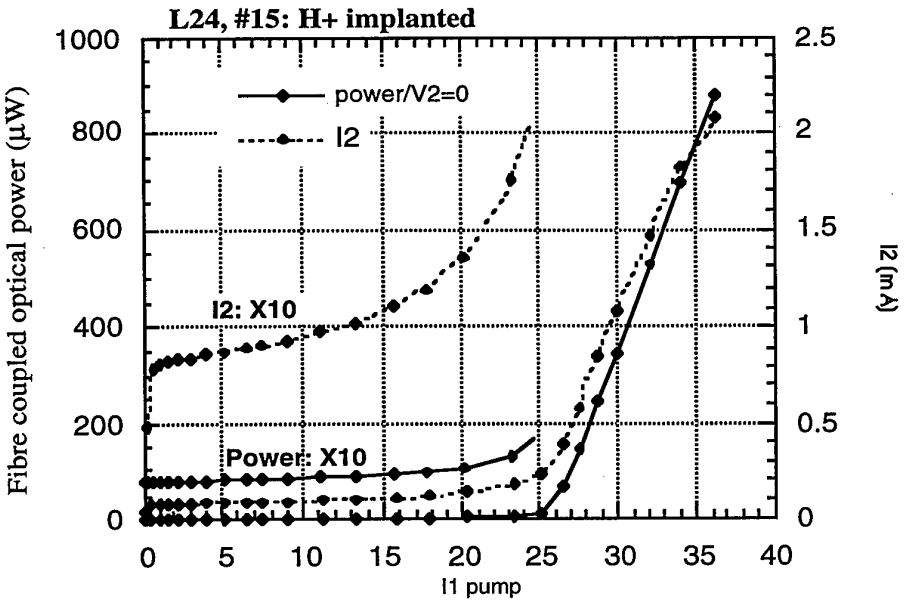

Figure 4.3b *Power output and tuning section leakage current of H+ implanted two-section laser as a function of CW pumping current.*

The initial current jump in I2 from the tuning section at low pumping current I1 is due to carrier diffusion and drift from the gain section: the increase in I2 due to photo-current only occurs at much higher I1.

In the O+ implanted scheme, O+ is implanted through the whole guiding and active layer, and theoretically, the μ and D in the upper p-cladding, upper core and the whole MQW active layer are all changed due to the implantation. Extremely low values of μ and D are expected leading to very high isolation resistance and elimination of lateral carrier diffusion. Figure 4.4 shows the result using the same assessment method for detecting current leakage as in Figure 4.3. It is clearly seen that no sudden I2 jump at low I1 occurs. This is clear evidence that there is no lateral carrier leakage from gain to tuning section in the device. The current I2 is purely the photo-generated current in the tuning section.

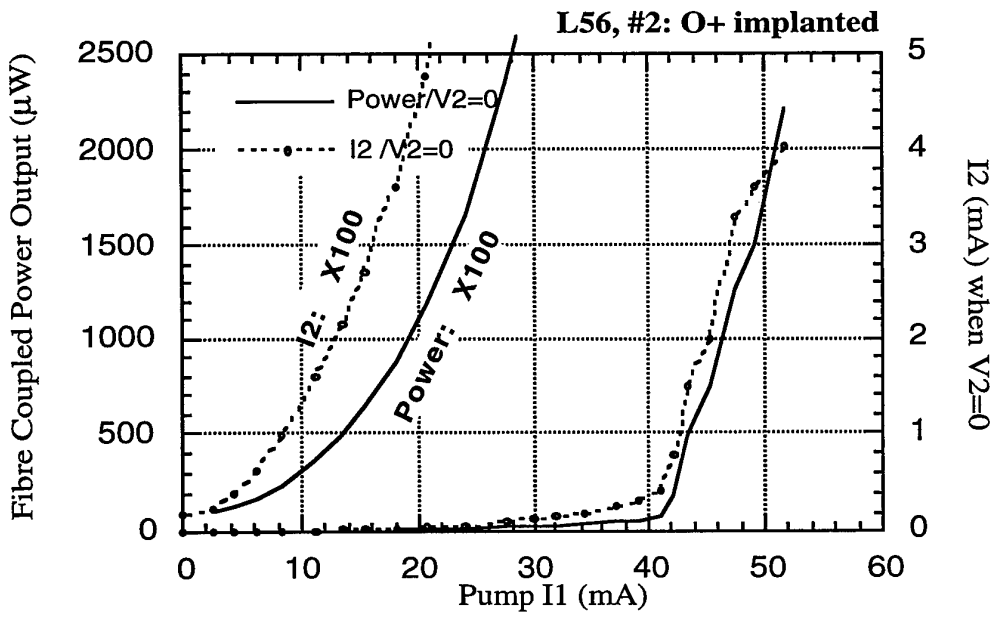

Figure 4.4. *Power output and tuning section leakage current of O+ implanted two-section laser as a function of CW pumping current.*

The higher threshold current seen in Figure 4.4 is not completely due to the O+ implantation. It is partially due to low doping density in the epitaxial p^+ cap layer of L56 compared to L24, resulting in a worse p-contact.

4.2. O+ implantation details and L-I characteristics

Many experiments were run in order to determine optimum implantation doses and annealing temperatures. Successful room temperature operating CW lasers were obtained using O+ implantation with the doses below, followed by RTA at temperatures in the 650 - 750 °C range for 15 seconds.

Energy	*Dose(cm^{-2})*
100KeV	1~2E14
500KeV	8E13~1E14
2 MeV	6~8E13

The laser of Figure 4.4 used the above energies and doses, with annealing by RTA at 650 °C for 15 seconds. Its CW L-I curves with the tuning section open-circuit or shorted are presented in Figure 4.5. The isolation resistance is greater than 200MΩ, and in most device >1GΩ.

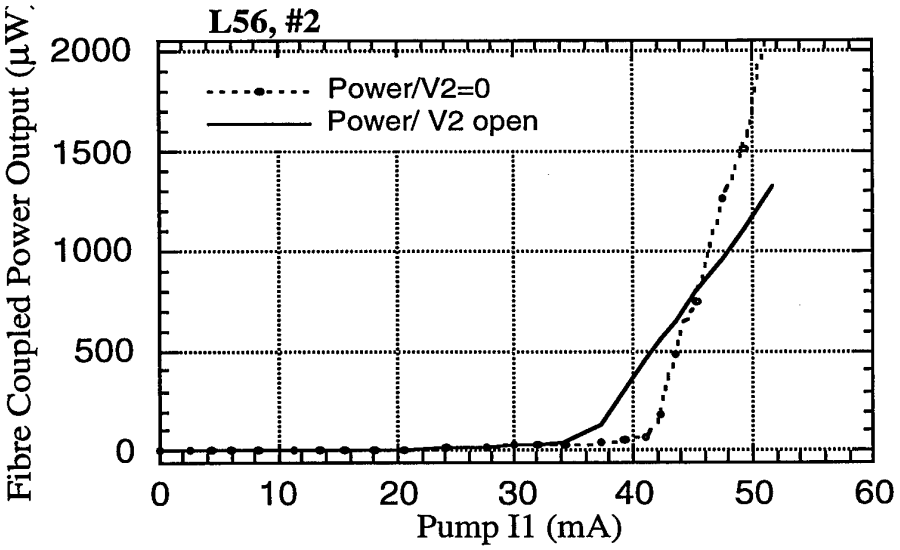

Figure 4.5. *CW L~I curves for O+ implanted two-section laser.*

It is seen that a lower threshold current is obtained with an open-circuit tuning section than short-circuit, but higher slope efficiency is obtained by shorting the tuning section.

All the two section lasers tested showed a multi-mode lasing spectra, but single section lasers from the same wafer including no O+ implanted region showed a mode suppression ratio of only 5 to 10 dB. Subsequent investigation indicated that on this wafer the active layer position was not at the expected depth, due presumably to error in growth calibration, so that the ridge guides were not single mode.

4.3. Power degradation for O+ implanted laser

Ageing degradation of the H+ implantation isolated device was observed, such as power decreasing with time under constant pumping current, and threshold current increasing in day-to-day assessment. For the O+ implantation isolated device, ageing degradation was found to be far less obvious. After two weeks day-to-day running of L56/#2 for assessment, no definite or obvious power drop, or threshold current increase was observed, showing satisfactory lasing stability.

It is understood that the selection of suitable implanting doses and annealing temperatures are the key factors in achieving a stable, low-loss isolation region.

Obviously, the success in producing highly insulating, very low-loss isolation regions by using suitable O+ implantation offers a new technique which could be very useful not only in laser-modulator integration, but also equally importantly in the whole integrated optoelectronics area.

4.4. Static reverse bias tuning

The O+ implanted lasers did not include quantum well disordered tuning sections so that a large change in output power with tuning section voltage would be expected. Figure 4.6 shows the power change with reverse bias, with tuning section leakage current I2 as the reference.

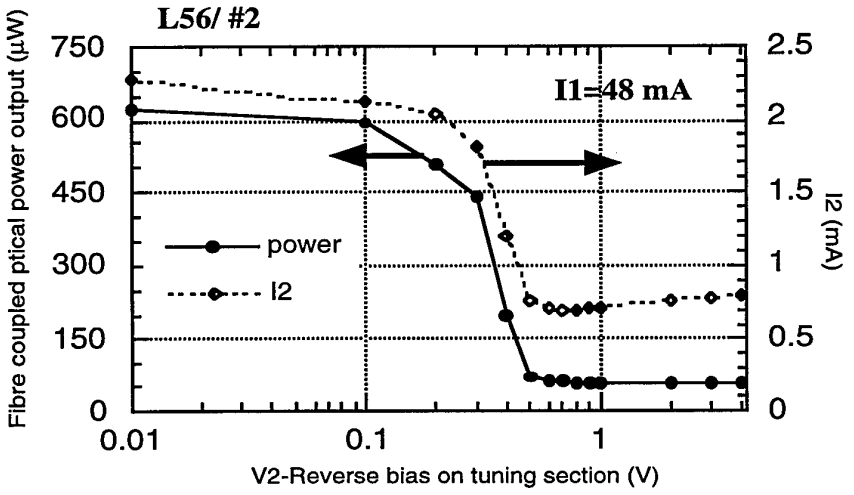

Figure 4.6. *Output power variation with applied reverse bias on the tuning section when the gain section is pumped at 48 mA.*

It is seen that the output power drops rapidly for low applied reverse bias. At 0.5 V reverse bias, the power almost drops to its minimum value. Further increase in reverse bias has little effect on the power output. The large power variation with bias is due to the very high absorption variation with reverse bias, which is the direct result of the non-optimised exciton peak in the tuning section. This absorptive tuning section functions like a saturable passive absorber and may cause passive mode locking [4.2]. Chapter 5 describes work on selective band gap shifting techniques to detune the lasing wavelength from the exciton peak of the tuning section.

4.5 Comparison between different isolation schemes

Good electrical isolation is necessary in order to enable a reverse bias to be applied to the tuning section without affecting the forward biased gain section. Three different

schemes have been studied so far: shallow etch isolation [4.3], H+ implanted isolation [4.4] and O+ implanted isolation [4.5], as illustrated in Figure 4.7a. In the shallow etch scheme, the top p^+-contact layer is removed by a wet etch in the transition area between gain and tuning sections, resulting in a reasonably high isolation resistance (1~15KΩ) between the two sections. This is due to the low p-type doping level in the upper cladding and guiding layer. The leakage current when bias was applied laterally across gain and tuning section, as shown in Figure 4.7b, was very high. The reason for this is due to the potential drop and carrier density gradient between gain and tuning section, causing carriers to diffuse and drift from gain to tuning section through the active layer as shown in equation (4.1). Both μ and D vary slowly with doping levels; therefore, unless the value of μ and D are changed completely by some method, for instance by ion implantation, μ and D remain high throughout the upper cladding, guiding and the active layers. Carriers therefore drift and diffuse through these layers easily, despite a large isolation resistance being obtained relative to non-etched samples (typical resistance 100~600 Ω). By using this etch scheme, a successful CW laser with threshold current 20 mA was obtained.

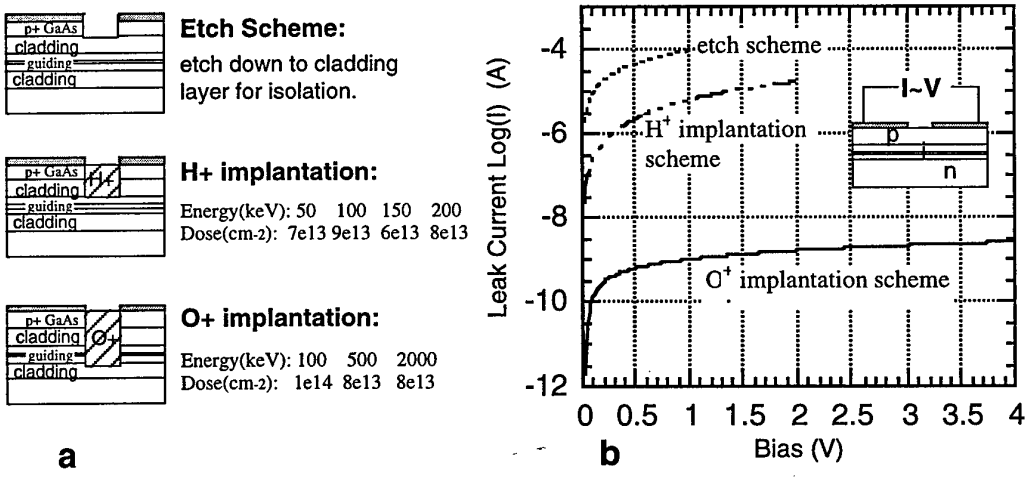

Figure 4..7 *Three isolation schemes adopted (a) and their corresponding measured current leakage characteristics (b).*

In the H+ implanted isolation scheme, protons were implanted in the isolation region but the depth was controlled to be above the core layer since it was found that H+ implantation into the guiding and active layer suppressed laser operation a dose level of $3x10^{14}$ cm^{-2}, and degraded the laser performance seriously even at very low dose levels (10^{12}~10^{13} cm^{-2}). This was consistent with the results from other researchers [4.6] Even after rapid thermal annealing (RTA) at an elevated temperature (200 - 500

°C), no full recovery of device performance was obtained in contrast to some predictions [4.7] This result indicated that the defects and deep energy levels associated with proton bombardment were very harmful to the laser diode and difficult to remove, therefore, great care has to be taken in choosing implantation depth and doses. Figure 4.7a indicates a typical H+ implantation condition for the two section laser. A CW laser with threshold current 24 mA and 10kΩ ~ 2MΩ isolation resistance was achieved. Figure 4.7b shows the leakage current between gain and tuning section as a function of bias between them, a reduced but still obvious leakage current is obtained. This is because carrier leakage through the guiding and active layers is still possible.

Dramatic leakage current suppression was achieved by using the O+ implantation scheme where O+ was implanted through the whole upper cladding and guiding (including the active) layers to achieve a strict isolation between gain and tuning section, as shown in Figure 4.7a. The key factors in achieving a CW laser with this isolation scheme are the selection of suitable implantation doses and the RTA condition. Due to hopping conductivity [4.8] in the post-implanted sample, the resistivity is low for non-annealed or annealed below 500°C samples, but the optical loss is high due to implantation damage. After annealing at temperatures between 600 ~ 700 °C the sample shows maximum resistivity with acceptably low optical loss (judged by the fact that no obvious threshold current increase compared to the lasers made from the same wafer but with no implanted region). Annealing at higher temperature reduces the resistivity dramatically with no further significant optical loss reduction. The result shown in Figure 4.7b was obtained by RTA at 650°C for 15 seconds after implantation. A room temperature CW operating laser with threshold current 34mA and isolation resistance 600MΩ ~ 2GΩ was achieved.

4.6 References

4.1 HUANG, X. and SEEDS, A. J.: AFOSR Contract F61708-94-C0009 Final Report, December 1996.

4.2 VAN DER ZIEL, J.P., TSANG, W.T., LOGAN, R.A. and AUGUSTYNIAK, W.M.:'Pulsating output of separate confinement buried optical guide laser due to deliberate introduction of saturable loss', *Appl. Phys. Lett.,* 1981, 39, p. 376.

4.3. WHITE, I. H., WATTS, J. J. S., GARRETT, B.: 'Experimental observation of spectral tuning in twin-segment double quantum well (DQW) AlGaAs diode laser', *Electron. Lett.*, 1989, 25(15), pp. 953-954.

4.4. HOFSTETTER, D., ZAPPE, H. P., and DANDLIKER, R.:'Monolithically integrated optical displacement sensor in GaAs/AlGaAs', *Electron. Lett.*, 1995, 31(24), pp. 2121-2122.

4.5. BERTHOLD, K., LEVI, A. F. J., PEARTON, S. J., MALIK, R. J., JAN, W. Y. and CUNNINGHAM, J. E.:'Bias-controlled intersubband wavelength switching in a GaAs/AlGaAs quantum well laser', *Appl. Phys. Lett.*, 1989, 55(14), pp. 1382-1384.

4.6. HWANG, R. Y., LEE, C. P. and LEI, T. F.:'GaAs/AlGaAs laser arrays with and without proton isolation', *Journal of the Chinese Institute of Engineers*, 1989, 12(2), pp. 255-261.

4.7 DYMENT, J. C., NORTH, J. C. and D'ASARO, L. A.: 'Optical properties and electrical properties of proton bombarded p-type GaAs', *J. Appl. Phys.*, 1973, 44, pp. 207-213.

4.8. PEARTON, S. J.:'Ion implantation in III-V semiconductor technology', *Int. J. Modern Physics B*, 1993, 7(28), pp. 4687-4761.

Chapter 5 Fabrication of Low Parasitic Capacitance Lasers

Due to the large bonding pads needed for connection to the two sections, it is likely that parasitic capacitance will limit high frequency assessment. Our early dynamic tuning assessment was limited to below 500MHz due to high parasitic capacitance (~22pF). The only choice to overcome this limitation is to develop a low parasitic contacting scheme. We have therefore developed an air-bridged mesa etched two section tunable laser. A new set of masks for this purpose has been designed and fabricated. Shown in Figure 5.1 is the diagram of the device structure and a lithography mask for the bonding electrode.

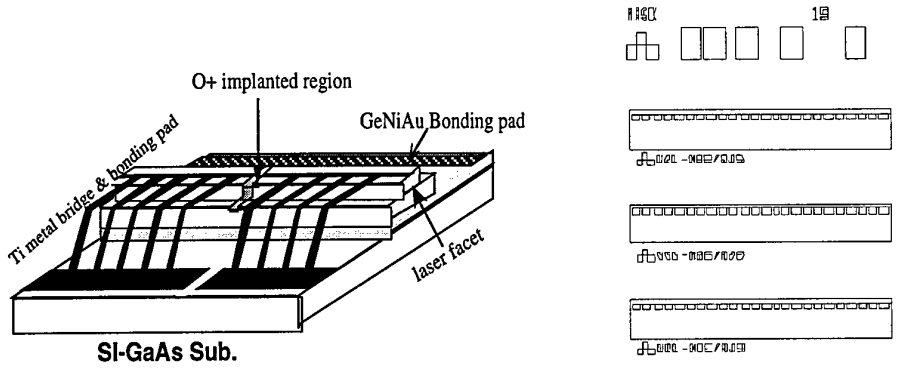

Figure 5.1 *Schematic diagram of air-bridged two-section tunable laser and its top contact metalisation mask.*

The laser is fabricated on a semi-insulating substrate so that the bond-pad capacitance is low. After fabricating the ridge and N contact, a deep trench etch is used to isolate the ridge from the bonding pad on one side. Photoresist is then used to fill the trench followed by p-contact metal evaporation and lift-off to leave the air bridge in place. Figure 5.2 shows the room temperature CW L-I characteristics of this laser which has a cavity length of 500 μm with a junction width of 24 μm. An SEM picture of the air-bridged two section laser is shown on the next page. During the fabrication, due to the lack of metal sputtering and plating facilities, we used a complicated photolithography - resist filling-metal thermal evaporation-metal lift off-resist stripping process which required good metal adhesion to the semiconductor surface, therefore, Cr/Au was used for p-contact metalisation, resulting in higher threshold current and low maximum power output. To overcome this, a modified multi-layer metalisation scheme, has been used for the final batch of GaAs/AlGaAs tunable lasers.

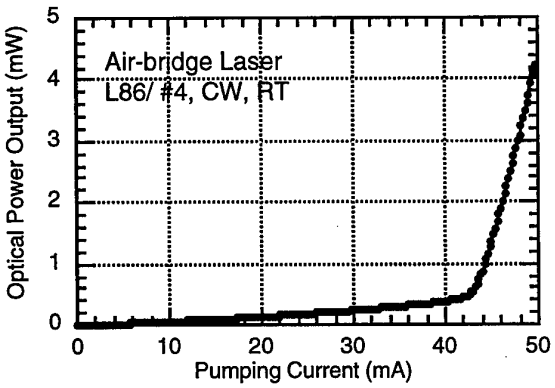

Figure 5.2 L-I characteristics of an air-bridged laser for room temperature CW operation.

Measurement of device capacitance gave a value of ~2pF for the laser shown in Figure 5.1, an order of magnitude capacitance reduction. By further reducing the junction width to ~14μm and adopting the O+ implantation isolation of Chapter 4, this value can be reduced to less than 1pF which will increase the cut-off frequency to above 3GHz for a 50Ω RF source impedance.

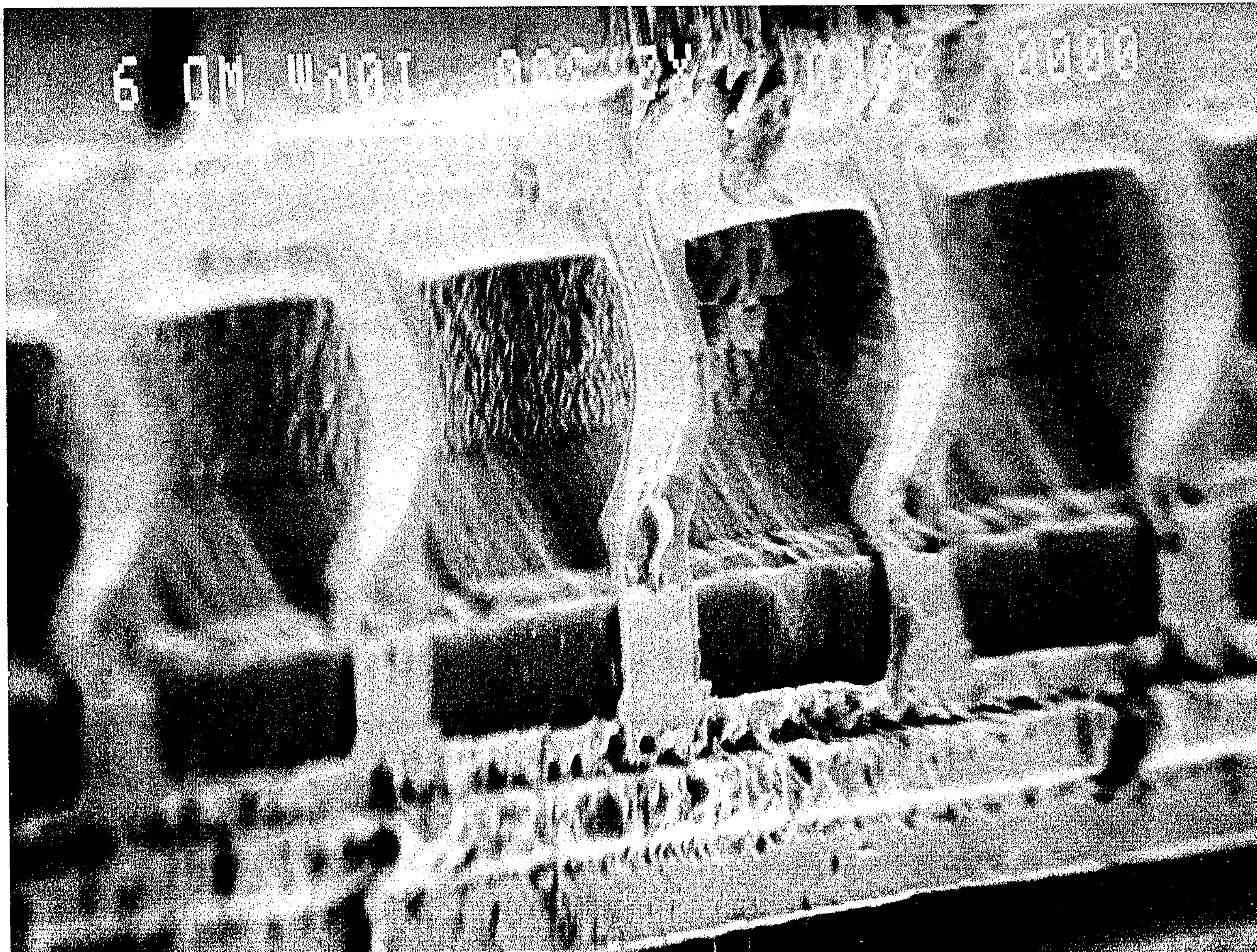

Chapter 6 Band Gap Shifting Experiments and Further Developments in GaAs/AlGaAs Laser Fabrication

It has been shown in Chapters 3 and 4 that band gap detuning is important in order to obtain FM with small power variation. A transparent tuning section is also important to prevent passive mode locking, therefore, band gap shifting techniques have been explored. In our previous report [6.1] we described initial experiments on quantum well disordering techniques which showed clear differential shifts in photoluminescence wavelength for samples of wafer depending on the dielectric cap used. In this chapter we describe extensive further work on disordering techniques including the successful fabrication of a room temperature CW operating laser with a disordered tuning section. We conclude the chapter with further work on the effect of different caps leading to the procedure used for the final batch of GaAs/AlGAAs tunable lasers.

6.1. Band gap shifting by impurity-free vacancy diffusion

The task for band gap shifting is to have the band gap of the MQW in the tuning section increased (exciton edge blue shifted), while keeping the MQW in the gain section unchanged. If this is achieved, the lasing wavelength will be on the low absorption red side of the exciton edge of the tuning section. Impurity free vacancy diffusion (IFVD) is a suitable technique to achieve this purpose [6.2, 6.3]. The most common dielectric to produce large band gap shift is SiO_2, and one of the dielectric films reported [6.2] to best protect MQW from band gap shift is SrF_2. Figure 6.1a shows the band gap shift result using RTA of the sample at 900 °C for 30 seconds after dielectric coating. Although large relative band gap de-tuning (17nm) was produced, the SrF_2 capped section presented very bad surface morphology and good quality lasers could not be produced as observed by another group who used the same technique [6.3]. It is believed that the reaction of GaAs and SrF_2 at high temperature is the reason.

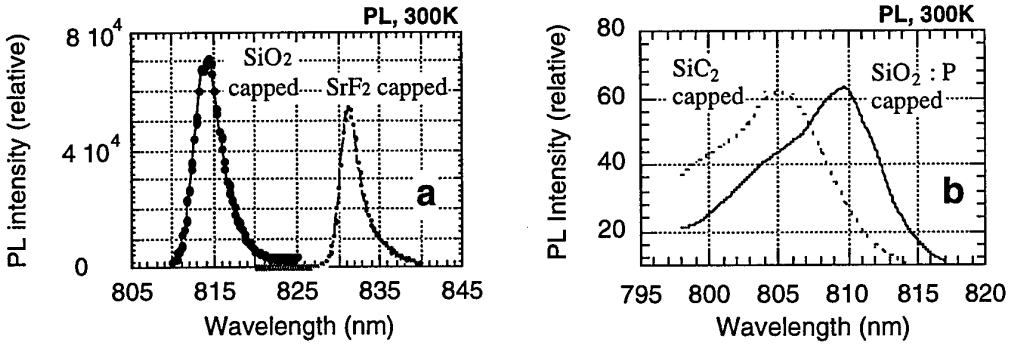

Figure 6.1 *Band gap shifting experimental results: (a) capped with SiO_2 or SrF_2; (b) capped with SiO_2 or SiO_2:P ; all samples were annealed at 900 °C for 30 seconds.*

Instead of using SrF_2, SiO_2:P can also be used as a protecting film [6.4] during annealing. An initial result is shown in Figure 6.1b, where the P content failed to reach the required concentration of ~5% by weight. Small but clear band gap de-tuning was still produced. More importantly, no surface degradation has been found after annealing.

6.2 Further development of the SiO_2:P/SiO_2 disordering system

Although large relative band gap de-tuning was easily achieved by using SrF_2/SiO_2 system, the SrF_2 capped section tends to present very bad surface morphology and it is difficult to have good quality lasers produced from such wafers [6.3] As a new technique introduced recently [6.4] (private communication with Dr. C. Pasquale, Department of EEE, University of Glasgow), SiO_2:P, which is 5% in weight of phosphorus heavily doped SiO2 deposited by chemical vapour deposition (CVD), is reported to have the property in preventing band gap shift while maintaining good surface morphology after RTA. In order to optimise the shift, especially to control the relative shift over a much wider range (~10nm) as required by the laser design, more experiments have been carried out.

By placing SiO_2:P or SiO_2 coatings on adjacent parts of a single test wafer, cleaving the wafer and applying RTA to the different samples, a systematic series of band gap shifting results can be obtained. Figure 6.2 shows the photoluminescence (PL) results as a function of anneal time and temperature. It is seen that over the RTA temperature range 900 to 960 °C, the biggest relative band gap shift is only 6 nm. This is much less than the required 10nm relative band gap shift. We also observe that the absolute band

gap shifts, which are defined as the PL peak shift after annealing compared to its peak before annealing, are both as large as 10nm blue shift for SiO2:P and SiO2 coated samples when annealing at 940 °C for 1 minute.

Group 1: RTA 900 °C, 1min

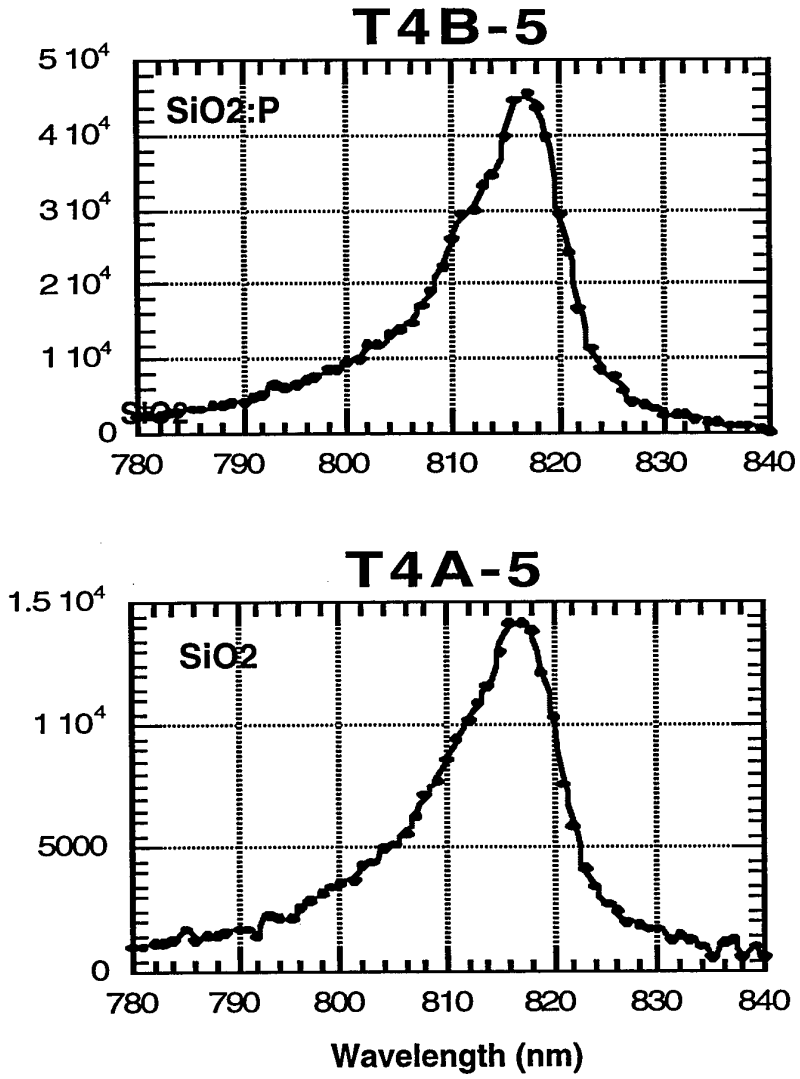

Figure 6.2a *PL measurement results for SiO2:P and SiO2 coated sample after RTA on different conditions: Group 1, nearly no relative band gap shift.*

Group 2: RTA 920 °C, 1min

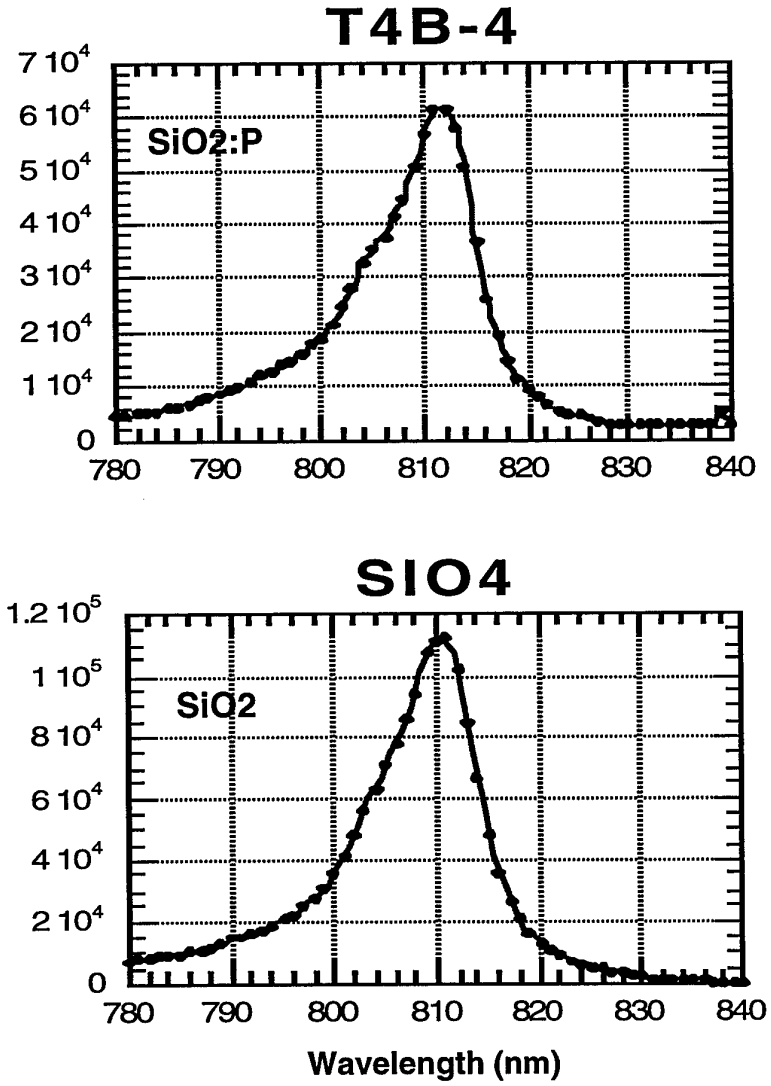

Figure 6.2b *Group 2, only 1nm band gap shift.*

Group 3: RTA 940 °C, 1min

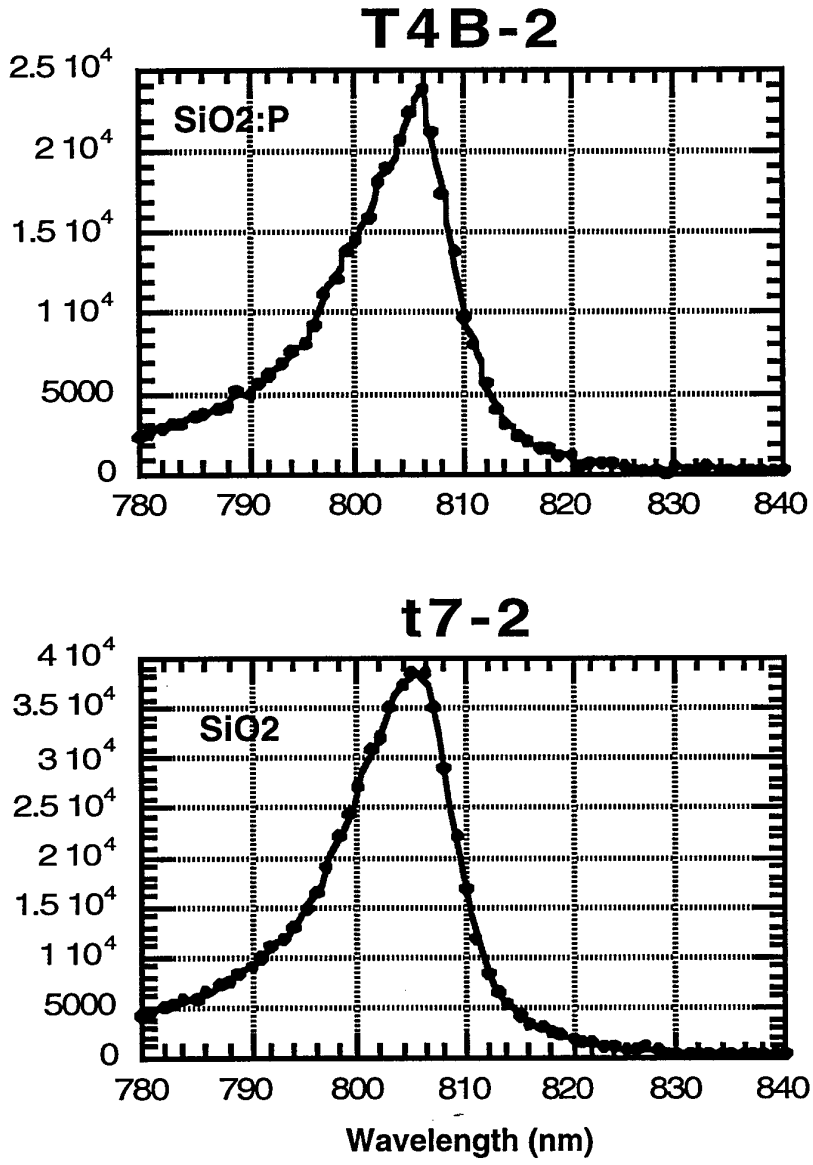

Figure 6.2c *Group 3, roughly 1nm shift obtained.*

Group 4: RTA 940 °C, 2 min

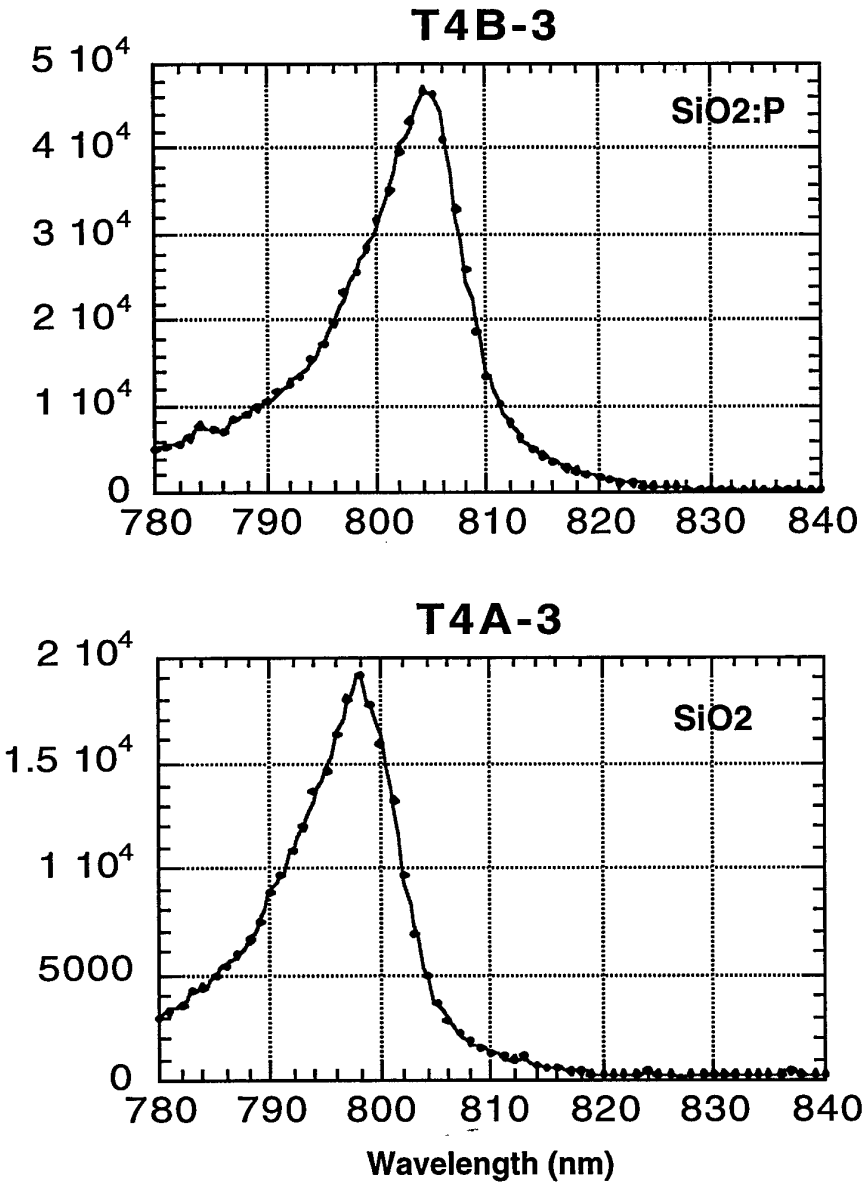

Figure 6.2d *Group 4, 6nm relative shift obtained.*

Group 5 : RTA 960 °C, 1min

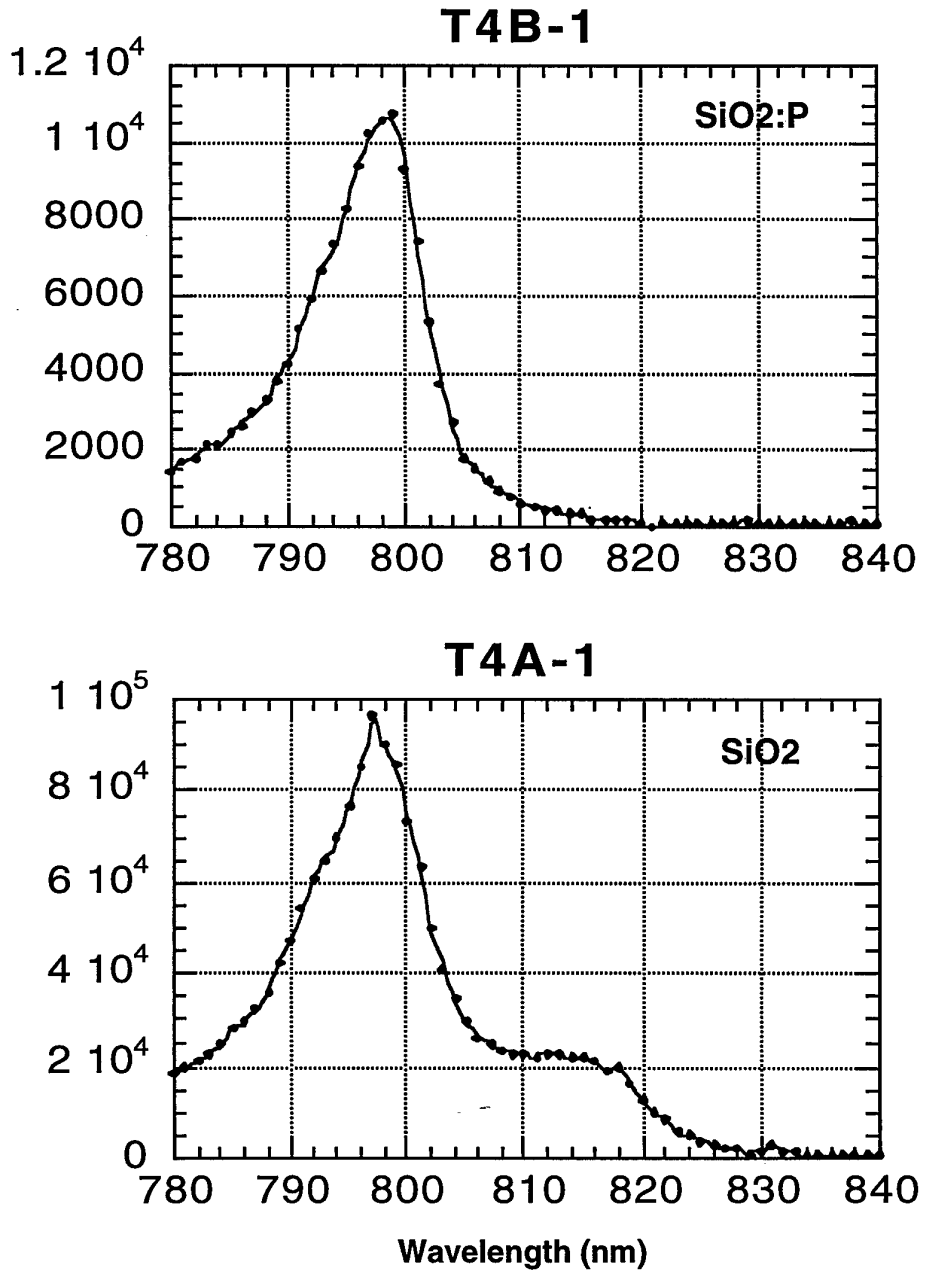

Figure 6.2e *Group 5, at most 2nm relative shift obtained.*

From these results, it is obvious that the SiO2:P/SiO2 system fails to satisfy our requirements for band gap shifting. The reason for this may be inadequate control of the P doping, which was not carried out at UCL. In the light of this experience further experiments were conducted on the SrF_2/SiO_2 system.

6.3 Further development of the SrF_2:P/SiO_2 disordering system

In our earlier experiments, SrF2/SiO2 had been used and no laser was fabricated successfully due to very bad surface morphology after RTA, although large (> 10nm) relative band gap shift, with very good repeatability, was obtained. We decided to make a more extensive study of this system.

First, different deposition conditions have been applied in order to achieve minimum surface morphology damage. In our previous experiments, only 40 A current was applied to the SrF_2 boat, resulting in a low density deposited SrF2 film (~100nm in thickness). In our new experiments, a wide range of heating currents, from 40 to 80A, were used, with film thicknesses of 100nm to 200nm. We found that the best surface morphology is maintained when using 70A heating current, with no obvious relation to film thickness. That is, a suitably dense SrF_2 film is quite helpful in reducing surface morphology damage after RTA. It is also found that proximity cap annealing (by using a clean GaAs wafer face down to cover the processed wafers during annealing) is necessary during RTA. The film thickness has no important effect on preventing band gap shift with films thickness in the range 100 to 200 nm.

Figure 6.3 shows the PL results by using SrF_2 and SiO_2 coating films and RTA at temperatures from 900 to 940 °C using the evaluation methods of Section 6.2. The results show that, starting from 920 °C, a very pronounced relative band gap shift is achieved. Higher temperatures produce larger shifts but give worse surface morphology. It is also found that at the same annealing temperature, a longer annealing time results in a larger shift. By using dense SrF2 film deposition method and 920 and 940 °C RTA, successful room temperature CW operation of a two section disordered laser was obtained.

Group 1: RTA 900 °C, 1min

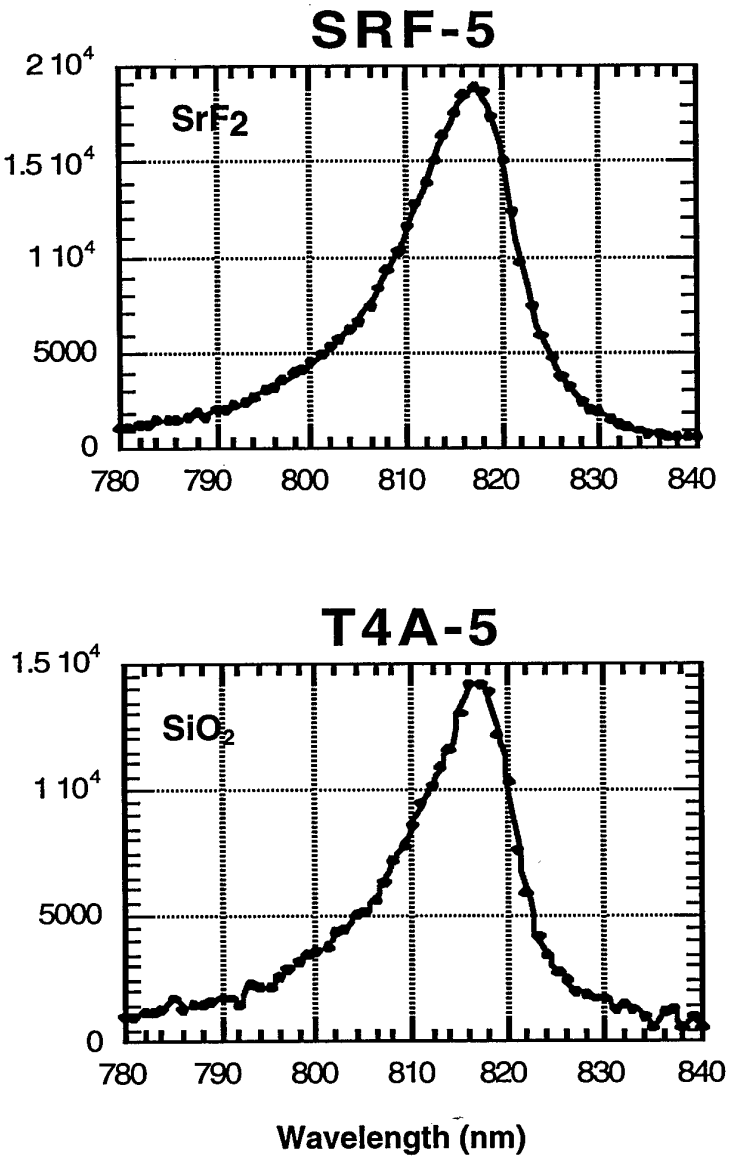

Figure 6.3a *PL spectra of SrF2 and SiO2 coated samples after RTA; Group 1: almost no shift.*

Group 2: RTA 920 °C, 1min

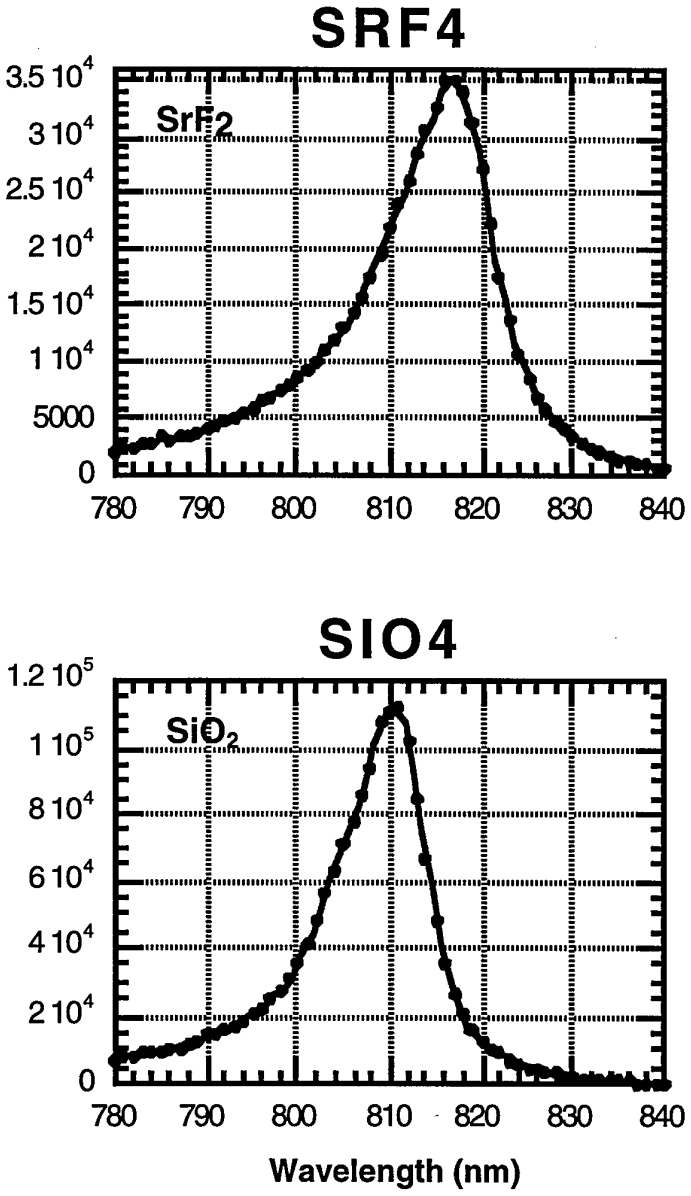

Figure 6.3b *Group 2: 7nm relative shift is achieved.*

Group 3: RTA 940 °C, 1min

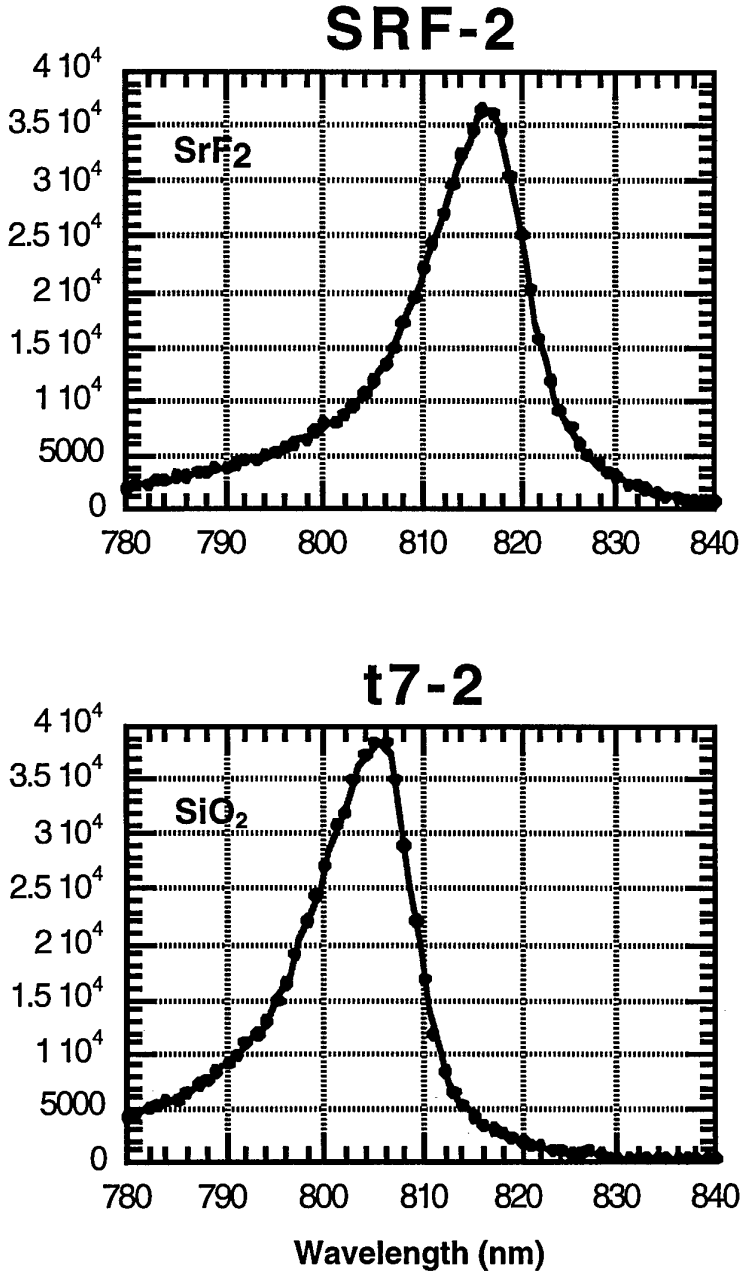

Figure 6.3c *Group 3: 12nm relative shift is achieved.*

6.4 The fabrication and assessment of a band gap shifted CW operating two section laser

By using the above techniques on the SrF_2/SiO_2 system, successful CW operation of a two section laser was obtained. The fabrication procedure was the same as reported previously [6.1] with the disordering carried out as the first process steps because of the high temperature anneal requirement.

Figure 6.4 shows the L-I plot for a two section laser, with the 400μm long gain section SrF_2 coated and the 100μm long tuning section SiO_2 coated before RTA. Pumping current was applied to the tuning section only.

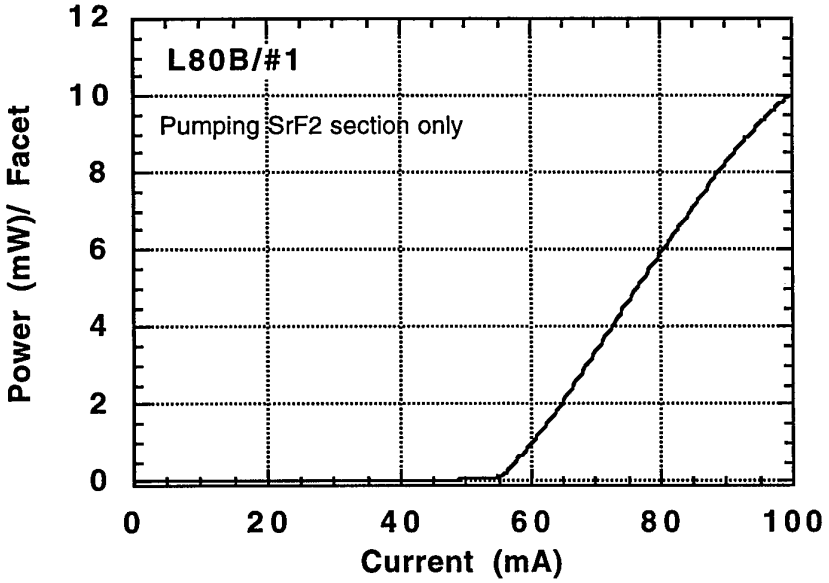

Figure 6.4 *L-I plot of a band gap shifted two section laser under CW operation.*

6.4.1 Device fabrication details

The laser was made from QT935 wafer grown at the Sheffield III/V Facility on an N+ substrate. First, pure SiO_2 is deposited by PECVD processing with a thickness of 200nm. Secondly, part of the SiO_2 is removed by wet HF etching where the band gap intermixing is to be prohibited, followed by dense SrF2 film thermal deposition in an evaporator with thickness of 150 nm. Wafers are then sent to Surrey University for

RTA. We use 920°C and 2 minutes as the annealing condition, with a clean bare GaAs wafer covering the annealing wafers during RTA. Wafers are then processed as normal ridge waveguide lasers.

The two section laser fabricated is a broad electrode contacted laser with no effort taken to reduce the parasitic capacitance. The final band gap shifted lasers are however fabricated on a semi-insulating substrate for improved high frequency performance.

6.4.2. The assessment of the band gap shifted laser

In order to confirm the relative band gap shift and to assess the shift amount, detailed optical spectrum measurement have been performed on the fabricated lasers. Figure 6.5 is the spontaneous emission spectrum of Laser #1 (Figure 6.4) with pumping current just below its threshold current (55mA in this case). It is seen the exciton peak is at 843nm. Figure 6.6 shows the spontaneous emission spectrum and the L-I plot of Laser #6 which is from the same wafer and adjacent to #1, but it is a single section laser (300μm cavity length) from the SiO_2 coated portion. That is, its band gap should have been intermixed and blue shifted. Indeed, the spectrum shows its exciton peak at 830nm when pumping just below its threshold current (47mA in this case).

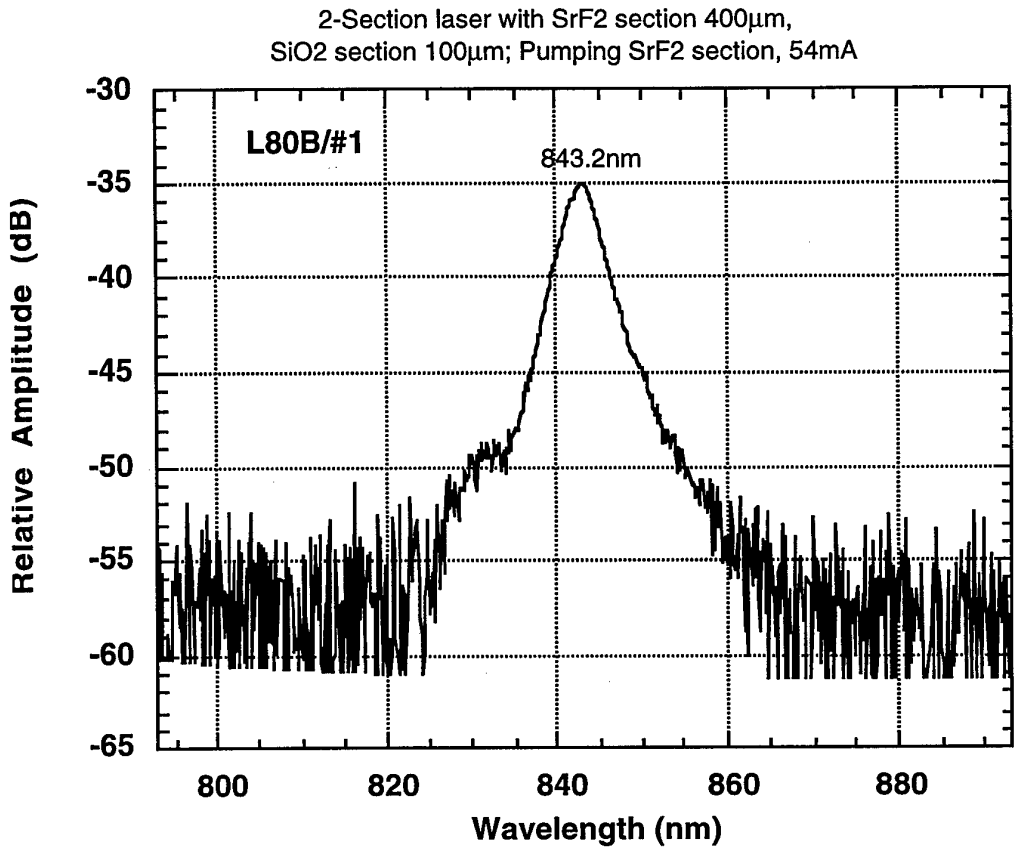

Figure 6.5 *The spontaneous emission spectrum of #1 under pumping current just below threshold current on the SrF2 section.*

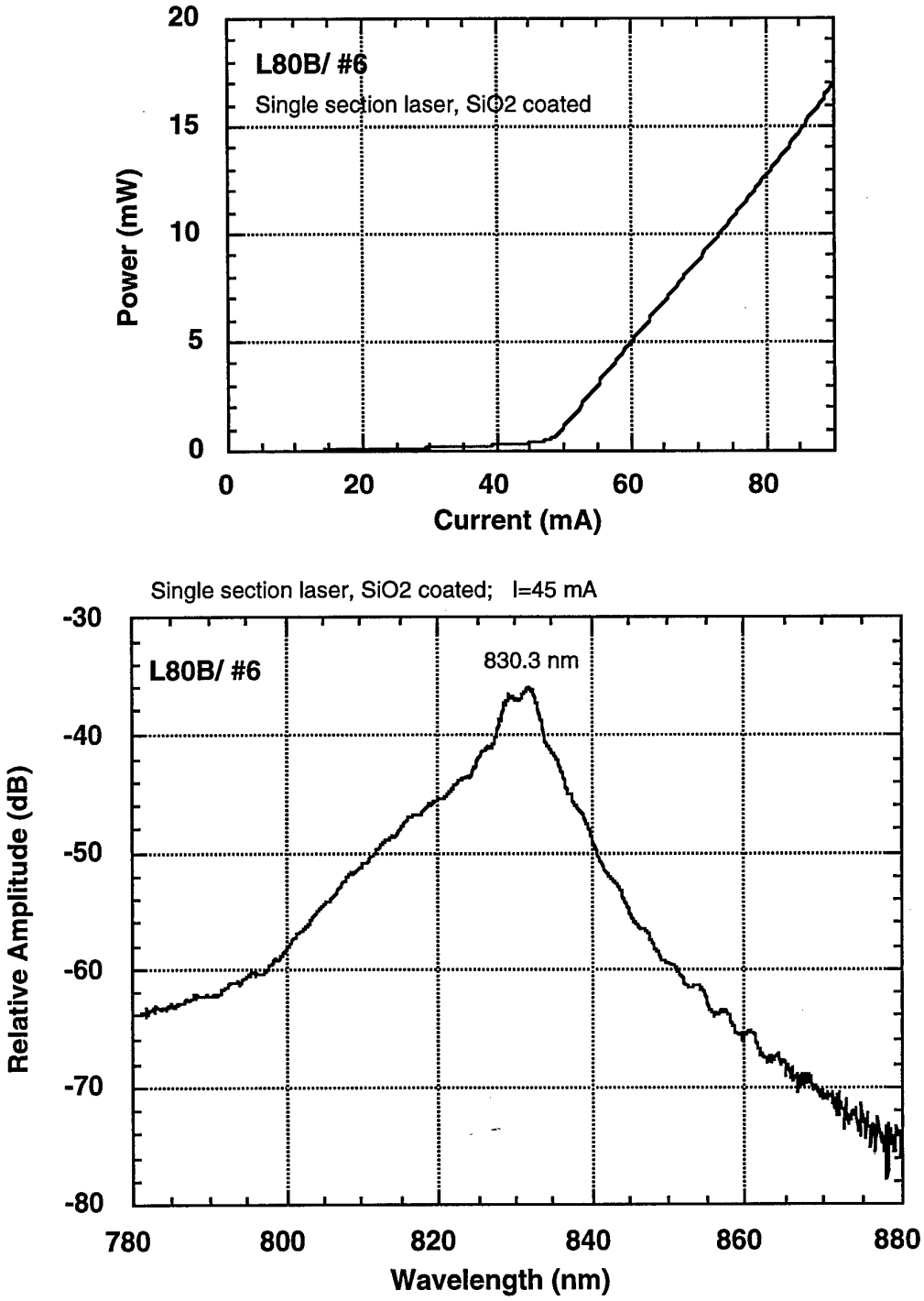

Figure 6.6 *L-I plot and spontaneous emission spectrum of SiO2 coated single section laser #6 under pumping current just below threshold current.*

It is seen clearly that the exciton peaks on the same wafer, but from SrF2 and SiO2 coated portion, shows a 13nm relative band gap shift, which is quite consistent with

the result obtained in Group 2 of Figure 6.3.

Another measurement was performed to confirm this relative band gap shift. We cleaved a two section laser with equal SrF_2 and SiO_2 section lengths. If relative band gap shifting does happen, pumping the SiO_2 coated section should give higher threshold current as the SrF_2 coated section acts as an absorber. However, pumping the SrF_2 coated section should give a lower threshold current as the SiO_2 coated section will have low loss. Figure 6.7 shows the results.

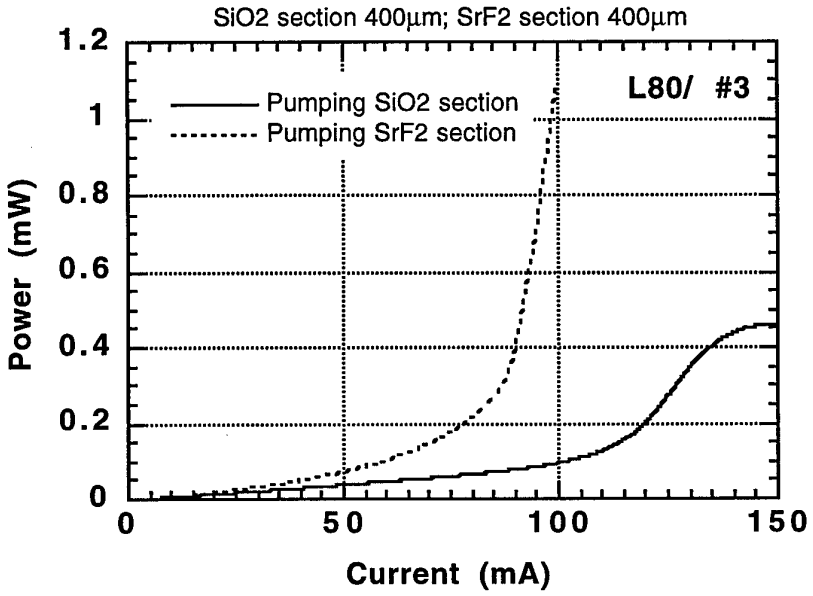

Figure 6.7 *L-I plots of a two-section laser with equal lengthened sections when pumping either the SiO2 or SrF2 coated section.*

It is clearly seen, when pumping the SiO_2 coated section, that as expected the threshold current is much higher and the maximum output power is also limited.

Lasing spectra were also measured under different pumping levels. Figure 6.8 shows the spectra obtained. Single mode operation with better than 10dB mode suppression ratio was achieved, but the working range (a certain pumping current range within which the single mode operation is maintained) is rather limited. We find this is due to improper ridge etch during fabrication. It is worth remarking that after RTA, the portion coated with SiO2 or SrF2 may have different etching speed even in the same etchant. Further measurements on tuning performance are given in Chapter 7.

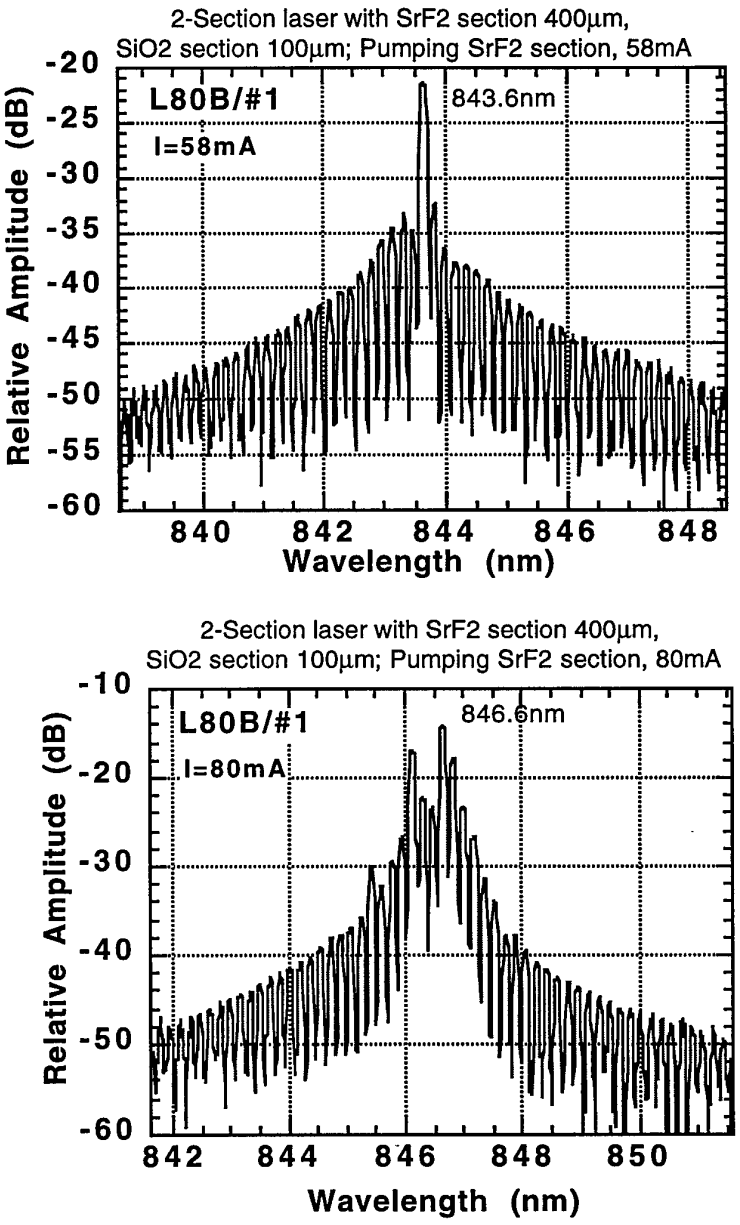

Figure 6.8 *Lasing spectrum of #1, a two-section band gap shifted laser under CW operation.*

6.5 Further experiments with other capping regimes.

Following the successful fabrication of two section disordered lasers using the SrF_2/SiO_2 technique we have completed our sutudy of cap anneal disordering by PL studies on Si_3N_4/SiO_2, Ar etched/SiO_2 and uncoated/SiO_2 surfaces. GaAs proximity caps were used in RTA in each case. Figure 6.9 shows the results.

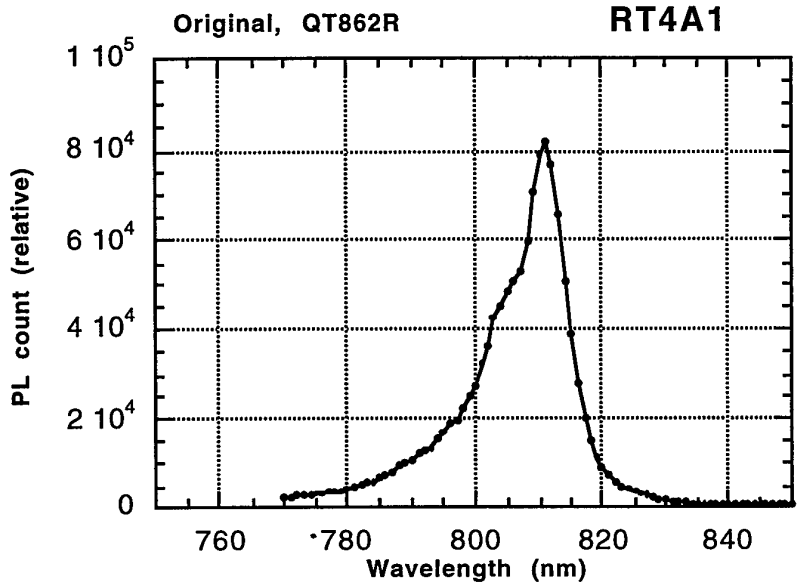

Figure 6.9a *PL spectra for different cap anneal conditions: Uncapped sample before RTA.*

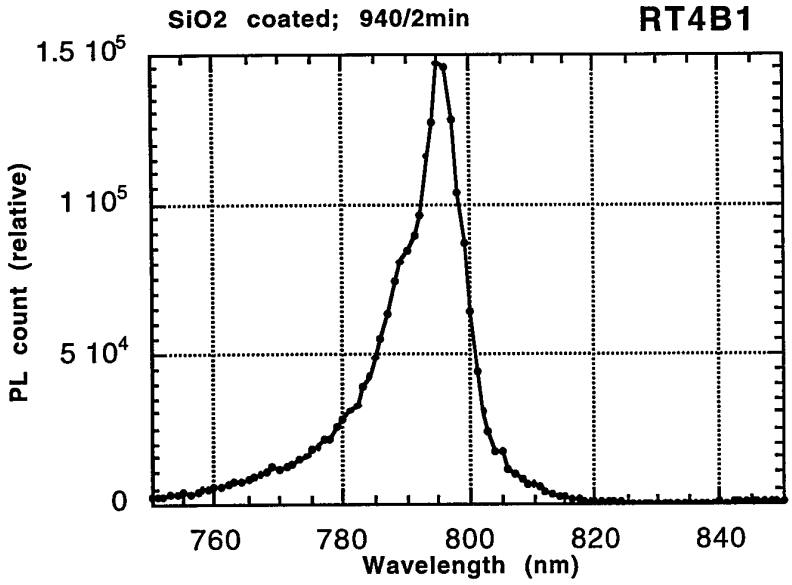

Figure 6.9b *SiO2 coated sample after RTA. 15nm shift.*

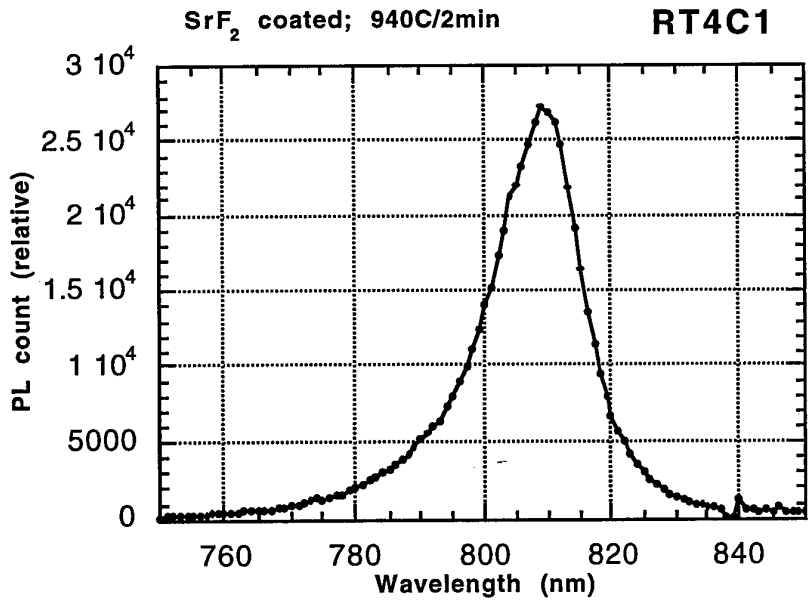

Figure 6.9c *SrF2 coated sample. 1nm shift.*

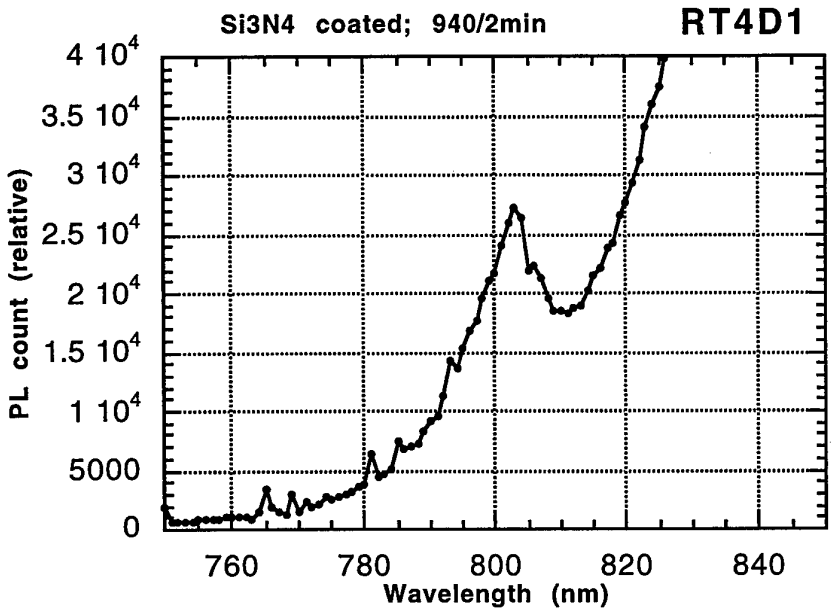

Figure 6.9d *Si3N4 coated sample. 6 nm shift. Strong background PL emission of GaAs is observed on this sample due to the unsuccessful top GaAs layer removal.*

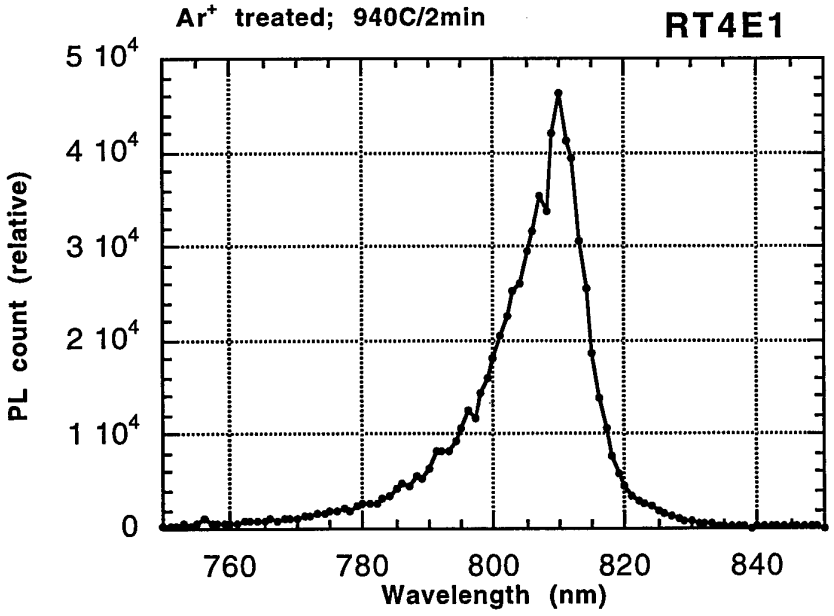

Figure 6.9e *Ar+ plasma treated sample. 0 nm shift.*

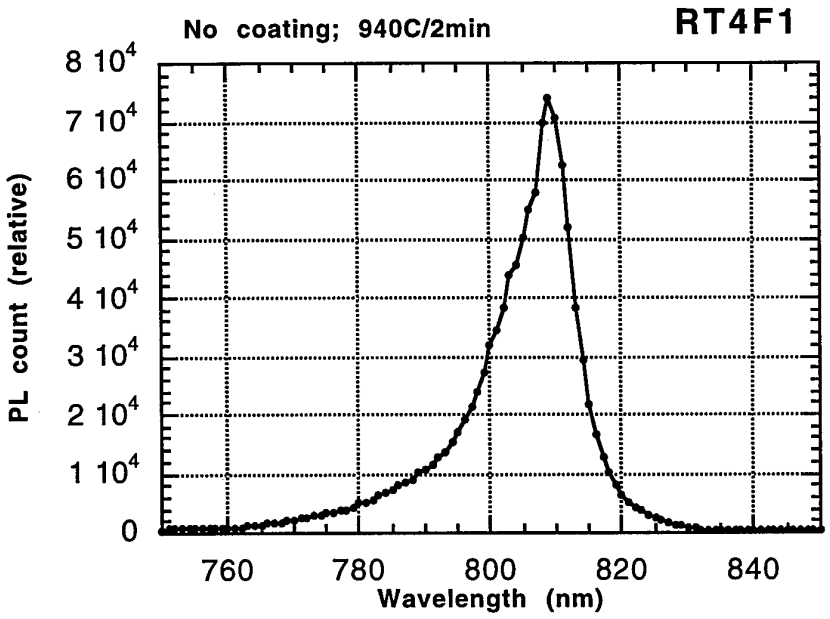

Figure 6.9f *No cap. 1 nm shift.*

Reviewing these results it is clear that using the proximity cap technique SrF_2, Ar+, and uncapped wafers all give negligible shift under the conditions used. Moreover the uncapped and Ar+ wafers have excellent surface morphology after RTA. The Si_3N_4 cap gives a significant shift and this may be due to incorrect composition. Thus for laser processing use of the uncapped or Ar+ treated wafers with SiO_2 where disordering is required may be a simple and effective route.

6.6 Conclusion

In our work on disordering we require a shift of about 10 nm to add to the normal offset of the laser gain peak from the e1-hh1 exciton absorption peak, so as to give total detuning close to 20 nm for optimised tunable lasers. We have studied a range of capped annealing techniques for this purpose. Adequate shifts were not obtained for the SiO_2:P/SiO_2 technique and we suspect that this may be due to lack of doping control at the deposition stage. The SrF_2/SiO_2 technique gives very reproducible shifts but careful control of SrF_2 deposition conditions is required to maintain surface morphology adequate for high quality laser fabrication. Recent work on uncapped/SiO_2 and Ar+ etched/SiO_2 techniques indicates that reproducible shifts with good surface morphology are obtainable. These are therefore the preferred techniques for laser fabrication.

6.7 References

6.1 HUANG, X. and SEEDS, A. J.: AFOSR Contract F61708-94-C0009 Final Report, December 1996.

6.2. GONTIJO, I., KRAUSS, T., MARSH, J. H. and DE LA RUE, R. M.:'Post growth control of GaAs/AlGaAs quantum well shapes by impurity-free vacancy diffusion', *IEEE J. Quantum Electron.*, 1994, . QE-30(5), pp. 1189-1195.

6.3. MARSH, J. H.:'Quantum well intermixing', *Semicon. Sci. & Technol.*, 1993, 8, pp. 1136-1155.

6.4 HAMOUDI, A ., RAO, E. V. K., KRAUZ, P., RAMDANE, A., OUGAZZADEN, A., ROBEIN, D. and THIBIERGE, H.:'Controlled disordering of compressively strained InGaAsP multiple quantum wells under SiO:P encapsulant and application to laser-modulator integration', *J. Appl. Phy.*, 1995, 78(9), pp. 5638-5641.

Chapter 7 Fabrication and Testing of Low-Parasitic Quantum-Well Disordered Two-Section Tunable Laser

7.1 Introduction

In this chapter the fabrication and testing of the final AlGaAs/GaAs tunable laser structure is described. This laser incorporates a quantum-well disordered tuning section to give reduced loss and loss variation with tuning in the tuning section, drawing on the techniques described in Chapter 6. It also offers a much increased upper limit to the FM frequency response through the use of low parasitic contacting techniques, drawing on work from Chapter 5. After describing the fabrication procedures used in Section 7.2, the static light/current characteristics and spectral behaviour are described in Section 7.3, including measurements to confirm the effectiveness of the quantum well disordering techniques. Section 7.4 describes the linewidth measurements made on the laser. Static tuning characteristics are presented in Section 7.5, with dynamic tuning characteristics presented in Section 7.6. Finally, Section 7.7 gives conclusions for the work and suggests areas for further development.

7.2 Device Fabrication Procedures

7.2.1. Device fabrication processes.

In order to achieve a low parasitic capacitance laser we adopted air-bridge and polyimide coating planarisation techniques in our laser fabrication procedures. Together with our well-developed band gap shifting and etched isolation techniques, we successfully fabricated band gap shifted two section lasers with low parasitic capacitance. The air-bridged and polyimide planarised laser processing is described below.

7.2.2. Air-bridge laser fabrication.

The laser is fabricated on a semi-insulating substrate. First, band gap shifting is carried out as high temperature annealing is required. The whole wafer is coated with PECVD SiO_2, and by using photolithography and wet etching in HF the SiO_2 layer covering the gain section is removed. The wafer is then exposed to Ar+ plasma in a reactive ion etcher for 5 minutes to retain the exciton peak position for the gain section during RTA. The wafer is then transferred to the Surrey Ion Beam Facility for RTA at 940°C for 1 minute. Spontaneous emission spectra measurements from lasers made from gain

or tuning section material confirmed that a 7nm exciton peak shift was achieved. A longer anneal time will result in larger de-tuning.

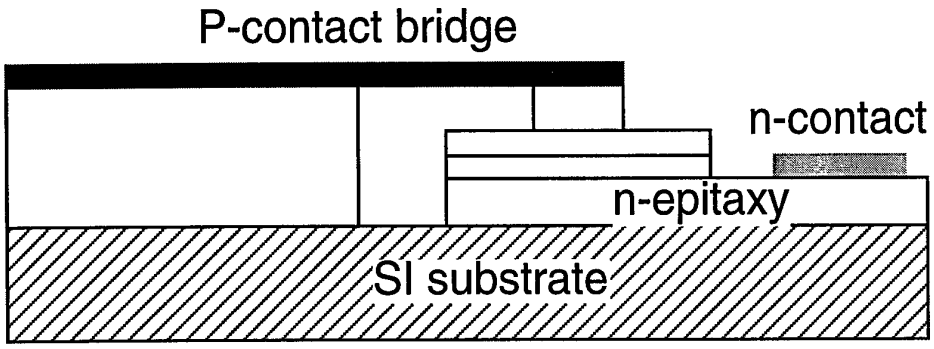

Figure 7.1 *Structure of air-bridged laser*

The wafer now is ready for normal ridge waveguide laser processing to realise the structure of Figure 7.1. Due to epitaxial growth calibration errors, no accurate actual epitaxy layer thickness data is supplied. As the ridge height is so crucial to single mode lasing performance an extra processing run was carried out using a wafer from the same growth run, but using an N+ substrate and without band gap shift. A series of ridge etch depths ranging from 1.4 μm to 1.9 μm were used. From the threshold current and far field pattern test, the optimum ridge depth was found to be 1.7 to 1.85 μm, instead of the designed 1.3 to 1.5 μm. Wet etch is used to achieve a 1.75 μm ridge depth on the band gap shifted wafer, with a ridge width of 4 μm.

In order to have suitable electrical isolation between the two sections, a 30μm gap is etched in the ridge between the two sections with etch depth 0.5 to 0.7 μm. The next step is to etch on one side of the ridge, down to the N+ contact layer. As the required etch depth is quite deep (4.5 to 5 μm), thicker resist and faster etch rate are needed. $H_2SO_4/H_2O_2/H_2O$ etchant is used to give an etch rate of ~2 μm/min. On the other side of the ridge, another lithography/etch step is used to make an 10μm wide gap surrounding the p-bonding pad with etch depth as deep as 10 μm down to the SI substrate. The wafer is then coated with 400nm SiO2 by PECVD, and a window is opened by lithography/and wet etch onto the n-contact site. GeAu/Au is used as the n-contact metal and lift-off is used to pattern the metal. A two-layer p-contact metal system is used for p-contact. First, a 4 μm wide-line window is opened on the ridge and Zn/Au/Ni/Au metal is deposited as the first p-contact metal. Low contact resistance is achieved by using such a metal system. Second, in order to ensure a continuous metal layer bridge from bonding pad to the ridge, the deep isolation gap between the bonding pad and the ridge is filled with thick photoresist followed by thick Au evaporation (~400nm), using a rotating tilted stage so that good coverage is

achieved. The Au is then etched to the pattern required by photolithography and wet etch, followed by removal of the unwanted support photoresist. The substrate is then thinned down to ~100 μm and a Au/Sn/Au metal is deposited on the backside to achieve good eutectic bonding to the heat sink at a later stage.

7.2.3. Polyimide coated laser

The laser is fabricated on an N+ substrate to give the structure shown in Figure 7.2. The fabrication procedure is the same as described above for the air-bridged laser until the completion of the ridge isolation gap etch between the two sections.

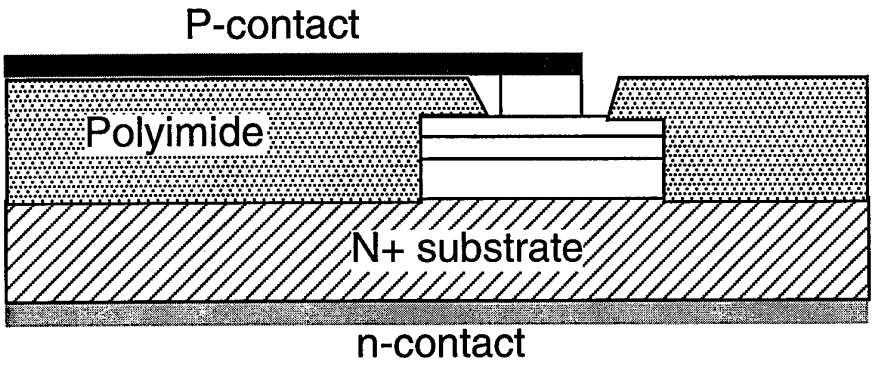

Figure 7.2 *Polyimide contacted laser*

Instead of etching down on one side of the ridge to the N+ contact layer we now etch on both sides of the ridge down to ~3 μm, to leave a ~20μm wide junction. 400nm thickness SiO_2 is then deposited by PECVD on the wafer. The wafer is then carefully cleaned and coated with polyimide (Pirl II), to a thickness of ~4 μm. It is then baked at temperatures 120, 150, 200 250 and 300 °C, each for 30 minutes, to achieve half-curing. Photolithography is then used to open a 6μm line-window on the polyimide above the ridge and the polyimide is removed by positive resist developer. It is crucial to ensure polyimide is removed completely from the ridge, or the device will not lase. As normally residual polyimide is left behind after such a removal process, the wafer is etched in acetic acid to clean the residual. Another lithography step is followed to open a 4 μm width window above the ridge to permit removal of the SiO_2 from the ridge. The wafer is then processed as for the air-bridged laser to obtain the two-layer p-contact metallisation. After thinning the substrate, n-contact metal (GeAu/Au/SnAu) is deposited on the backside of the wafer.

7.3. L-I and Optical Spectra Results

Successful room temperature CW operating lasers were fabricated using both contacting techniques. Optical spectra show that single mode operation with better than 10 dB MSR is achieved over a very wide gain section bias current range.

7.3.1. Air-bridged lasers

Figure 7.3 shows L-I plots for the air-bridged laser with tuning section open or shorted. Figure 7.4 shows the corresponding optical spectra when gain section current ranges from 48mA to 80mA. It is seen single mode operation is achieved over this current range.

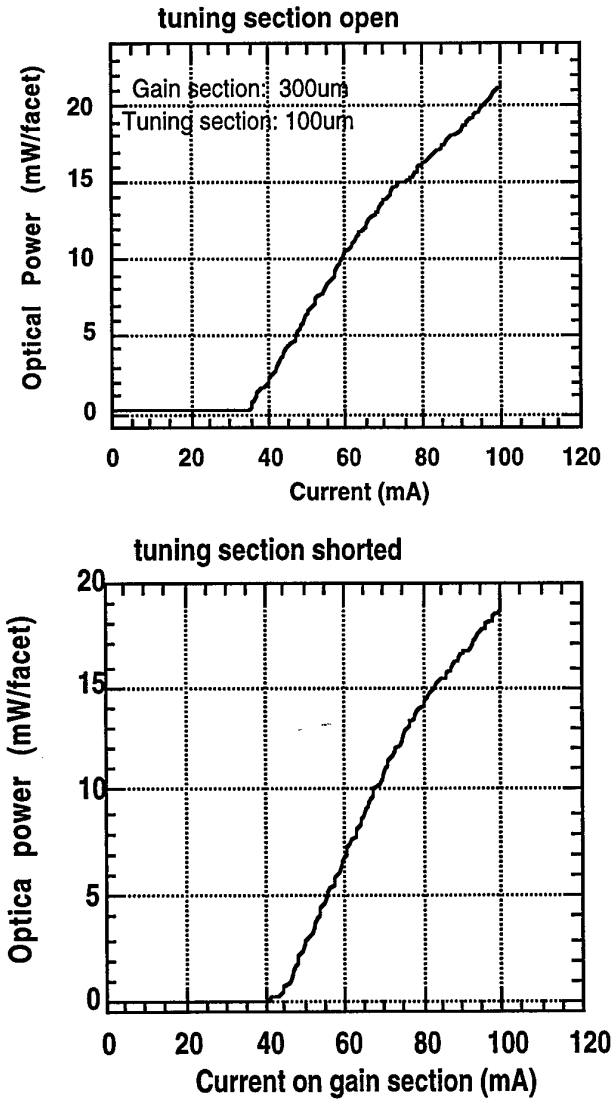

Figure 7.3 *L-I plots for air-bridged laser*

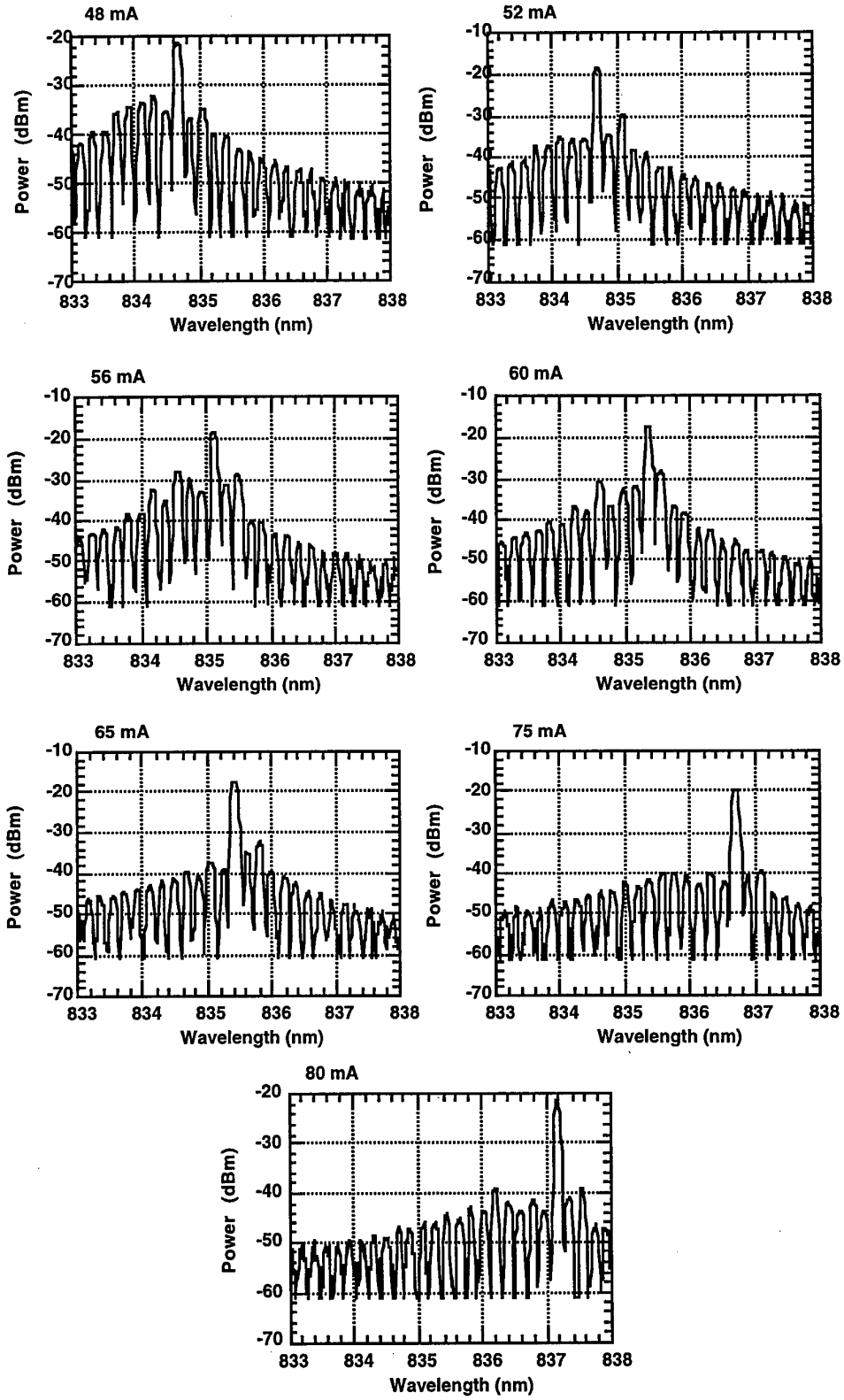

Figure 7.4. *Optical spectra of air-bridged laser.*

7.3.2. Polyimide coated laser

Figure 7.5 shows the L-I plots for tuning section open and shorted. Figure7.6 shows the optical spectra for different gain section currents , when the tuning section is shorted. It is seen better than 10 dB MSR is achieved over a 30mA current range.

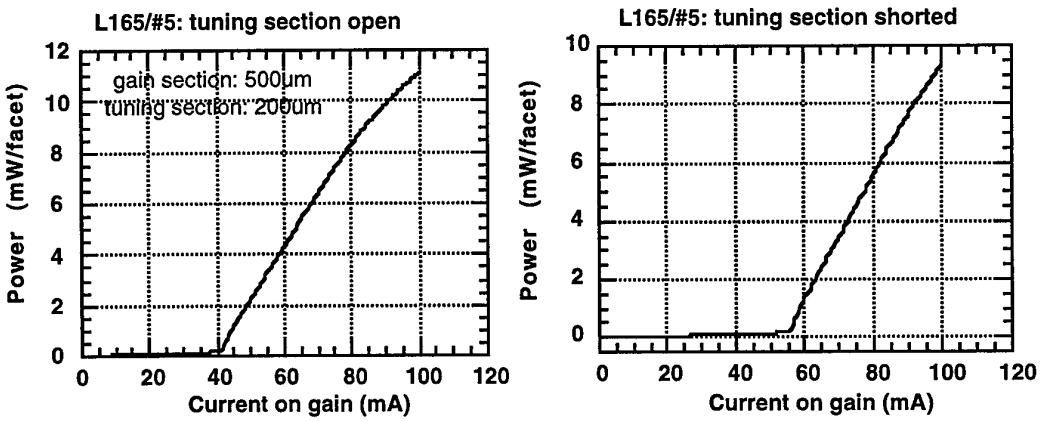

Figure 7.5 *L-I plots for polyimide coated laser.*

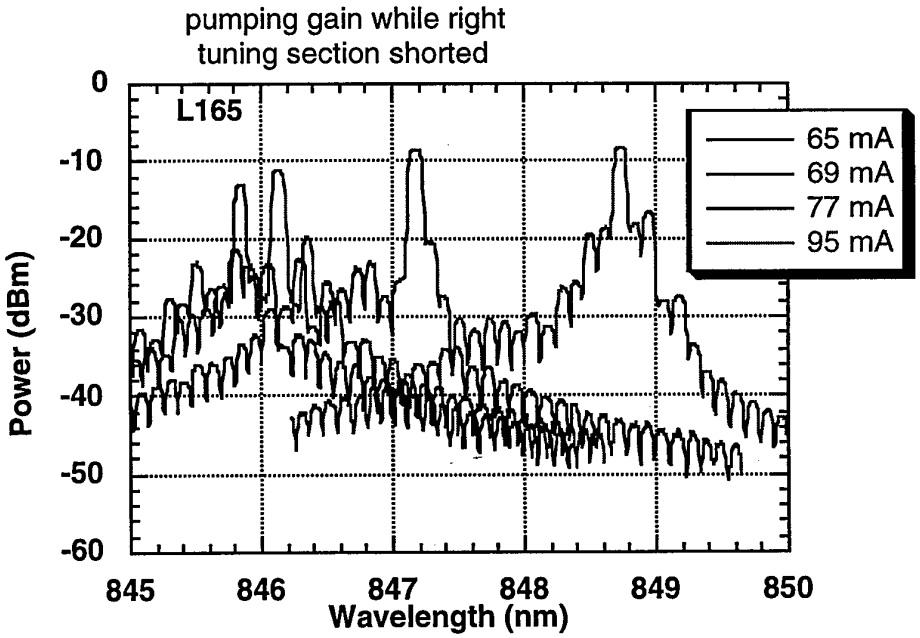

Figure 7.6. *Optical spectra of polyimide coated laser.*

7.3.3. Disordering process characterisation.

In order to confirm the shift of exciton peak and the de-tuning between gain and tuning section, single section lasers cleaved from gain section or tuning section were checked at just below threshold current, as shown in Figure7.7. It is seen that 7 nm detuning was achieved after a 1 minute anneal at 940°C.

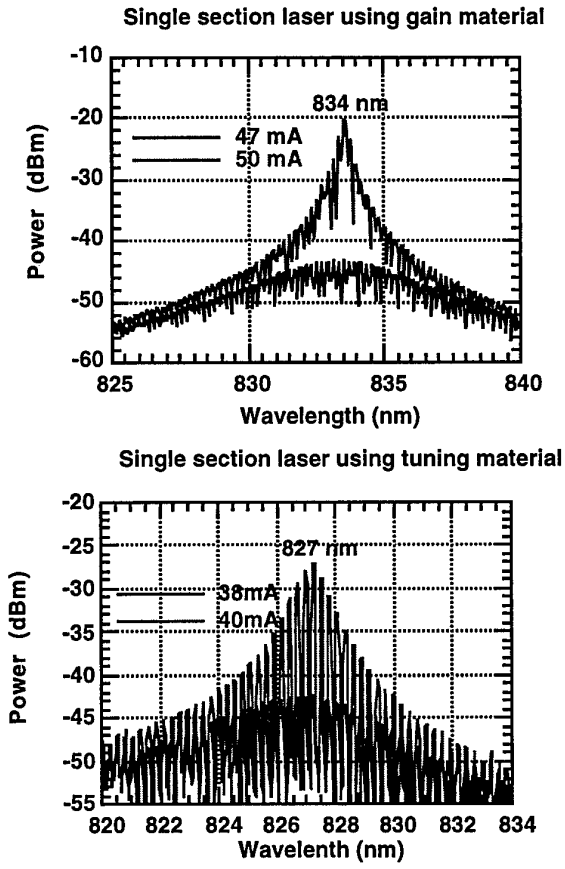

Figure 7.7. *Exciton peak de-tuning between gain and tuning section.*

A further test on a polyimide coated two section laser fabricated on an N+ substrate with band gap shifting by a 2 minute anneal at 940°C is shown in Figure 7.8, where the pumping current is applied to the short tuning section (100μm) while the long gain section (400μm) is left open. Spontaneous emission energy is absorbed by the gain section where the exciton peak is at longer wavelength, and photoluminescence occurs, resulting in a twin-peaked emissionspectrum. It is seen that 20nm de-tuning is achieved.

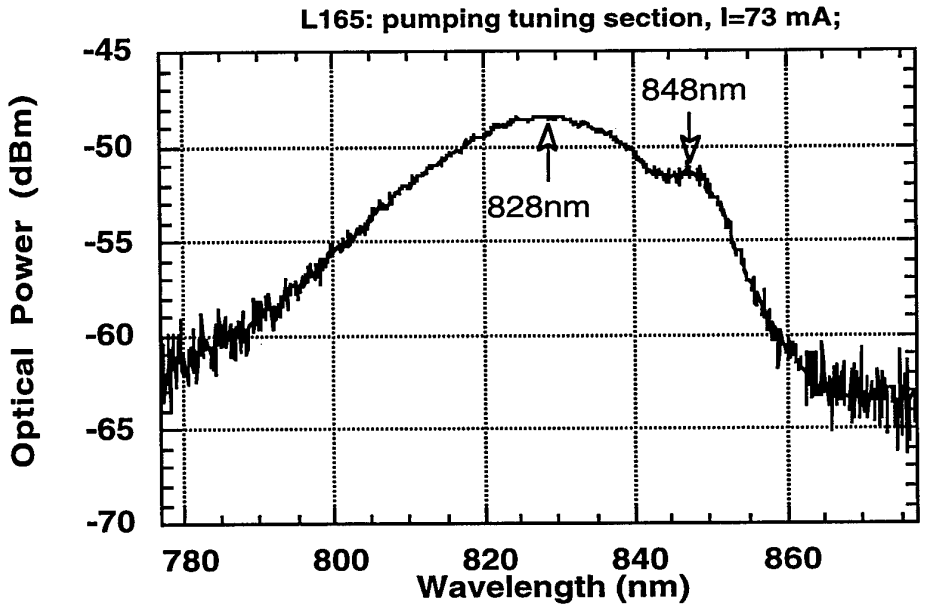

Figure 7.8 Emission spectrum from a polyimide coated two section laser with tuning section only pumped.

7.4 Linewidth measurement results

Line width measurements were made on an air-bridged two-section laser by using a self-homodyne system. Figure 7.9 shows the measured and Lorentzian fitted curve. Figure 7.10 shows the linewidth variation with optical power output and its inverse. It is seen that the linewidth varies between 8 and 11 MHz and follows the theoretically predicted reciprocal power dependence.

An estimate of the expected linewidth can be obtained from the modified Schawlow-Townes equation [7.1]

$$\delta f = \frac{hc\mu}{2\pi\lambda P\tau_p^2}\left(1+\alpha_H^2\right) \qquad (7.1)$$

where μ is the inversion parameter given by

$$\mu = \frac{N_{2t}}{N_{2t}-N_{1t}} \qquad (7.2)$$

and τ_p the photon lifetime given by

$$\tau_p = \frac{n}{c\left[a - \frac{1}{l}\ln\sqrt{R_1 R_2}\right]} \tag{7.3}$$

with P the intracavity power, α_H the Henry factor, N_{1t} the ground state threshold density, N_{2t} the inversion state threshold density, n the cavity effective index, a the cavity loss factor, l the cavity length, R the facet reflectivities, h Planck's constant, $c$the velocity of light in vacuo and λ the wavelength.

Selecting appropriate parameters for our laser of P=10mW, λ=850nm, μ=0.3, α_H=3.5, with a=30cm^{-1}, R=0.3, l=0.6mm, and n= 3.4 giving τ_p = 2.3 ps gives a predicted linewidth of 2.8 MHz in reasonable agreement with measured values, considering the uncertainties in parameter estimation.

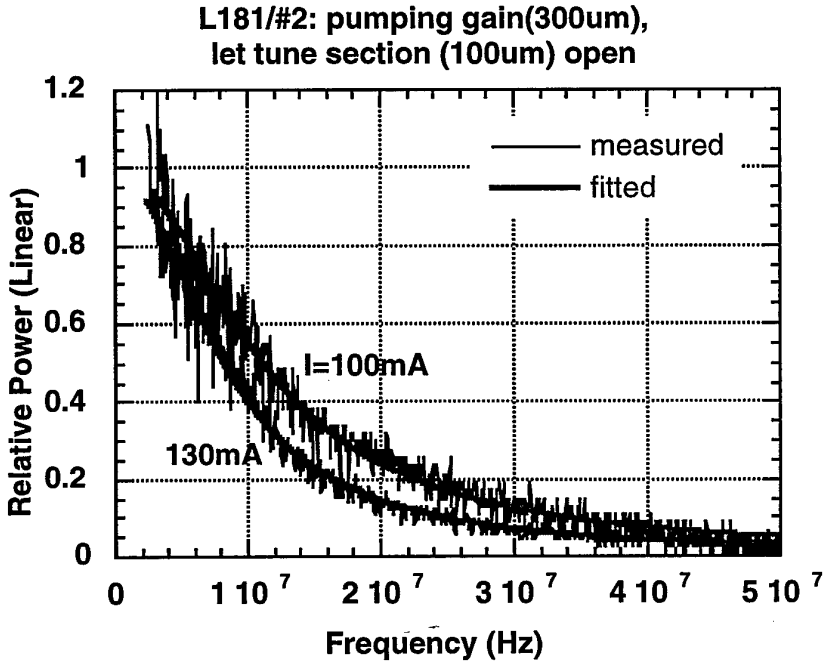

Figure 7.9 *Linewidth measurement and fitting results on an air-bridge two-section laser.*

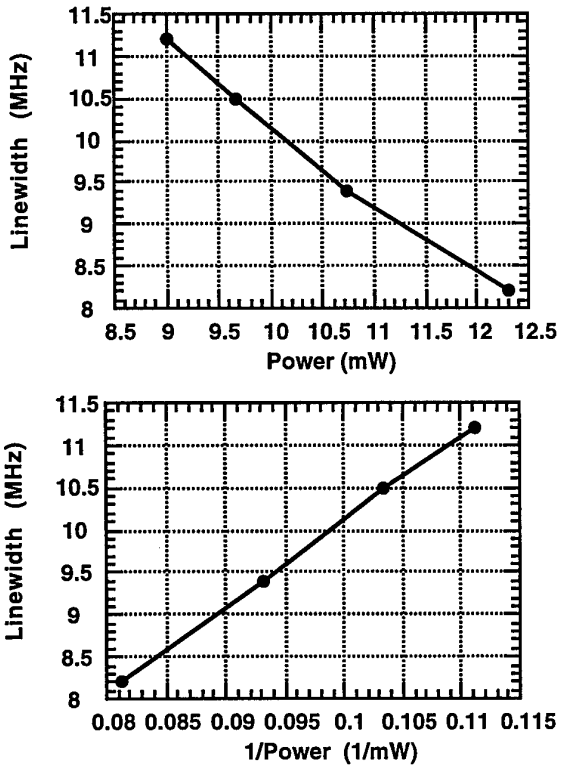

Figure 7.10 Linewidth variation with power.

7.5. Static Tuning Performance

The static tuning performance was evaluated using a high resolution scanning Fabry-Perot interferometer. A typical result is show in Figure 7.11. Linear tuning over nearly 25 GHz with slope 12 GHz/V is obtained. The direction of tuning is as expected for a tuning section having exciton peak shifted substantially shorter in wavelength than the operating wavelength. Linear characteristics such as these are highly attractive in optical FM systems, as discussed in Chapter 2.

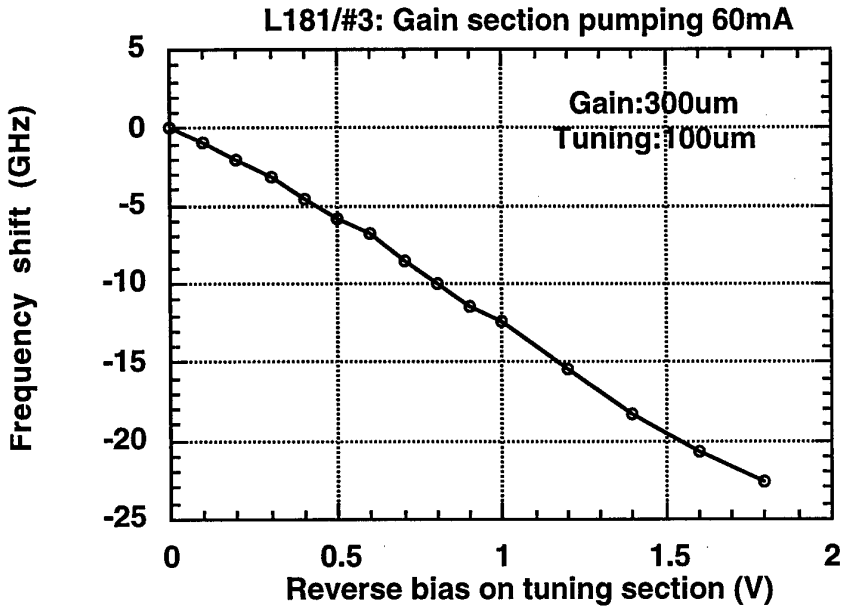

Figure 7.11 *Static tuning result of air-bridged two-section laser.*

7.6. Dynamic Tuning Performance

The purpose of fabricating air-bridge or polyimide coated lasers was to reduce the parasitic capacitance of the laser tuning section. Using a capacitance bridge tuning element capacitances of 1pF to 3pF were measured for the air-bridged laser with cavity lengths of 300 μm to 600 μm and 2 to 5 pF for polyimide coated laser with cavity length 300 μm to 800 μm, a reduction of an order of magnitude relative to the oxide isolated devices fabricated earlier in the programme. The geometrically calculated capacitance for the tuning element itself ranged from 0.8 pF to 2.5 pF so that it is clear that significant parasitic capacitance was present in the polyimide coated lasers. This is thought to be due to inadequate polyimide coating thickness, with a measured thickness of about 3 μm. For a 2 pF device capacitance and eliminating any other parasitic parameters a cut-off frequency of 3 GHz would be expected in a 50 Ω terminated system. In our experiments, as there is no specially designed low parasitic mount yet available, a normal laser mount was used for laser mounting and testing which added significant parasitic elements. The relatively long bonding wire (1 ~ 2 mm) in particular contributes a 1 nH to 2 nH inductance.

A F-P interferometer was used as an optical frequency discriminator to measure the dynamic tuning characteristics. The central frequency of the optical signal was set at the half way point of the discriminator characteristic by adjusting the voltage applied to the piezo-electric translators of the interferometer. FM responses were taken with

and without terminating impedances, and with the tuning section 0.6V DC reverse biased, as shown Figure 7.12 and Figure 7.13. Both static tuning and FM phase response measurements confirm the red shift, which is as expected. The FM response is uniform within ± 2.5 dB up to 2GHz, and then rolls off due to parasitic parameters. The FM efficiency is about 12.5GHz/V. With RF power -5dBm, a peak frequency deviation of 5.5GHz was achieved with residual IM index of ≤0.05. A specially interesting feature of this laser is that when the pumping current was varied from 56 to 80mA, the FM response stayed almost the same. Thus the optical output power and tuning performance can be controlled independently. This represents a great advantage over CIE tuned multi-section DFB lasers.

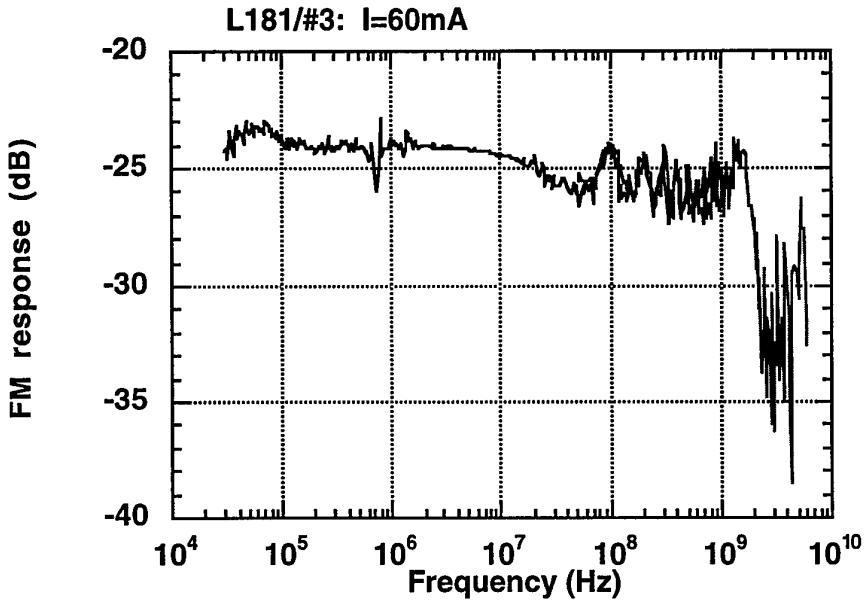

Figure 7.12. *FM response of air-bridged laser, without terminating impedance.*

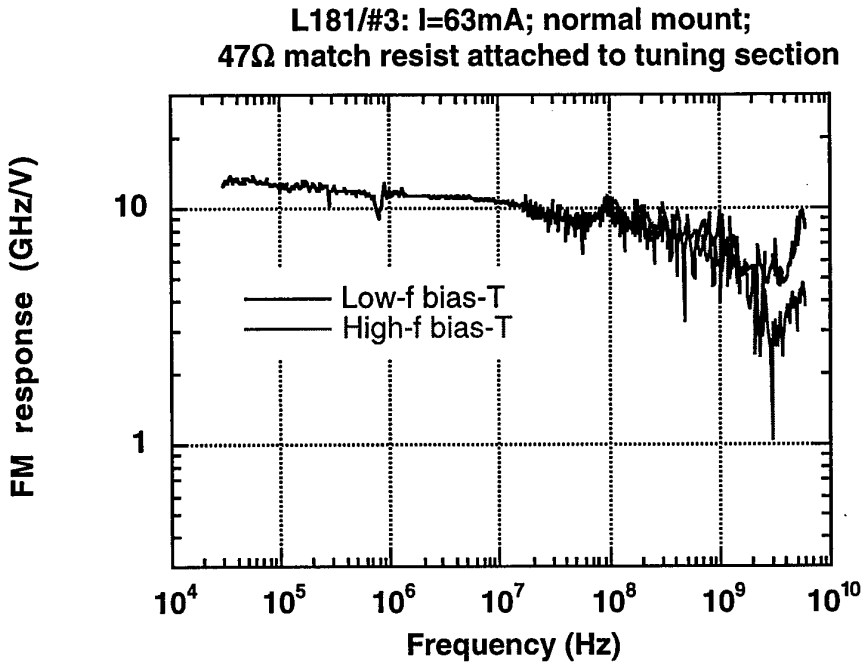

Figure 7.13. *FM response of air-bridged laser, with 47 Ω terminating impedance.*

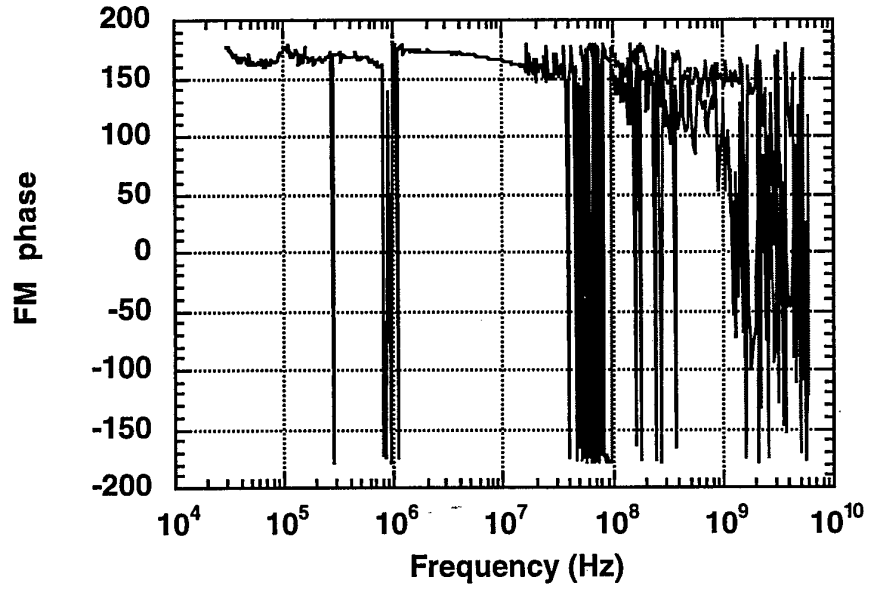

Figure 7.14. *As Figure 7.13, FM phase.*

7.7 Conclusion

In the fabrication of the lasers described above we have brought together the various techniques developed within this programme to produce reverse bias tuned quantum well lasers offering room temperature CW output power comfortably in excess of 10mW/facet, sidemode suppression exceeding 10 dB over 2:1 current ranges with best

values exceeding 20 dB, linewidths of < 10 MHz, FM tuning slopes of 12 GHz/V, residual intensity modulation below 5% for 5 GHz peak deviation and FM frequency response uniform within ± 2.5 dB from 10 kHz to over 2 GHz. When these lasers are mounted on microwave sub mounts we expect the upper cut-off frequency to be raised to between 3 GHz and 5 GHz. Further increases would be posssible by using more complex fabrication procedures. A specially attractive feature of these lasers is the independence of the tuning response from changes in gain section bias current, in complete contrast to current tuned lasers.

Although the oxygen implantation isolation technique was fully developed for use in this laser fabrication system it was not used for the lasers reported here because sufficient isolation could be obtained using the etch isolation procedures. Nevertheless, a fabrication run using oxygen implantation isolation is being carried out for completeness.

Future work will be focused on transferring the techniques developed to the InP/InGaAsP materials system to produce lasers directly applicable to systems applications in the third telecommunications window.

7.8 References

7.1. HENRY, C. H.:'Theory of the linewidth of semiconductor lasers', *IEEE J. Quantum Electron.*, 1982, . QE-18(2), p. 259.

Chapter 8 Preliminary Work on InP-Based Semiconductor Laser

As further work will transfer the techniques we have developed to InP based semiconductor lasers, we have started some exploration of this material system.

8.1 Tuning section design

Based on the absorption measurements in GaInAsP/InP MQW structure made by Kurita [8.1], we calculated the absorption change and refractive index change for 8nm InGaAsP (1.3 μm) well/10nm InP barrier with 5 wells/4 barrier MQW structure by using the Kramers-Kronig relations. Figures 8.1 to 8.3 show the results obtained. From these further calculations for the design of a two-section, QCSE tuned MQW InGaAsP/InP tunable laser can be carried out.

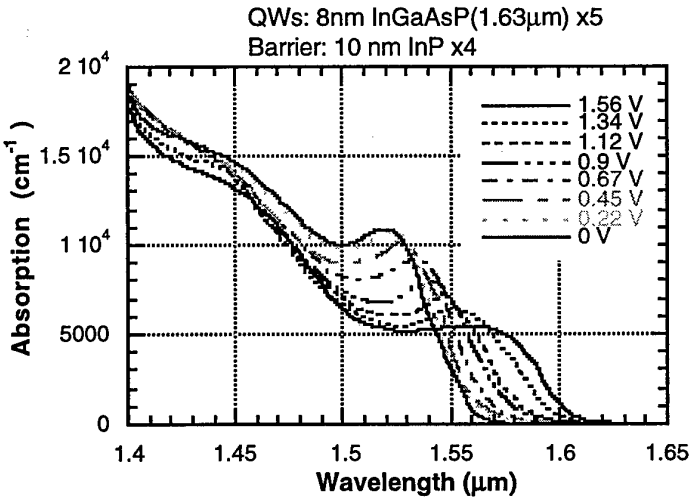

Figure 8.1 Measured absorption spectra for different reverse bias (after Kurita [8.1])

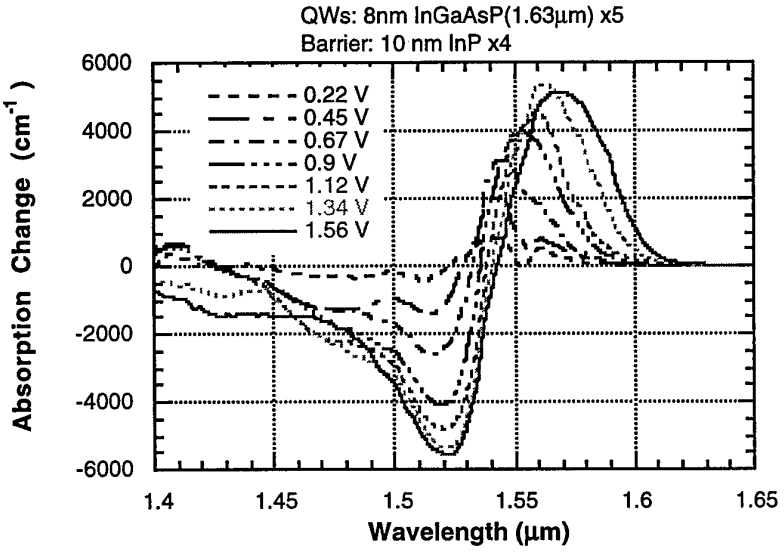

Figure 8.2 Absorption change spectra calculated from measured absorption.

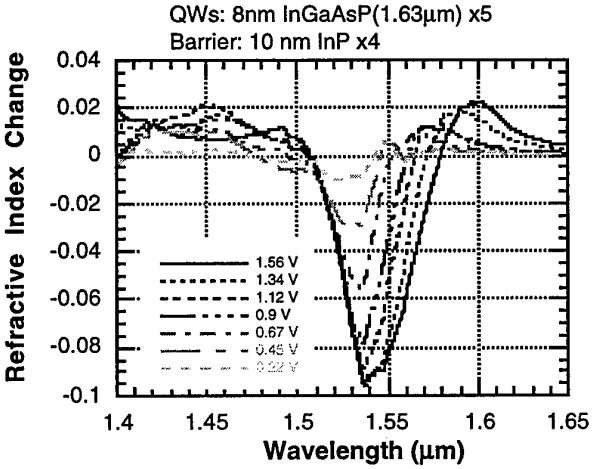

Figure 8.3 Refractive index change spectra calculated using K-K relations.

From the above results, we can decide the required tuning section length for π phase change as a function of bias and determine the insertion loss. Figures 8.4 and 8.5 show the results.

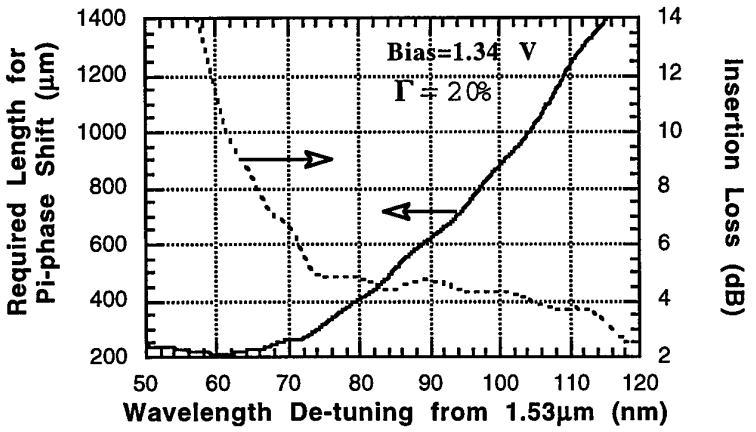

Figure 8.4 Tuning section length required for π phase shift (solid line) and the corresponding insertion loss (dashed line) for reverse bias 1.34V.

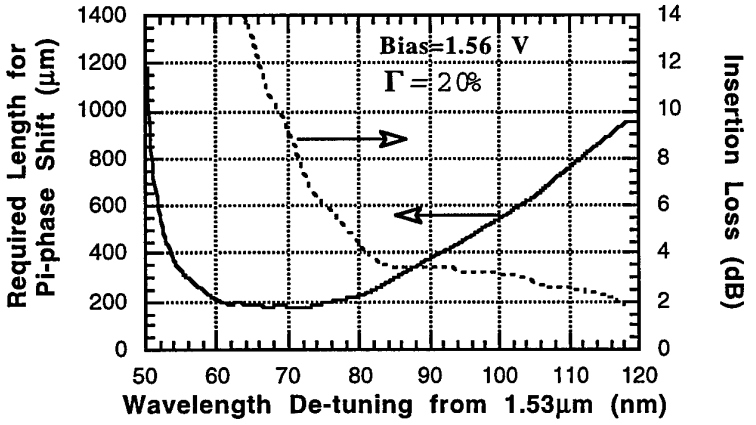

Figure 8.5 Tuning section length required for π phase shift (solid line) and the corresponding insertion loss (dashed line) for reverse bias 1.56V.

From these results, we can see that an InP tuning section generally requires much larger wavelength de-tuning (80~100nm from the zero bias e1-hh1 exciton peak) compared to the GaAs system. This is probably an intrinsic property of the InP system, due mainly to its lower exciton binding energy and higher phonon ionisation possibility [8.2], resulting in a lower oscillator strength and a less sharp absorption edge. It is also seen, that higher bias gives shorter tuning element length and lower insertion loss, as in the GaAs case.

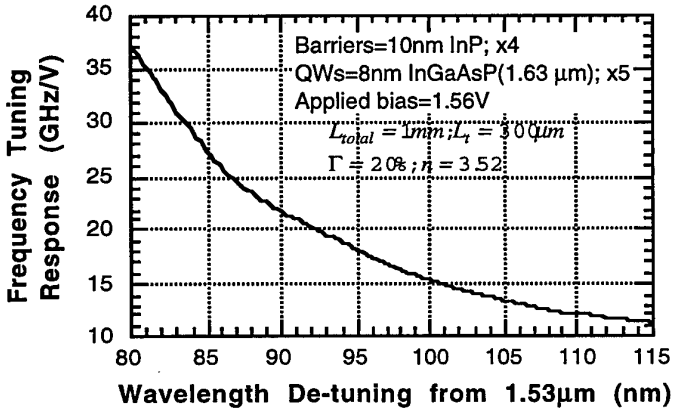

Figure 8.6 *Frequency tuning response spectrum for 300μm tuning section length in a 1mm long two-section laser for 1.56V applied reverse bias.*

Figure 8.6 shows the calculated tuning sensitivity variation with wavelength de-tuning for a tuning section length of 300μm in a 1mm long two-section laser with 1.56V applied reverse bias. For a minimum wavelength de-tuning from the zero bias exciton peak of 85nm, a tuning sensitivity variation of less than 3.5dB is obtained for a laser wavelength tuning range of 10nm, offering the possibility of a widely tunable laser for WDM application using the QCSE tuning technique.

8.2 Laser device fabrication

Initial attempts to fabricate InGaAs/InP and InGaAsP/InP active layer MQW lasers have been made. The designed epitaxial structures are shown in Figure 8.7, and the growth was carried out by Dr. Chris Button at EPSRC III-V Semiconductor Facility in Sheffield using AP-MOVPE. As both structures had not been grown at the Facility previously, the epitaxial quality is uncertain and successful stripe lasers were not obtained from the first run of supplied wafers. However, we had the chance to transfer our laser fabrication techniques from the GaAs system to the InP system. For example, using Zn/Au p-contact metal for 6μm stripe lasers, we achieved 10Ω series resistance at ~40mA pumping current, as shown in Figure 8.8, which is already slightly better than for our GaAs device.

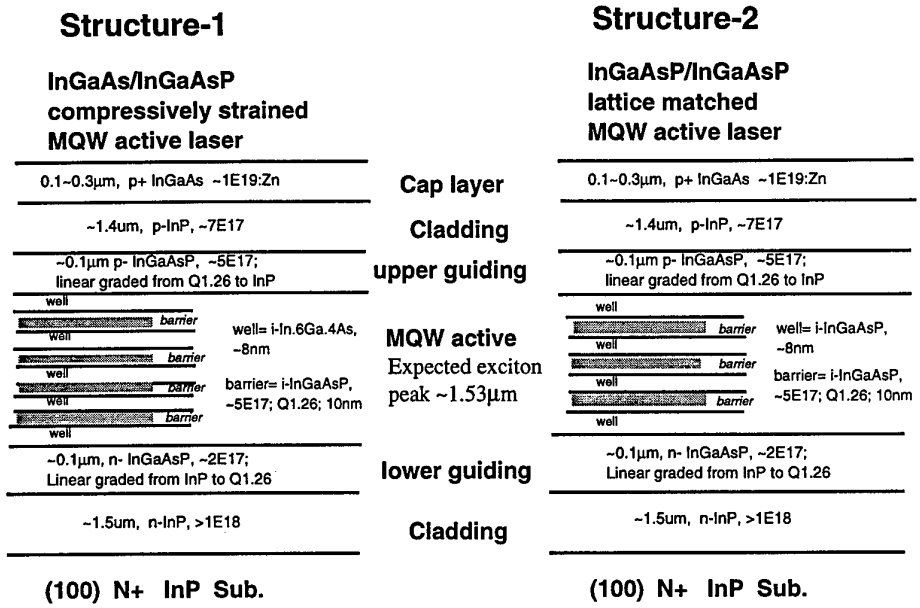

Figure 8.7 Two epitaxial structure designs for InP based lasers grown by MOVPE.

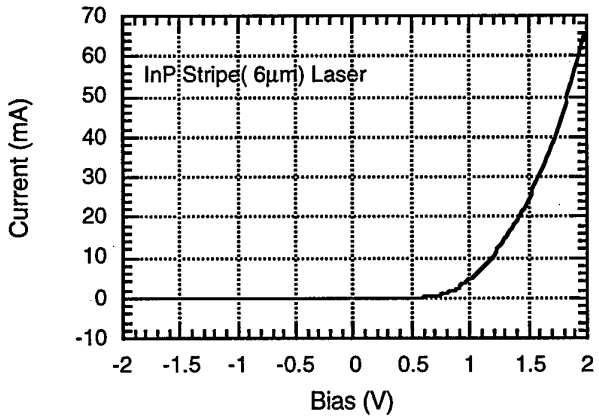

Figure 8.8 I-V plot for an InP based stripe laser.

For tunable laser applications, it is necessary to fabricate ridge waveguide lasers. However, in the InP material system using wet chemical etches it is quite difficult to achieve the same etch rate for InGaAsP and InP. It is equally difficult to have an anisotropic etch so as to obtain a vertically etched side wall. In processing experiments, we have found serious lateral etch effects (~3µm) in using wet etches to form the ridge, which destroyed any fine line of width below 6µm. Therefore, dry etch has to be used to define the ridge. Anisotropic dry etch could be realised by H_2/CH_4 reactive ion etch (RIE) [8.3]. By using our RIE facility and a SiO_2 mask, we have successfully achieved well defined 5µm ridges with total lateral etching less than

0.2μm, and a nearly straight side wall.

By using this dry etching technique, a ridge waveguide laser with 4μm ridge width has been processed. I-V characteristics for these devices showed low contact resistance but room temperature lasing was not obtained. Since a successful laser for room temperature CW operation is very much dependent on good quality epitaxial growth we are pursuing collaborations with Technion, Haifa (MOMBE), Dr. Dan Ritter, Centre for Electronic Materials, Imperial College, Professor G. Parry (MBE) and University of Maryland, LPS (MBE) in addition to our work with the Sheffield Facility on InP laser epitaxy. The collaboration with LPS has already proved fruitful. Figure 8.9 shows the measured CW light/current characteristics for a stripe laser test structure.

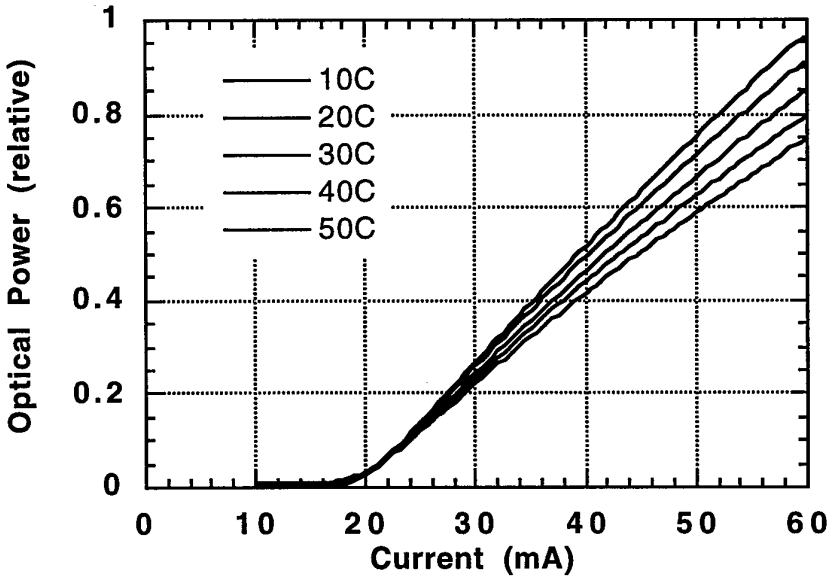

Figure 8.9 *Light current characteristic for InGaAsP/InP 50 μm x 200 μm stripe laser using LPS MBE-grown material.*

A calibrated measurement of output power was not made but the power was estimated at below 0.1 mW. This, combined with the very low threshold current and broad spectral output, is now the subject of a detailed study.

8.3 Fast Tunable Laser Design

Once we have succeeded in fabricating a satisfactory InP/InGaAsP MQW laser for room temperature operation we shall proceed to develop tunable laser structures. As shown in Section 8.1 a tuning range of 10 nm appears a practical goal. From our previous study of tunable lasers [8.4] integrated grating structures are required to give reliable single mode operation in the 1,550 nm wavelength band and such tunable lasers will require a large development effort to give the extremely narrow (kHz) linewidth performance we have obtained in our fiber grating laser (FGL) work, [8.5] and which, as discussed in Chapter 2 is essential for high performance optical FM links. We therefore plan to follow an evolutionary strategy that should deliver results of value to OFM systems at an early stage, while taking important steps towards the widely tunable structure. The first step is to realise an integrated QCSE tuned angled facet gain device which can be coupled to a fibre grating to give a narrow linewidth OFM source. As discussed in Chapter 3 and Section 8.1 the wavelength offset between gain section tuning section is critical to tuning performance. We shall follow two approaches to produce the required offset.

In the first evanescent wave coupling between a gain section grown above a narrower well waveguide layer is used. This approach has two advantages

1) Quantum well material for both gain and waveguide layers is grown in a single step, eliminating calibration drift between growth runs.

2) The waveguide layer can have a different number of wells from the gain layer, allowing separate optimisation of the two. This is particularly useful in controlling the confinement factor in the phase control section to obtain a convenient section length.

However, post growth adjustment of the offset is not possible and one overgrowth step is required.

The second approach, which eliminates the overgrowth step and allows post-growth optimisation is to grow a single gain and tuning layer and use quantum well disordering techniques to provide the offset between gain and tuning sections [8.6, 8.7]. This simplifies waveguide design but does not allow separate optimisation of the well number in tuning and gain sections.

Following successful realisation of QCSE tuned FGL devices for OFM systems we can then proceed to the tunable distributed Bragg reflector (DBR) laser shown in Figure 8.10. In this design coarse wavelength setting is achieved using CIE tuning of the grating section. The output power is maintained constant by adjusting the bias current applied to the gain section. Fine tuning and frequency modulation is achieved using the reverse biased phase control section. Such a laser can be fabricated in ridge guide form using a single overgrowth step.

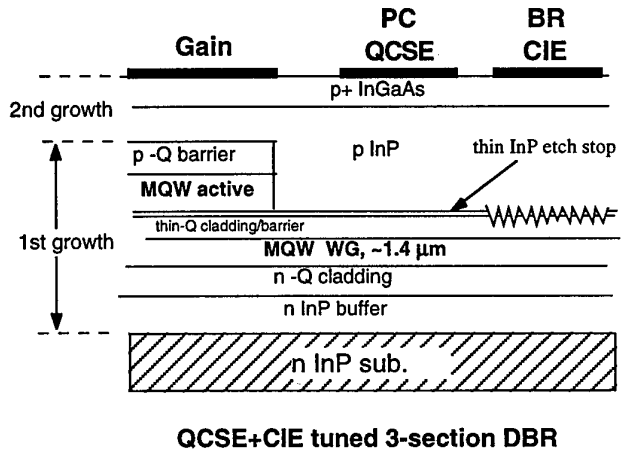

Figure 8.10 *QCSE-tuned three section DBR laser.*

Building on our experience with GaAs/AlGaAs ridge guide lasers we propose to fabricate all InP/InGaAsP tunable lasers as ridge guide structures in order to avoid the requirement for complicated overgrowth.

8.4 Conclusion

In this chapter we have reported our initial work aimed at extending the QCSE tuning concept to the InP/InGaAsP materials system to produce lasers for the 1,550 nm telecommunications window. We have estimated the required wavelength offset between the gain and tuning sections and shown that tunability over a 10 nm wavelength range should be possible while maintaining reasonable FM sensitivity.

In our initial fabrication experiments we have determined contacting parameters and fabrication procedures for stripe and ridge guide lasers in the InP/InGaAsP materials system and fabricated both types of lasers on two initial wafers grown by the EPSRC III/V Facility. Whilst good I-V characteristics, with low contact resistance, were displayed by the fabricated lasers, room temperature lasing was not obtained from the

first fabrication run. We are addressing this issue with a programme of wafer assessment, including evaluation of material from other sources of InP/InGaAsP epitaxy. Early results on MBE grown material from University of Maryland LPS are very encouraging.

Having identified the attractiveness of fibre grating lasers (FGLs) as sources for optical FM links in Chapter 2 we have developed a plan to realise FGL OFM sources at an early stage in our InP/InGaAsP laser programme. We shall then proceed to integrated grating tunable structures.

8.5 References

8.1 KURITA, Y., YOKOUCHI, N., MIYAMOTO, T., KOYAMA, F. and IGA, K.: 'Refractive index variation in GaInAsP/InP quantum confined structures grown by chemical beam epitaxy', *Jpn. J. Appl. Phys., Part 1*, 1995, 34(10), pp. 5626-5627

8.2. CHEMLA, D. S. and MILLER, D. A. B.:'Room temperature excitonic non-linear optical effects in semiconductor quantum well structures", *J. Opt. Soc. Am. B,* 1985, 2, pp. 1155-1173.

8.3. MCNAB, J. W. CRAIGHEAD, H. G., TEMKIN, H. and LOGAN, R. A.: 'Anisotropic reactive ion etching of InP in methane/hydrogen based plasmas', *J. Vac.Sci. Technol., B, 1991,* 9(6), pp. 3535-3537.

8.4. HUANG, X. and SEEDS, A. J.:'Wideband modulation and tuning of semiconductor lasers using novel quantum well structures', AFOSR Special Contract SPC-93-4072, Final Report, July 1995, pp. 2-26.

8.5 TIMOFEEV, F. N., BENNETT, S., GRIFFIN, R., BAYVEL, P., SEEDS, A.J., WYATT, R., KASHYAP, R. and ROBERTSON, M.:'High spectral purity millimetre-wave modulated optical signal generation using fibre grating lasers', submitted to *Electron. Lett.,* 1997.

8.6. MARSH, J. H.:'Quantum well intermixing', Semicon. Sci and Technol., 1993, 8, pp. 1136-1155.

8.7. MIYAZAWA, T, IWAMURA, H and NAGANUMA, M:'Integrated external-cavity InGaAs/InP lasers using cap-annealing disordering', Photonics Tech. Lett., 1991, 3, pp. 421-423.

Chapter 9 Conclusion

9.1 Summary of Programme

The objectives of this programme were to develop a quantum confined Stark effect (QCSE) tuned semiconductor laser and to investigate the potential of wide dynamic range optical frequency modulation analogue optical links using such lasers. The principal results of the work are summarised below.

9.1.1 Optical Frequency Modulation Links

Coherent analogue transmission systems were analysed and their performance compared with direct detection systems. The availability of high quality optical amplifiers for the 1,550nm optical fibre transmission window makes it possible to realise high quality IMDD transmission systems at that wavelength. For system spans beyond 100 km non-linear limitations in optical fibre, particularly stimulated Brillouin scattering (SBS), limit the maximum received optical power and hence the system dynamic range. The capability of coherent systems to select between many channels present on the same optical fibre makes them attractive in applications such as multiple antenna remoting. They also enable wide dynamic range transmission systems to be realised at wavelengths where high quality optical amplifiers are not available and for suitable modulation formats enable non-linear limits to be largely overcome.

Of the modulation techniques available for coherent systems, intensity modulation enables simple, linewidth insensitive links to be constructed. Frequency modulation offers the potential for modulated bandwidth signal to noise ratio trade-off at the expense of somewhat more exacting linewidth requirements and makes possible long distance wide dynamic range links. A key requirement in such systems is a source laser having narrow linewidth and uniform FM frequency response. This requirement can be met using the reverse biased quantum well laser tuning technique which has been studied in this programme, particularly if coupled with recently developed high performance fibre grating laser techniques.

For the future there is considerable scope for component development, leading to improved transmission system performance. Particular priorities for research include source modulator linearisation, narrow linewidth monolithic and fibre grating tunable laser development, the monolithic integration of OPLLs in opto-electronic integrated

circuit (OEIC) format to achieve wide demodulation bandwidth and improvements to receiver electronics to give enhanced demodulator linearity.

It is anticipated that whilst many single channel point to point transmission system requirements will be met by pre-amplified receiver IMDD systems, multi-channel and long distance networks will increasingly apply the coherent techniques discussed here. In particular the results of Chapter 2 indicate that signal to noise ratios of 156 dB.Hz at 1,000 km span and 142 dB.Hz at 5,000 km span could be achieved with suitably designed OFM systems.

9.1.2 Quantum confined Stark effect tuning modelling

The trade-offs between tuning section length and loss, FM sensitivity and residual intensity modulation, as a function of applied electric field and detuning between gain and tuning sections, have been analysed for the GaAs/AlGaAs materials system. The results show that for our device structure detunings of about 20 nm between the zero field e1-hh1 exciton peak wavelength and the emission wavelength are optimum. Since lasing normally occurs at an offset of about 10 nm to the red side of the peak a further shift of about 10 nm between tuning and gain sections is required.

9.1.3 Electrical isolation techniques

Good electrical isolation is necessary in order to enable a reverse bias to be applied to the tuning section without affecting the forward biased gain section. Three different schemes were studied: shallow etch isolation, H+ implanted isolation and O+ implanted isolation. In the shallow etch scheme, the top p^+-contact layer is removed by a wet etch in the transition area between gain and tuning sections, resulting in a reasonably high isolation resistance (1~15KΩ) between the two sections. This is due to the low p-type doping level in the upper cladding and guiding layer. This method has the attraction of relative simplicity but cannot eliminate diffusion leakage through the active region.

In the H+ implanted isolation scheme, protons were implanted in the isolation region but the depth was controlled to be above the core layer since it was found that H+ implantation into the guiding and active layer suppressed laser operation for a dose level of $3x10^{14}$ cm^{-2}, and degraded the laser performance seriously even at very low dose levels (10^{12}~10^{13} cm^{-2}). Even after rapid thermal annealing (RTA) at an elevated temperature (200 - 500 °C), no full recovery of device performance was obtained in

contrast to some predictions. This result indicated that the defects and deep energy levels associated with proton bombardment were very harmful to the laser diode and difficult to remove, therefore, great care has to be taken in choosing implantation depth and doses.

Dramatic leakage current suppression was achieved by using the O+ implantation scheme where O+ was implanted through the whole upper cladding and guiding (including the active) layers to achieve a strict isolation between gain and tuning section. The key factors in achieving a CW laser with this isolation scheme are the selection of suitable implantation doses and the RTA condition. Due to hopping conductivity in the post-implanted sample, the resistivity is low for non-annealed or annealed below 500°C samples, but the optical loss is high due to implantation damage. After annealing at temperatures between 600 ~ 700 °C the sample shows maximum resistivity with acceptably low optical loss (judged by the fact that no obvious threshold current increase compared to the lasers made from the same wafer but with no implanted region). Annealing at higher temperature reduces the resistivity dramatically with no further significant optical loss reduction. A room temperature CW operating laser with threshold current 34mA and isolation resistance 600MΩ ~ 2GΩ was achieved.

9.1.4 Low parasitic contacting techniques

The main limitation on the maximum tuning speed for the QCSE tuned laser stems from the parasitic capacitance of the tuning section. Two processes were developed to minimise this: the air-bridged contact technique, described in Chapter 5 and the polyimide technique described in Chapter 7. The air bridge technique requires a semi-insulating substrate and elaborate processing but gives parasitic capacitance limited by the mesa width of the laser. The polyimide technique can use an N+ substrate and offers much simpler processing but suffers two disadvantages. First, it is hard to obtain the polyimide thicknesses required to give negligible parasitic capacitance. Second, special arrangements have to be made to facilitate cleaving and contacts on polyimide tend to peel in bonding. With state of the art processing cut-off frequencies of about 40 GHz should be obtainable with either technique.

9.1.5 Quantum well disordering techniques

In our tunable laser structures we require a shift of about 10 nm to add to the normal offset of the laser gain peak from the e1-hh1 exciton absorption peak, so as to give

total detuning close to 20 nm for optimised tunable lasers. We have studied a range of capped annealing techniques for this purpose. Adequate shifts were not obtained for the SiO_2:P/SiO_2 technique and we suspect that this may be due to lack of doping control at the deposition stage. The SrF_2/SiO_2 technique gives very reproducible shifts but careful control of SrF_2 deposition conditions is required to maintain surface morphology adequate for high quality laser fabrication. Recent work on uncapped/SiO_2 and Ar+ etched/SiO_2 techniques indicates that reproducible shifts with good surface morphology are obtainable. These are therefore the preferred techniques for laser fabrication.

9.1.6 Realisation of QCSE tuned laser

We have brought together the various techniques developed within this programme to produce reverse bias tuned quantum well lasers offering simultaneously room temperature CW output power comfortably in excess of 10mW/facet, sidemode suppression exceeding 10 dB over 2:1 current ranges, with best values exceeding 20 dB, linewidths of < 10 MHz, FM tuning slopes of 12 GHz/V, residual intensity modulation below 5% for 5 GHz peak deviation and FM frequency response uniform within ± 2.5 dB from 10 kHz to over 2 GHz. When these lasers are mounted on microwave sub mounts we expect the upper cut-off frequency to be raised to between 3 GHz and 5 GHz and indeed subsequent to the major work on this report being completed an upper cut-off frequency of over 6 GHz has been achieved. Further increases would be posssible by using more complex fabrication procedures. A specially attractive feature of these lasers is the independence of the tuning response from changes in gain section bias current, in complete contrast to current tuned lasers.

Although the oxygen implantation isolation technique was fully developed for use in this laser fabrication system it was not used for the lasers reported here because sufficient isolation could be obtained using the etch isolation procedures. Nevertheless, a fabrication run using oxygen implantation isolation is being carried out for completeness.

9.1.7 InP/InGaAsP QCSE tuned lasers

Preliminary studies on the transfer of this work to the InP/InGaAsP materials system have been carried out towards the objective of producing lasers for the 1,550 nm telecommunications window. We have estimated the required wavelength offset between the gain and tuning sections and shown that tunability over a 10 nm wavelength range should be possible while maintaining reasonable FM sensitivity.

In our initial fabrication experiments we have determined contacting parameters and fabrication procedures for stripe and ridge guide lasers in the InP/InGaAsP materials system and fabricated both types of lasers on two initial wafers grown by the EPSRC III/V Facility. Whilst good I-V characteristics, with low contact resistance, were displayed by the fabricated lasers, room temperature lasing was not obtained from the first fabrication run. We are addressing this issue with a programme of wafer assessment, including evaluation of material from other sources of InP/InGaAsP epitaxy. Preliminary tests on material grown by the University of Maryland LPS have shown room temperature CW thresholds as low as 20 mA, although the output power was low and the emitted spectrum broad. Further investigation is in progress.

9.2 Future Work

This programme has established by analysis that the use of optical frequency modulation can allow the realisation of wide dynamic range analogue optical links with spans in the 100 km to 10,000 km range, where intensity modulation techniques suffer severely from non-linear propagation effects. A further attraction is the elimination of amplifier induced crosstalk in multi-channel wavelength division multiplexed systems. A system demonstrator programme to test these predictions experimentally would be desirable.

The programme has been successful in demonstrating a QCSE tuned laser having exceptionally ($\pm$ 2 dB) uniform FM frequency response at frequencies up to 6 GHz. A great attraction relative to carrier injection effect tuning is that the response is maintained almost independently of gain section pumping current.

The above two achievements indicate the main priority for future work as being the transfer of the QCSE tunable laser technology to the InP/InGaAsP materials system for operation in the third telecommunications window. The ultimate target for this work is to realise a source offering a total tuning range of about 10 nm combined with the fast and uniform tuning characteristics offered by the QCSE tuning technique.

Having identified the attractiveness of fibre grating lasers (FGLs) as sources for optical FM links in Chapter 2 we have developed a plan to realise FGL OFM sources at an early stage in our InP/InGaAsP laser programme. We shall then proceed to integrated grating tunable structures.

Appendix 2.1: Analysis and Experimental Demonstration of Optical FM Systems

SB

Optical Frequency Modulation Links: Theory and Experiments

Bo Cai and Alwyn J. Seeds, *Fellow, IEEE*

Abstract—**In this paper, the first theoretical analysis and experimental realization of an optical frequency modulation coherent detection (FMCD) link working at microwave frequencies is reported. Advantages over conventional optical intensity modulation direct detection (IMDD) links in terms of reduced effects of fiber nonlinearity, facilitation of multichannel operation, and bandwidth/signal-to-noise ratio (SNR) tradeoffs are identified. A detailed theoretical analysis of the SNR of FMCD links is carried out and compared to that for IMDD links. In the experimental FMCD link, a novel source laser tuning technique, based on the quantum confined Stark effect, is used. The experimental results are presented and compared with the predictions of the theoretical analysis.**

Index Terms— **Coherent optical communication, microwave photonics, optical fiber links, quantum well, semiconductor laser.**

I. Introduction

OPTICAL fiber provides a wide optical transmission bandwidth for analog optical links. Currently, most optical analog transmission systems use optical intensity modulation direct detection (IMDD) of the modulated optical signal in a depletion photo-detector [1], [2] and only utilize a fraction of this available bandwidth. In such a system, although the link dynamic range can be improved significantly by high power sources and optical amplifiers, as shown later in this paper, it is limited ultimately by shot noise and transmission medium (fiber) nonlinearity [3], [4].

An alternative approach, which can overcome these limitations, is to use optical frequency modulation coherent detection (FMCD) of the transmitter [5]. In such an approach, the signal is carried by the frequency rather than the intensity of the transmitter output. Apart from high signal-to-noise ratio (SNR), this approach also has advantages of constant transmission power, high detection sensitivity, and multichannel transmission capability.

An FMCD link consists of transmitter, receiver, and transmission medium, usually single-mode optical fiber. A frequency tuneable light source is used in the transmitter to convert an incoming electronic signal to an optical FM signal. At the receiver, the signal is down-converted using an optical local oscillator and detected by a depletion photo-detector. Demodulation is then carried out by an electronic frequency discriminator.

In this paper, optical FM analog links are analyzed and the first experimental demonstration is reported, including the use of a novel tuneable laser as the transmitter. In Section II, the performance of an FMCD link is analyzed in terms of its signal-to-noise ratio. Comparison is made with the SNR limits of IMDD links to demonstrate the advantages of the FMCD link. In Section III, the FMCD link experiment is detailed and link bandwidth and SNR results are presented. Conclusions are drawn in Section IV.

II. Basic Concept and Advantages of an Optical FMCD Link

An optical FMCD system is a direct emulation of RF FM broadcast and communications systems in the optical domain and uses the same basic concepts. In an optical link, the laser output provides a carrier of very high frequency (200–400 THz). As with RF carriers, there are two independent characteristics, amplitude and phase or frequency, which can be modulated with the signal to be transmitted. In optical FM (OFM) the carrier frequency deviates from its central frequency proportionately to the amplitude of the signal to be transmitted. Both random and impulse noise can be reduced by using a wide passband receiver containing an amplitude limiter. Therefore, for received carrier to noise ratios much greater than unity, FM systems can provide improved SNR relative to amplitude modulated systems.

The OFM system has three main features which distinguish it from its RF equivalent. First, the optical carrier frequency is very high relative to the bandwidth of the signal to be transmitted. As a result, a large frequency deviation relative to the signal bandwidth can easily be achieved with good linearity. On the other hand, a small relative carrier frequency drift will be significant compared with the signal bandwidth. Second, because no photo-detector has a bandwidth matching the optical carrier frequency, either demodulation in the optical domain or down conversion of the received signal from optical frequency to a much lower intermediate frequency is needed. Third, due to the high optical carrier frequency, the laser generates far more phase/frequency noise than an RF oscillator. This noise has to be considered in an optical FMCD link and, in fact, can be the major limiting factor on the signal-to-noise ratio.

The basic advantages of an FM system are well documented [6], [7]. The work reported here concentrates on the SNR

Manuscript received April 15, 1996; revised December 24, 1996. This work was supported by the U.K. Department of Trade and Industry/Science and Engineering Research Council LINK Opto-electronic Systems Program through the Wideband Optical Radio Frequency Networks (WORFNET) Project.

The authors are with the Department of Electronic and Electrical Engineering, University College London, London WC1E 7JE U.K.

Publisher Item Identifier S 0018-9480(97)02529-5.

performance of the FMCD link and the performance with that of the contrasts' well-established IMDD link.

A. SNR Limits of IMDD Links

In an IMDD system, as shown in Fig. 1, the analog signal to be transmitted can be represented by $m(t)$. The optical power at the detector is

$$P_o = P_u[1 + \gamma m(t)] \tag{1}$$

where P_u is the mean received optical power and γ is the modulation sensitivity ($\gamma m(t) > -1$).

The mean squared signal current at the detector output is

$$\langle I_s^2 \rangle = (RP_u\gamma)^2 \langle m^2(t) \rangle \tag{2}$$

where R is the photodiode responsivity.

Noise arises from the transmitter, any optical amplifiers used, and the photodetector. Fundamentally the noise is limited by the quantum nature of photon-matter interaction [8]. Taking into account the thermal noise of the electric circuit and the effective signal bandwidth B, can be derived the current variance for the whole link as

$$\sigma_I^2 = B[(RP_u)^2 RIN + 2qRP_u + 2P_nP_uR^2 + (2\Delta f_{\text{op}} - B)P_n^2R^2 + 4kT/R_l] \tag{3}$$

where RIN represents the excess intensity noise due to noncoherent behavior of the transmitter, q is the electronic charge, $P_n = 2hfG(l)\int_0^l g(z)/G(z)\,dz$ is the optical amplifier spontaneous emission (ASE) noise, l is the total link length, $g(z)$ is the gain coefficient at position z, $G(z) = \exp\{\int_0^z [g(z') - \alpha(z')]\,dz\}$ is the total link gain/loss at position z, k is Boltzmann's constant, T is the absolute temperature, R_l is the receiver load resistance, and Δf_{op} is the link optical filter bandwidth. Electrical pre-amplifier noise is neglected in the derivation of the above equation.

The terms in (3) correspond to the amplified transmitter RIN, detector shot noise, ASE-signal beat noise, ASE-ASE beat noise and thermal noise, respectively. The SNR of the link can be written as (see (4) at the bottom of the page). The SNR can be improved by increasing the power received at the detector. The detector received power P_u is, however, limited by stimulated Brillouin scattering (SBS) in the transmission fiber. For the worst case of a source laser of narrow linewidth relative to the SBS gain bandwidth (30 MHz at 1.55 μm), the SBS threshold for P_u in nonpolarization preserving single-mode fiber is given by [9]

$$P_{\text{SBS}} = \frac{21\pi D_e^2 G(l)}{2g_B \int_0^l G(z)\,dz} \tag{5}$$

where D_e is the effective fiber core diameter and g_B is the SBS gain factor.

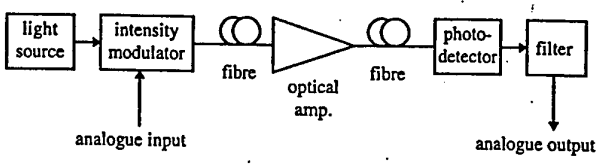

Fig. 1. IMDD transmission system.

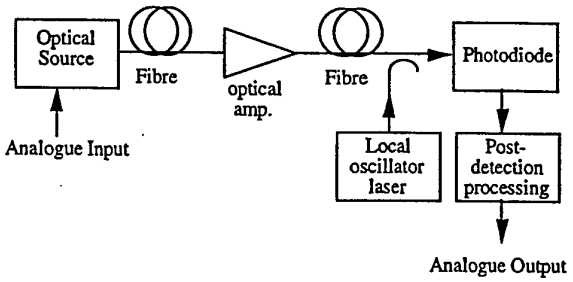

Fig. 2. Optical FMCD link.

Without optical amplifiers in the link, $g(z) = 0$. The SNR for such a passive IMDD fiber link with 100% modulation and $\langle m^2(t) \rangle = 0.5$ is plotted in Fig. 3. The results show a rapid SNR degradation with link length.

By inserting optical amplifiers in the link, the received optical power at the photo-detector will increase and so will the shot noise limited SNR. However, the optical amplifiers will also introduce ASE noise to the link. In an optimized transparent link, the signal is amplified by low gain, closely spaced optical amplifiers. In this ideal case, the optical gain can be considered distributed along the whole link exactly compensating the loss as it occurs. In such a case, if the fiber loss coefficient α is constant, then $g(z) = \alpha$, $G(z) = 1$, $P_n = 2hf\alpha l$. The SNR against link length for this case is plotted in Fig. 3. The results show that even in the ideally amplified case, the SNR of IMDD links is limited. For short links without optical amplifiers, the SNR is likely to be limited by RIN and shot noise and for long links with optical amplifiers, the SNR is likely to be limited by ASE. In reality, the SNR will be further reduced by other noise sources.

B. SNR Limits of FMCD Links

In an FMCD link, as shown in Fig. 2, the signal electric field at the photodiode is

$$E_s = \hat{E}_s \exp\left\{j\left[\omega_s t + 2\pi\Delta f \int_0^t m(\tau)\,d\tau + \varphi_s(t)\right]\right\}$$

where $\hat{E}_s$ and ω_s are the amplitude and frequency of the field, Δf is the maximum frequency deviation, $\varphi_s(t)$ is the random initial phase and $m(\tau)$ is the normalized signal varying from -1 to 1. The local oscillator electric field is

$$E_{\text{LO}} = \hat{E}_{\text{LO}} \exp\{j[\omega_{\text{LO}} t + \varphi_{\text{LO}}(t)]\}$$

$$\text{SNR} = \frac{(RP_u\gamma)^2 \langle m(t) \rangle^2}{B[(RP_u)^2 RIN + 2qRP_u + 2P_nP_uR^2 + (2\Delta f_{\text{op}} - B)P_n^2R^2 + 4kT/R_l]} \tag{4}$$

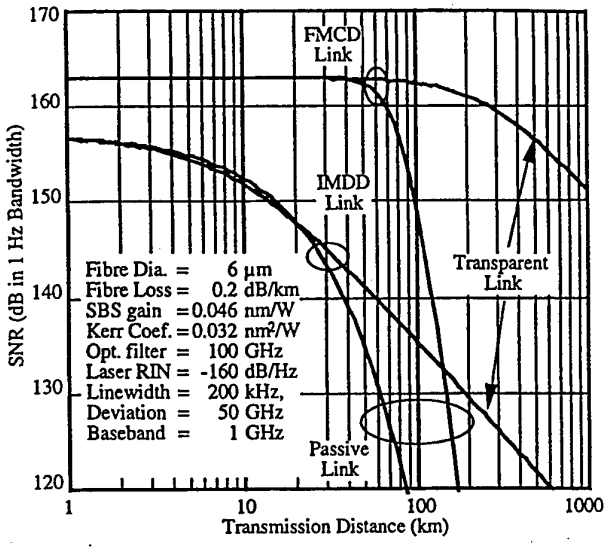

Fig. 3. SNR characteristics of IMDD and FMCD links.

with ω_{LO} being the local oscillator frequency and φ_{LO} the local oscillator phase. Assuming E_s and E_{LO} are polarization matched at the photodiode surface and taking into account that $\hat{E}_s^2 \propto P_u$ and $\hat{E}_{LO}^2 \propto P_{LO}$, the output current of the photodetector can be expressed as

$$I(t) = I_0 + I_s \cos\left[\omega_{IF} t + 2\pi\Delta f \int_0^t m(\tau)\, d\tau + \varphi_s - \varphi_{LO}\right]$$

where $I_0 = R(P_{LO} + P_u)$, $I_s = 2R\sqrt{P_{LO}P_u}$ and $\omega_{IF} = \omega_s - \omega_{LO}$. At the FM discriminator output, the mean squared signal current is

$$\langle i_s^2 \rangle = \Gamma_{FM}^2 \Delta f^2 \langle m^2(t) \rangle \tag{6}$$

where Γ_{FM} is the FM detector gain.

When the local oscillator output power P_{LO} is significantly higher than received signal power P_u the major noise current is contributed by an additive intensity noise related to I_0 and a phase noise φ_n.

The additive noise can be divided into quadrature and in-phase components. The influence of quadrature components on an FM system is well documented [10]. At the FM detector output, the current variance due to quadrature components σ_{qu}^2 is:

$$\sigma_{qu}^2 = \frac{(B\Gamma_{FM})^2}{3I_s^2}[I_0^2 RIN + 2qI_0 + 2P_n RI_0 + (2\Delta f_{op} - B)P_n^2 R^2 + 4kT/R_l]B. \tag{7}$$

Compared with the photodetector output, the FM detecting and RF filtering processes improve SNR by a factor of $3(\Delta f/B)^3$. For a typical $\Delta f/B$ ratio of 10, a SNR improvement of 35 dB can be achieved.

The in-phase components cause link transmission optical power fluctuation. Through the Kerr effect in the transmission fiber, such fluctuation will generate phase noise at the link output [11], [12]. At the FM discriminator output, the current variance due to the in-phase components σ_{in}^2 can be linked to optical intensity noise by

$$\frac{d\sigma_{in}^2}{dz} = \frac{2hfB}{3}[B\Gamma_{FM}K_G(z)]^2 \left[\frac{P_u G(z)}{G(l)} + \frac{2\Delta f_{op} - B}{2} P_n(z)\right] g(z) \tag{8}$$

and the boundary conditions determined by transmitter noise at the fiber input

$$\sigma_{in}^2(0) = \frac{B}{3}\left[\frac{B\Gamma_{FM}K_G(0)P_u}{G(l)}\right]^2 \left[RIN + \frac{2hfG(l)}{P_u}\right] \tag{9}$$

where $K_G(z) = \int_z^l G(z')\kappa_2(z')\, dz'$, κ_2 is the transmission medium nonlinear coefficient and for fiber $\kappa_2 = 8n_2/\lambda D_e^2$, n_2 is the Kerr coefficient. Equation (8) characterizes the influence of ASE noise along the transmission line and (9) that of the transmitter at the input of the link.

The laser phase noise passes through the FM discriminator directly and causes noise at the output. The current variance σ_{ph}^2 is

$$\sigma_{ph}^2 = \frac{\Gamma_{FM}^2}{2\pi}\int_{-\infty}^{\infty} |H(f)|^2 S_f(f)\, df \tag{10}$$

where $H(f)$ is the transfer function of the link, $S_f(f)$ the sum of transmitter and LO laser frequency noise spectral density. Assuming that $\langle m^2(t) \rangle = 0.5$, that the link transmission bandwidth is rectangular ($|H(f)|^2 = 1$ for $f \subset [-B, B]$, $|H(f)|^2 = 0$ otherwise) and the frequency noise is white, then $S_f = 2\pi\delta f$ and (10) reduces to

$$\sigma_{ph}^2 = \Gamma_{FM}^2 B\delta f/\pi \tag{11}$$

where δf is the sum of transmitter and local oscillator (LO) laser spectral linewidth.

Combining (6)–(11) the SNR of an optical FMCD link can be expressed as

$$\text{SNR} = \frac{\Gamma_{FM}^2 \Delta f^2 \langle m^2(t) \rangle}{\sigma_{qu}^2 + \sigma_{in}^2 + \sigma_{ph}^2}.$$

Both passive and ideally amplified link results for typical operating parameters are calculated and plotted in Fig. 3.

Fig. 3 shows that the SNR of an FMCD system is primarily determined by the transmitter and LO laser linewidth δf and the maximum frequency deviation Δf which is, in turn, limited by photodiode bandwidth. For long links, the SNR can be improved by bandwidth-SNR tradeoff. Compared with IMDD, FMCD links can show significant advantages in SNR performance.

III. Experiments

An FMCD link has been constructed, as shown in Fig. 4, to demonstrate the principles described above. The input signal modulates the optical frequency of the tuneable optical source and the resulting signal passes through the link to the receiver. An LO laser is offset from the source center frequency by the intermediate frequency (IF), which is made greater than the peak source frequency deviation. Balanced photo detection is preferred to minimize the contribution from LO laser intensity

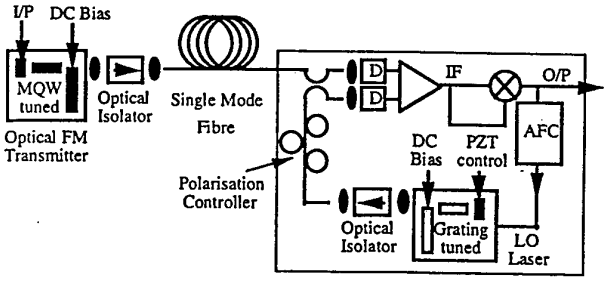

Fig. 4. Experimental optical FMCD link.

noise. The effect of intensity noise is further reduced by using a limiting IF amplifier. Signal recovery is by delay line microwave frequency discriminator, which also drives the LO laser frequency control circuit to compensate for system drift.

One of the biggest challenges in implementing such a system is to build a suitable tuneable optical source as the transmitter laser. The continuous tuning range of the source must be reasonably large in order to take full advantage of the available bandwidth of the photo-detector and the linewidth of the source must be narrow enough, relative to its tuning range, to achieve large signal-to-noise ratio. Furthermore, the bandwidth of the link will depend on the FM frequency response of the source; a wide and uniform FM frequency response is required to realize wide link bandwidth. To fulfill these crucial demands, a novel source laser tuning technique based on the quantum confined Stark effect (QCSE) in quantum-well materials is used in a multiple quantum-well (MQW) tuned external cavity laser [13]. In the MQW-tuned external cavity laser, a part of the laser cavity is formed by the MQW material. Due to QCSE, the refractive index of the MQW material can be modulated at very high speed by an electric field applied across it. This causes modulation of the optical length of the laser cavity and, therefore, of the emitted optical frequency.

Fig. 5 shows the MQW-tuned external cavity laser. A 300-μm long GaAs/AlGaAs channelled substrate planar (CSP) laser diode (Hitachi HLP 1400) was used as the laser gain section. One of the laser diode facets was antireflection coated with a single quarter wavelength SiO layer to reduce the Q factor of the laser diode internal cavity modes. The output from this facet was coupled into the tuning element through a graded refractive index (GRIN) lens of 0.29 pitch to form an external cavity laser of optical resonator length 15 mm. The conjugation between the laser diode facet and tuning element window enables the use of a small window area tuning element. The laser diode and MQW tuning element were temperature controlled independently and their relative positions were aligned with piezoelectric translator (PZT) micropositioners.

The tuning element was a PIN-type reflection phase modulator consisting of three sections: 1) the P-doped Bragg reflector section used 12 pairs of 692 Å AlAs/594 Å $Al_{0.2}Ga_{0.8}As$ layers to give a 20-nm wide reflection band centered on 828 nm with power reflection greater than 95%; 2) the intrinsic MQW section comprised 75 pairs of 60-Å $Al_{0.3}Ga_{0.7}As$ barriers and 52 Å GaAs wells, giving a maximum refractive

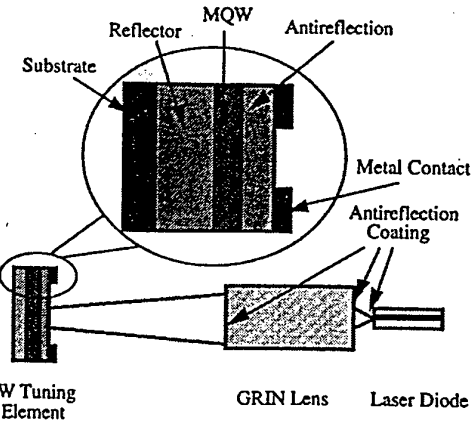

Fig. 5. MQW tuned external cavity laser.

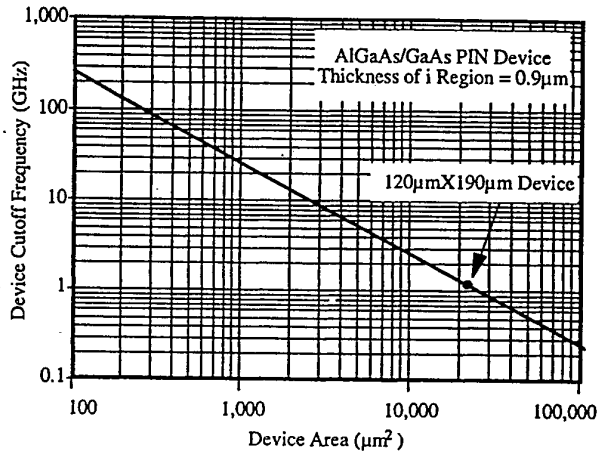

Fig. 6. Cutoff frequencies for different tuning element areas.

index change of 3% at a wavelength of 828 nm under an applied electric field strength of 55kV/cm; and 3) the N-doped antireflection section used 3-1/2 pairs of 692 Å AlAs/587 Å $Al_{0.17}Ga_{0.83}As$ layers giving a 15-nm-wide antireflection band centered on 828 nm with residual power reflection less than 1%. The performance evaluation and wavelength calibration of the three sections were carried out on three separately grown test wafers. The Ga concentration level in both Bragg reflector and antireflection sections was carefully chosen to give adequate reflection and antireflection bandwidth without significant increase of absorption. The whole structure was grown on a semi-insulating substrate using atmospheric pressure metalorganic vapor phase epitaxy (MOVPE) and the conventional reagents of trimethylgallium, trimethylaluminum, and arsine.

Electrically, such a PIN structure is comparable to a parallel plate capacitor. Its capacitance, and therefore the cutoff frequency is directly affected by the device area. For the wafer structure used, the calculated -3 dB cutoff frequencies for different device areas are plotted in Fig. 6. In order to achieve high-frequency operation, Mesa-type tuning elements of area 120 μm$\times$ 190 μm with 50 μm$\times$ 50 μm windows, as shown in Fig. 7, were fabricated from this material using conventional processing techniques.

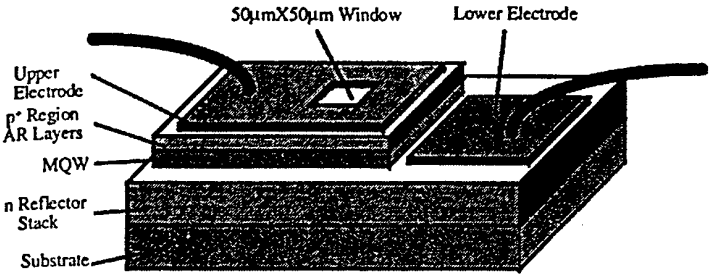

Fig. 7. MQW tuning element structure.

With 5 V reverse bias change on the MQW PIN tuning element, a continuous tuning range of 2.3 GHz was achieved. Harmonic distortion products were better than 30 dB below the signal and unwanted intensity modulation less than 0.3 dB for a peak deviation of 1.5 GHz. The tuning range could be increased by either reducing the external cavity length or increasing the thickness of the MQW section in the tuning element. As the tuning range achieved was sufficiently large to demonstrate the principles of the FMCD link, no effort was made to increase it further.

The laser spectral linewidth was measured to be less than 100 kHz, limited by the resolution of the self homodyne system used.

The FM response of the laser was measured independently by two methods, an adjustable Hi–Bi fiber optical frequency discriminator and a high resolution scanning Fabry–Perot interferometer.

An FM response uniform within ±1.6 dB from 20 kHz to 1.3 GHz was achieved [13]. The flatness at low frequency clearly shows the absence of the thermal effects which are normally dominant for forward biased, current tuned lasers. The higher frequency limit is due to the capacitance of the MQW tuning element used.

The uniform FM response results confirm the superiority of the tuning mechanism based on QCSE in MQW material over conventional current tuning. The residual IM was about 4% for a peak frequency deviation of 2 GHz.

The LO laser was realized using a grating-tuned external cavity configuration. The output from the SiO antireflection coated facet of the gain section (Hitachi HLP 1400) was collimated by a diffraction limited 10 × 0.17 numerical aperature (NA) microscope objective lens and diffracted by an 8 mm × 8 mm, 1200 pair lines/mm, blazed grating, mounted on a miniature PZT mirror mount, forming a 15-mm length external cavity. Both the lens position and grating angles were independently controlled using PZT devices. A full width at half maximum (FWHM) linewidth of less than 100 kHz and sidemode suppression of greater than 30 dB at an output power level of 4 mW were measured using the delayed self-homodyne technique and an optical spectrum analyzer, respectively. By rotating the grating, a large discrete tuning range of over 5 nm which is desired for channel selection potential was achieved.

The optical outputs from both the transmitter and LO laser were combined in a 3-dB fiber coupler and illuminated the photodiode active area. The polarization state of the output

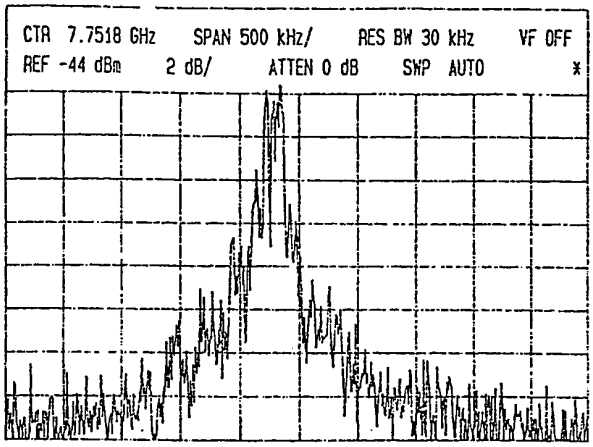

Fig. 8. Detected heterodyne spectrum.

from the LO laser was adjusted to match that of the transmitter laser with a fiber polarization controller. In this demonstration set-up, only a single detector was used to simplify the front-end design. The photodiode, mounted on an SMA connector, was an indium tin oxide (ITO) Schottky GaAs diode with a 3-dB cutoff frequency of 18 GHz and responsivity of 0.4 A/W (quantum efficiency of 60%). The transmitter and LO laser power at the detector were approximately 6 and 200 μW, respectively.

Although the laser emission wavelengths were aligned by grating tuning of the LO laser, further alignment was needed to obtain the desired intermediate frequency f_{if}. This alignment was realized by adjusting the temperature, bias level, and external cavity length of both lasers. The heterodyne signal at 8 GHz is shown in Fig. 8. The linewidth of the beat signal is about 200 kHz, slightly wider than expected due to relative frequency shift during the scanning period of the microwave spectrum analyzer. With a total linewidth of 200 kHz and maximum frequency deviation of over 2 GHz, the achievable SNR limited by laser frequency noise is greater than 130 dB · Hz.

The heterodyne signal in the microwave domain enables a detailed evaluation of laser noise due to the high spectral resolution available. The noise was in the form of both fast jitter and slow drift within a few MHz range. The structure of the noise indicates that the noise was caused by very weak external feedback and instability of both external cavity lasers due to the coupling of residual reflections to the laser diodes. The noise can be reduced by a better experimental environment or better thermal and mechanical isolation from the environment. The slow drift of frequency can be controlled by an automatic frequency control (AFC) loop.

The baseband signal was recovered using a microwave delay line frequency discriminator. The circuit used is shown in Fig. 9. Post-detector amplification was provided by a two-stage IF amplifier. The amplified signal was split by a 90° 3-dB hybrid coupler. The mixer reflections were reduced by circulators in both paths. The phase shifter in one of the paths provided an adjustable delay of 0 to 250 ps. The signals from the two paths were compared in a diode ring double-balanced mixer. Designed as a first-order discriminator, the delay time τ_d and

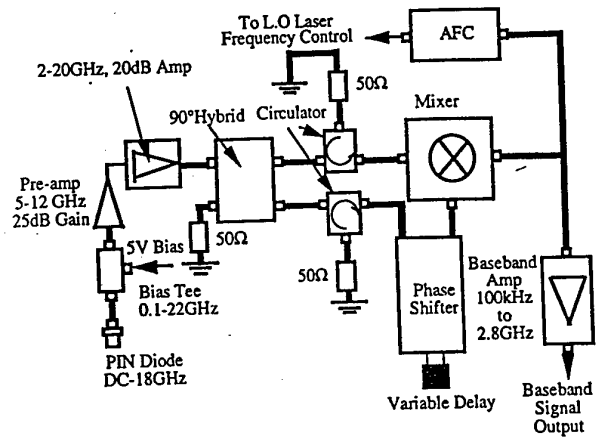

Fig. 9. Signal detection and demodulation circuit.

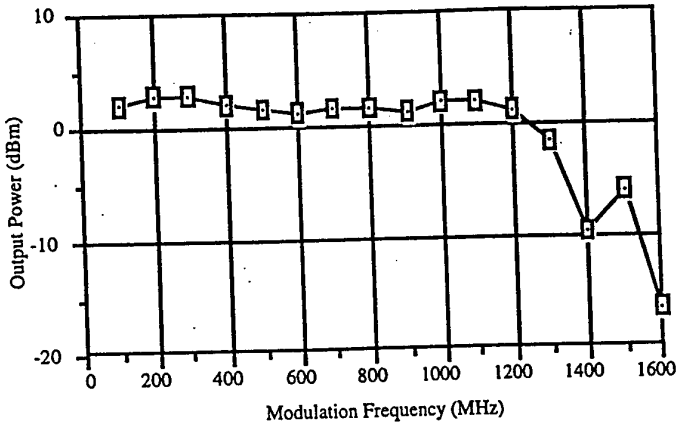

Fig. 10. Link frequency response.

intermediate frequency f_{IF} have the relationship

$$\tau_d \cdot f_{IF} = 1/2$$

for $f_{IF} = 8$ GHz, $\tau_d = 62.5$ ps. The demodulated signal from the mixer output was amplified by a baseband amplifier.

Replacing the photodiode with a microwave signal generator and the baseband amplifier with a voltage/current recorder, the static discriminator response was characterized and ripples were observed in the discriminator conversion curve. This is due to imperfect matching at the double-balanced mixer ports and limited the obtainable link linearity.

The flatness of the link transmission frequency response was measured by monitoring the link output signal at different input signal frequencies for a given input signal power. In this case, an input power of 15 dB was used to modulate the MQW tuning element in the transmitter laser. The measurements were taken at 100-MHz frequency intervals. The measured results are plotted in Fig. 10. The results show that with this novel tuning technique an uniform link transmission response to 1.3 GHz (−3 dB) was achieved and the earlier optical spectrum measurements of the transmitter laser FM response were confirmed. The main limitation on the high-frequency response is caused by tuning element depletion capacitance, and the technique could be extended to millimeter-wave frequencies with low parasitic capacitance tuning elements.

The maximum signal-to-noise ratio was estimated by measuring the link output signal and noise power at a given frequency with input signal power set at the 1-dB compression point. The measurement was carried out at 500 MHz, which is the center of the designed bandwidth. For a received optical signal power of 6 μW at the photodetector, a midband output SNR of 120 dB · Hz was achieved after correcting for the spectrum analyzer log amplifier response. This represents an improvement of some 20 dB over an intensity modulated link with the same received power [14]. The characteristic triangular shape of the link noise spectrum confirmed the theoretically predicted SNR-bandwidth tradeoff ability of the link. However, the measured SNR is lower than the value of 130 dB · Hz predicted from laser linewidth limited SNR because the LO laser power is not sufficient to achieve shot noise limited carrier-to-noise ratio (CNR) and full limiter action at the mixer for FM SNR improvement. The link nonlinearity due to imperfection in the microwave frequency discriminator construction also contributes to the reduction of the SNR.

The nonlinearity of the link was observed by harmonic distortion measurement and was mainly contributed by the microwave frequency discriminator. With very irregularly shaped ripples in the FM conversion curve, the conventional means used to quantify the nonlinearity of a link can not be applied. An indirect assessment on the linearity of the link without the influence of the ripples was made using measured transmitter linearity and a perfect sinusoidal FM conversion curve for the frequency discriminator. The results show that the maximum harmonic peaks are more than 30 dB below the signal at the 1-dB compression drive level of 18 dB and high linearity should, therefore, be possible with improved frequency discriminator construction.

IV. Conclusions

An analog optical FMCD link working at microwave frequencies has been analyzed and demonstrated in this paper for the first time. In the experiments, a bandwidth of 1.3 GHz and a SNR of 120 dB·Hz were achieved for a received optical power of 6 μW. With the external cavity type source and LO lasers used, the bandwidth can be expanded to 6 GHz by reducing the tuning element depletion capacitance. The SNR obtained was limited by photodiode power handling/LO laser-power capabilities. The SNR can be improved to 130 dB·Hz by using a high-power handling photodiode and increasing the LO laser launch power to above −3 dB. Combining the QCSE tuning technique used in these experiments and narrow linewidth laser techniques developed by [15], an optical FMCD link with 50-GHz bandwidth and 160 dB · Hz should be achievable.

Acknowledgment

The authors would like to thank their industrial and academic colleagues for their contributions to this paper. The authors would also like to thank Dr. J. S. Roberts at the EPSRC

III-V Centre, Sheffield University, for growing MQW epitaxial layer required for the source laser tuning elements.

REFERENCES

[1] C. H. Cox, G. E. Betts, and L. M. Johnson, "An analytic and experimental comparison of direct and external modulation in analog fiber-optic links," *IEEE Trans. Microwave Theory Tech.*, vol. 38, pp. 501–509, May 1990.

[2] W. E. Stephens and T. R. Joseph, "System characteristics of direct modulated and externally modulated RF Fiber optic link," *J. Lightwave Technol.*, vol. 5, pp. 380–387, Mar. 1987.

[3] E. P. Ippen and R. H. Stolen, "Stimulated brillouin scattering in optical fibers," *Appl. Phys. Lett.*, vol. 21, p. 539–540, Dec. 1972.

[4] A. R. Chraplavy, "Non-linear effect in optical fibers," in *Topics in Lightwave Transmission Systems*, T. Li, Ed. San Diego, CA: Academic, pp. 267–295, 1991.

[5] B. Cai and A. J. Seeds, "Optical frequency modulation link for microwave signal transmission," in *IEEE Microwave Theory Techniques '94, Dig.*, San Diego, CA, 1994, pp. 163–166.

[6] V. D. Pol, "The fundamental principles of frequency modulation," *Proc. Inst. Elect. Eng.*, vol. 93, pt. III, pp. 153, 1946.

[7] T. Kimura, "Coherent optical fiber transmission," *J. Lightwave Technol.*, vol. 5, pp. 414–428, Apr. 1987.

[8] E. Desurire, "Erbium-doped fiber amplifiers: Principles and applications," New York: Wiley, 1994.

[9] R. G. Smith, "Optical power handling capacity of low loss optical fibers as determined by stimulated raman and brillouin scattering," *Appl. Opt.*, vol. 11, pp. 2489–2494, Nov. 1972.

[10] J. Fagot and P. Magne, *Frequency Modulation Theory: Application to Microwave Links*, New York: Pergamon, 1961.

[11] J. P. Gordon and L. F. Mollenauer, "Phase noise in photonic communications systems using linear amplifiers," *Opt. Lett.*, vol. 15, pp. 1351–1353, Dec. 1990.

[12] S. Ryu, "Signal linewidth broadening due to fiber nonlinearities in long-haul coherent optical fiber communication systems," *Electron. Lett.*, vol. 27, pp. 1527–1529, Aug. 1991.

[13] B. Cai, A. J. Seeds and J. Roberts, "MQW-tuned semiconductor laser with uniform frequency response," *IEEE Photon. Technol. Lett.*, vol. 6, pp. 496–498, Apr. 1994.

[14] A. J. Seeds, "Microwave optoelectronics," *Opt. Quantum Electron.*, vol. 25, pp. 219–229, Apr. 1993.

[15] M. Okai, T. Tsuchiya, K. Uomi, N. Chinone, and T. Harada, "Corrugation-pitch-modulated MQW-DFB laser with narrow spectral linewidth," *IEEE Photon. Technol. Lett.*, vol. 2, p. 529–530, Aug. 1990.

Bo Cai received the B.Eng. and M.Eng. degrees from Xi'an Institute of Technology, Institute of Optics and Electronics, Chinese Academy of Sciences in 1982 and 1985, respectively and the Ph.D. degree from University College London, U.K., in 1991, all in optical engineering and optoelectronics.

Since 1991, he has been with University College London working on fast tuneable lasers, wideband optical links and other aspects of high-speed optical transmission systems. He is currently engaged in research on dense wavelength division multiplex optical communication systems.

Alwyn J. Seeds (M'81–SM'92–F'97) received the B.Sc. degree in electronics and the Ph.D. degree in electronic engineering from the University of London, U.K., in 1976 and 1980, respectively.

From 1980 to 1983 he was a Staff Member at Lincoln Laboratory, Massachusetts Institute of Technology (MIT), where he worked on monolithic millimeter-wave integrated circuits for use in phased-array radar. In 1983, he was appointed Lecturer in Telecommunications at Queen Mary College, University of London, U.K. In 1986 he moved to University College London, U.K., where he is currently Professor of Opto-electronics and leader of the Microwave Opto-electronics Group. He is the author of over 100 papers on microwave and opto-electronic devices and their systems applications and presenter of the video "Microwave Opto-electronics" in the IEEE Emerging Technologies series. His current research interests include microwave bandwidth tunable lasers, optical control of microwave devices, mode-locked lasers, optical phase-locked loops, optical frequency synthesis, dense WDM networks, optical soliton transmission, and the application of optical techniques to microwave systems.